PL-TR-95-2154

SEISMIC STUDIES OF THE CASPIAN BASIN AND SURROUNDING REGIONS

Keith Priestley
Stephen Mangino

University of Cambridge
Department of Earth Sciences
Madingley Rise, Madingley Road
Cambridge CB3 OEZ
UNITED KINGDOM

14 November 1995

Final Report
15 September 1993-14 November 1995

Approved for Public Release; Distribution Unlimited

PHILLIPS LABORATORY
Directorate of Geophysics
AIR FORCE MATERIEL COMMAND
HANSCOM AFB, MA 01731-3010

This technical report has been reviewed and is approved for publication.

JAMES F. LEWKOWICZ
Contract Manager

JAMES F. LEWKOWICZ, Director
Earth Sciences Division

This report has been reviewed by the ESC Public Affairs Office (PA) and is releasable to the National Technical Information Service (NTIS).

Qualified requestors may obtain additional copies from the Defense Technical Information Center. All others should apply to the National Technical Information Service.

If your address has changed, or if you wish to be removed from the mailing list, or if the addressee is no longer employed by your organization, please notify PL/TSI, 29 Randolph Road, Hanscom AFB, MA 01731-3010. This will assist us in maintaining a current mailing list.

Do not return copies of this report unless contractual obligations or notices on a specific document requires that it be returned.

REPORT DOCUMENTATION PAGE

Form Approved
OMB No 0704-0188

1. AGENCY USE ONLY (Leave blank)

2. REPORT DATE
14 NOVEMBER 1995

3. REPORT TYPE AND DATES COVERED
FINAL REPORT(15 Sep 93-14 Nov 95)

4. TITLE AND SUBTITLE
SEISMIC STUDIES OF THE CASPIAN BASIN AND SURROUNDING REGIONS

5. FUNDING NUMBERS
PE 61102F
PR2309 TA G2 WU BM
Contract F49620-92-J-0475

6. AUTHOR(S)
KEITH PRIESTLEY
STEPHEN MANGINO

7. PERFORMING ORGANIZATION NAME(S) AND ADDRESS(ES)
University of Cambridge
Department of Earth Sciences
Madingley Rise, Madingley Road
Cambridge CB3 OEZ, UNITED KINGDOM

8. PERFORMING ORGANIZATION REPORT NUMBER

9. SPONSORING/MONITORING AGENCY NAME(S) AND ADDRESS(ES)
Phillips Laboratory
29 Randolph Road
Hanscom AFB, MA 01731-3010
Contract Manager: James Lewkowicz/GPEH

10. SPONSORING/MONITORING AGENCY REPORT NUMBER
PL-TR-95-2154

11. SUPPLEMENTARY NOTES

12a. DISTRIBUTION/AVAILABILITY STATEMENT
APPROVED FOR PUBLIC RELEASE DISTRIBUTION UNLIMITED

12b. DISTRIBUTION CODE

13. ABSTRACT (Maximum 200 words)

In order to investigate the anomalous crust and upper mantle structure of the south Caspian Basin, we installed a network of six three-component seismograph stations within the countries of Turkmenistan and Azerbaijan. Improved knowledge of the crust and upper mantle structure of the south Caspian Basin is important in a seismic verification context because of the anomalous effect it has on regional seismic waveforms. Our objective is to determine the velocity structure of this region using both body wave receiver function and surface wave modeling techniques. We present receiver function inversion results for four sites and fundamental mode Rayleigh wave observations for two great circle paths across this region. Also presented are results of a study of Russian deep seismic sounding data from a nuclear source recorded along a 2600km long profile in Siberia. This analysis supports the earlier observation that the 410km discontinunity beneath the Siberian Platform consists of a velocity increase over a 35km depth.

14. SUBJECT TERMS
Seismic studies
Caspian Basin
Upper mantle structure
Surface wave modeling techniques

15. NUMBER OF PAGES
84

16. PRICE CODE

17. SECURITY CLASSIFICATION OF REPORT	18. SECURITY CLASSIFICATION OF THIS PAGE	19. SECURITY CLASSIFICATION OF ABSTRACT	20. LIMITATION OF ABSTRACT
unclassified	unclassified	unclassified	SAR

CONTENTS

VELOCITY STRUCTURE OF UPPER MANTLE TRANSITION ZONES BENEATH CENTRAL EURASIA FROM SEISMIC INVERSION USING GENETIC ALGORITHMS

VELOCITY STRUCTURE IN THE REGION OF THE SOUTH CASPIAN BASIN FROM TELESEISMIC RECEIVER FUNCTION MODELING

Velocity Structure of Upper Mantle Transition Zones beneath Central Eurasia from Seismic Inversion using Genetic Algorithms

Fernando A. Neves, Satish C. Singh and Keith F. Priestley

Bullard Laboratories, Madingley Rise, Madingley Road, Cambridge CB3 0EZ, UK

SUMMARY

We present velocity constraints for the upper mantle transition zones beneath Central Siberia based on observations of the 1982 "RIFT" Deep Seismic Sounding (DSS) profile. The data consist of seismic recordings of a nuclear explosion in northwestern Siberia along a 2600–km long seismic profile extending from the Yamal Peninsula to Lake Baikal. We invert seismic data from the mantle transition zones using a non–linear inversion scheme using a genetic algorithm for optimization and the WKBJ method to compute the synthetic seismograms. A statistical error analysis using a graph–binning technique was performed to provide uncertainty in the velocity models.

Our best model for the upper mantle velocity discontinuity near 410 km depth has a two–stage velocity gradient structure with velocities increasing from 8.65 to 9.30 km/s over a depth range of 400–415 km, a gradient of 0.043 s^{-1}, and from 9.30 to 9.65 km/s over a depth range of 415–435 km, a gradient of 0.0175 s^{-1}. This derived model is consistent with other seismological observations and mineral physics models. The model for the velocity discontinuity near 660 km depth is simple, sharp and includes velocities increasing from 10.10 km/s at 655 km depth to 10.65 km/s at 660 km depth, a gradient of 0.055 s^{-1}.

Key words: mantle transition zones, seismic inversion, genetic algorithm.

INTRODUCTION

The size and sharpness of the 410–km and 660–km seismic discontinuities provide important constraints in assessing petrological models of upper mantle phase changes and chemical layering. Laboratory studies (Ito & Takahashi, 1989) suggest that the velocity discontinuity at 410 km depth corresponds to a phase change over 20 km from peridotite to β–spinel structure. This result contradicts seismological studies of P'P' precursors (Lees et al. 1983;

Benz & Vidale, 1993) that suggest a simple and sharp 410–km discontinuity. The velocity discontinuity at 660 km depth corresponds to a phase change over 5 km from δ–spinel to perivoskite and magnesiowustite (Helffrich & Bina, 1994). Benz & Vidale (1993) have shown that the short–period frequency content of reflections from the 660–km discontinuity is sharp, corresponding to transition zones of 4 km or less.

Most of the previous seismic studies of the upper mantle transition zones have used low–frequency body wave or surface wave data, which results in poor resolution. Furthermore, a number of different source signatures are used in earthquake body wave studies, requiring a comparison of different waveforms or solving for the earthquake source, both resulting in possible ambiguities between velocities and earthquake source mechanism. Several recent upper mantle studies are based on very long refraction profiles in Asia (Mechie et al., 1993; Cipar et al., 1993; Priestley et al., 1994). The one–dimensional (1–D) model for the latter study, derived from travel–time forward modeling techniques and amplitude matching using reflectivity synthetic seismograms, has a 35–km thick transition zone (8.64–9.45 km/s) at 410 km depth and 4–km thick (10.25–10.62 km/s) at 660 km depth. As pointed out by Priestley et al. (1994) there is a clear evidence from the recorded section that lateral heterogeneity exists in the upper mantle along the profile.

In order to present seismic velocity models of upper mantle discontinuities that provide quantitative constraints on the petrology, error estimates on the velocity are necessary. Previous studies have used forward modeling techniques which give insight into the velocity structure, but they offer only qualitative estimates of the uncertainties associated with the velocity model features. Since the objective function which describes the goodness of fit between observed and synthetic seismograms is highly non–linear, a linear inversion scheme can provide neither a unique solution nor an error estimate. In this study we have used a non–linear global inversion scheme that can provide a statistical error analysis and model resolution. By obtaining the smallest structural details that are statistically resolvable, an inversion–derived velocity model can help discriminate between alternative seismic interpretations.

NON–LINEAR GLOBAL INVERSION

Seismic inversion schemes consist of three steps: forward modeling, evaluation of an

objective function and optimization of the objective function. The main objective of an inversion analysis is to find a "best" model that explains the observations. The forward modeling is achieved by efficiently solving the wave equation. The objective function is a measure of goodness between data and synthetic seismograms. Depending upon the nature of the objective function, a local (linear) or a global (non–linear) method of optimization is used. Linearized methods of optimization depend strongly on the starting model, and hence are prone to being either trapped in local optima or becoming unstable. As a result, these methods fail if the initial model is too far from the most likely model. In addition, they may require derivative of the objective function, and the computation of, which could be difficult and costly. A non–linear global optimization avoids nearly all of the limitations of the linear methods. For instance, by using an initial population of many randomly chosen velocity models, one does not require a starting velocity model. Instead of trying to find a "best" model that explains the observations, the global methods search for a family of velocity models which explain the data to a desired level of confidence. It is also possible to quantify the degree of confidence on each of the final estimated velocity models. Non–linear global inversion methods are attractive for problems where efficient forward modeling schemes are available.

Misfit Function

There are many measures of goodness of fit, and the choice of a specific one depends on the problem and the kind of data being analyzed. In general, a least–squares misfit between the data and synthetic seismograms should be used. However due to the absence of true amplitude information in the data that are analyzed here, we have used the semblance functional $E(\mathbf{m})$ defined as (Landa et al., 1989)

$$E(\mathbf{m}) = \sum_{k=0}^{K} \frac{\left\{\sum_j U_j[kdt + \tau(\mathbf{m})]\right\}^2}{\sum_j \left\{U_j[kdt + \tau(\mathbf{m})]\right\}^2} \tag{1}$$

where U_j represents the seismic trace for the j^{th} receiver, τ is the traveltime calculated by raytracing through the model $\mathbf{m}$, dt is the time sampling interval and Kdt is the time window

for semblance calculation. Our goal is to find the model $\mathbf{m}$ which maximises the semblance functional $E(\mathbf{m})$ calculated for all seismic traces in a time window along the traveltime trajectory defined by a forward modeling scheme. A time window length of 2 s (K=20) was used for the analysis.

Our choice of the semblance function was motivated primarily to avoid traveltime picking of the data. This is important since the seismic phases we are analyzing are secondary arrivals and hence of low signal–to–noise ratio. Furthermore, since the true amplitude information on the data was not available, we could not use a norm based on the full wavefield.

In order to perform a global search, which is computationally time consuming when compared to local search methods, we need a fast forward modeling scheme. The WKBJ synthetic seismogram method (Chapman, 1978) provides such a solution. We have used the WKBJ seismogram algorithm extended to laterally inhomogeneous media using the Maslov asymptotic theory (Chapman & Drummond, 1982) as a 2–D forward modeling technique. For the traveltime calculation we have applied a dynamic raytracing algorithm, where non–geometrical signals caused by inhomogeneities in the Earth are modeled. This algorithm is an extension of geometrical ray theory and agrees with geometrical ray theory for high–frequency direct and turning rays (Chapman et al., 1988). The Maslov algorithm was chosen because it is a fast and accurate 2–D forward modeling scheme to evaluate the objective function for a large number of models. We have adopted the 2–D raytracing scheme in order to take into account propagation effects generated by lateral heterogeneities within the crust and upper mantle.

Genetic Algorithms

The objective function $E(\mathbf{m})$ generally has many peaks and the methods based on local optimization often fail to find the largest value of the objective function if the starting model is not close enough to the final model. To avoid this problem, a global method, Genetic Algorithm (GA), is used. The GA works with a group of M velocity models simultaneously, each represented by a bit–string (Goldberg, 1989). The initial search space for each velocity is divided into $2n$ parts described by n bits. The initial population of M velocity models is generated randomly within each velocity bound.

At each iteration the GA essentially consists of three operations (Fig. 1) : selection, crossover and mutation.

Selection: From the initial population of M–bit strings, an interim population of M parents is generated by selecting models from the original group with likelihood of selection determined by a probability depending on the objective function. The probability of selecting the k^{th} velocity model is written as (Sambridge & Drijkoningen, 1992)

$$P(\mathbf{m}_k) = \left[\sum_{j=1}^{M} \exp(BE_j)\right]^{-1} \exp(BE(\mathbf{m}_k)) \qquad (2)$$

where $B = (E_\sigma)^{-1}$. E_σ is the standard deviation of the objective function $E(\mathbf{m}_k)$ ($k = 1, ..., M$) within the population that is being evaluated by GA. E_j ($j = 1, ..., M$) is the current value of the objective function $E(\mathbf{m}_k)$. Note in Fig. 1 that model 1 with the highest objective function was selected twice, model 2 and 3 once, model 4 with the lowest objective function was rejected.

Crossover: From the parent population of M–bit strings a new generation of M–strings is generated, each of which is obtained by mixing bit–strings from two parents. All the M parents are randomly paired to produce $M/2$ couples. A probability for performing this step is assigned. The value designated for this probability is chosen by preliminary tests on the data. If this probability is greater than a generated random number between 0 and 1, then the current pair is to be crossed over. The location where the strings are cut is also determined randomly. Our GA algorithm uses a single–point crossover, with the cut position restricted to occur only at velocity boundaries (Fig. 1).

Mutation: This final process allows any bit in an individual string to flip between 0 and 1. The main goal of this process is to add some degree of local diversity (since only individual bits are affected) into the whole inversion process. Therefore, no genetic feature is permanently lost, something that would reduce the model space. A mutation probability (usually rather low) is used to control the likelihood of this process.

A Posteriori Probability Density (PPD) is assigned to each evaluated model, which is defined as (Basu & Frazer, 1990) :

$$\Psi(\mathrm{m}) = \frac{\exp(E(\mathrm{m})/\sigma)}{\sum \exp(E(\mathrm{m})/\sigma)} \tag{3}$$

where $E(\mathrm{m})$ is the semblance (objective) function value for model m and σ is the variance in $E(\mathrm{m})$ for all the models sampled by the GA. Here we have assumed that the data are statistically independent. The square root of variance is a measure of uncertainty or standard error of the estimated parameter. The denominator $\sum \exp(E(\mathrm{m})/\sigma$ is summed and evaluated at the end of all the runs and is used to normalize the PPD. Since it is impossible to plot the PPD in the M–dimensional model space, we have used the graph–binning technique proposed by Frazer & Basu (1990) where each model parameter was assigned the model's PPD and summed into model parameter bins. Nolte & Frazer (1994) argue that there is no theoretical basis for using GA to compute the PPD. However, we agree with Stoffa & Sen (1991) that many independent GA runs with different initial populations followed by a graph–binning technique can provide an estimate of the PPD.

APPLICATION TO DATA

The Siberian RIFT Profile

During the past 30 years, the Soviet Ministry of Geology (now the Center of Regional Geophysical and Geological Research) has conducted an extensive seismic exploration program of the Eurasian crust and upper mantle. Many of these profiles used nuclear explosions as seismic sources for recording long–range profiles (up to 4000 km) and chemical explosives for recording short–range (up to 750 km) profiles (Scheimer & Borg, 1984; Benz et al., 1992). Analysis of these data by Russian seismologists has largely been by forward modeling of the travel time data. Recently, data from several of these profiles have been analyzed by forward modeling of the waveform data (Cipar et al. 1993; Priestley et al. 1994).

The 1982 RIFT profile extends 2600 km across the Siberian platform from the Yamal Peninsula to Lake Baikal (Fig. 2). Seismic data were recorded from three nuclear explosions and thirty–four chemical explosions along this profile. The northernmost shot point (SP245) is located within the West Siberian rift on the northwest edge of the Siberian platform.

This aborted rift is buried beneath approximately 15 km of sediments (Cipar et al., 1993). The central section of the profile extends across the Tunguska basin (site of SP173), a region of widespread intraplate flood basalts. The southern portion of the profile crosses the presently active Baikal rift (site of SP35); this rift occurs within a recent regional uplift and is characterized by high heat flow and a low velocity upper mantle (Belousov et al. 1991).

We analyze the data from SP245 in this study. SP245 was located at 69.206°N 81.647°E, had a body wave magnitude of mb = 5.2, and was recorded in a SE–direction to a distance of 2400 km (Fig. 2). Analysis of the seismograms from the chemical explosions along this profile provides detailed crust and uppermost mantle velocity structure (Fig. 4) (Pavlenkova, personal communication).

SP245 was recorded at 182 sites, each equipped with three–component seismometers and a Taiga seismic recording system, (Chichinin et al., 1969). We analyze only the vertical component data in this study. The seismometers have a natural frequency of 1.5 Hz, and the recording system has a usable bandwidth between 0.5 and 20 Hz. The station locations are accurate to 0.1 km, which is lower than the accuracy of station locations for most modern crustal refraction studies. However, the source–receiver distances are much more accurate than in most mantle studies using earthquake data because the source location is accurately known. These data were commercially digitized and corrected for amplitude scaling to produce trace normalized record sections (Cipar et al., 1993). The seismic section for SP245 is shown in Fig. 3.

The nature of the wave field from these data have been discussed by Priestley et al. (1994). Crustal arrivals are prominent at short offsets, especially the crustal (Pg) phase. The uppermost mantle refracted arrival (Pn) is observed as a first arrival starting at a distance of ~ 150 km. The Pn arrival is observed to about 600 km but has variable amplitude. Since this amplitude variation can be correlated over large distances, it is likely to be due to variations in the lithospheric structure. The upper mantle velocity is about 8.2 km/s (Priestley et al., 1994). In this study we concentrate our effort on reflected/refracted arrivals from the upper mantle transition zones. The phase from the 410–km discontinuity is a clear secondary arrival beginning at about 1600 km and 15 s reduced time with a reduction velocity of 8.2 km/s, and becomes the first arrival at about 2200 km. The phase from the 660–km discontinuity

starts at about 2100 km range and 13 s reduced time.

Initial Models

Since we are interested in the details of the velocity discontinuities at 410 km and 660 km depths, we allow the velocity model to vary only in the vicinity of these zones and fix the model elsewhere. For the crust we include the 2–D velocity model determined from a study of refraction data recorded from the chemical explosions along the "RIFT" profile (Pavlenkova, personal communication). This crustal model is very complex, so instead of using this model for the crust, we have used a smoothed version (Fig. 4) of it. The smoothed crustal velocity model still contains significant lateral velocity variations which generate differential time delays at different ranges. These will certainly affect the depth and thickness estimates of mantle features. It is therefore important to use a 2–D raytracing technique for the crustal part of the profile. However, having only one line and one shot available, it is impossible to resolve lateral variations in upper mantle structures. Thus, we have used a hybrid method consisting of 2–D raytracing for the crust and a 1–D inversion scheme for the upper mantle transition zones. The 1–D upper mantle velocity model used in this study (Fig. 5, thin line) was derived by Priestley et al. (1994).

Model Parameterization

The velocity model in the vicinity of the transition zone was parameterized as a function of depth V(z) at various node points with linear interpolation applied between the node points. This implies that velocity gradient is parameterized. The separation between nodes was determined by the dominant frequency content of the seismic data. The dominant frequency of the P–waves for the upper mantle arrivals is around 1.5 Hz, giving a resolution of 4–5 km. Therefore, we have parameterized the velocity model for the region with velocity nodes every 5 km. The structure in the vicinity of the 410–km discontinuity was parameterized by 8 nodes equally spaced at 5 km and in the vicinity of the 660–km discontinuity by 4 nodes. This was based on the maximum resolution of 5 km provided by the data and also by the maximum thickness of the transition zones given by previous studies (Priestley et al. 1994). Thus we restrict the thickness of the 410–km transition zone to be less than 35 km and the thickness

of the 660–km transition to be less than 15 km.

Inversion

The inversion was run for 200 iterations with an initial population of 50 models, and with probabilities of crossover and mutation equal to 0.6 and 0.05, respectively. These values were obtained from preliminary tests on the data and must be tuned for each particular problem or data set. This tuning represents an unsatisfactory aspect of the GA method (Sambridge & Drijkoningen, 1992). The initial population of models was chosen randomly within the velocity range defined from the model–T. The velocity range was defined as $V_T \pm 0.5$ km/s, where V_T is the velocity of model–T. The velocity deviation in this range is greater than a typical accuracy of $\pm$ 0.1–0.2 km/s provided by a ordinary wide–angle seismological survey. A positive velocity gradient constraint was imposed to avoid the presence of low velocity zones.

The evaluation of the semblance functional (eq. (1)) requires knowledge of neither the source wavelet nor the instrument response. However, we have used the source function described in Evernden et al. (1986) to calculate the synthetic seismograms so that the synthetic seismograms can be visually compared to the data. Evernden et al. (1986) present an empirically determined formula for the far field amplitude spectrum generated by explosions. The attenuation model used in computing the synthetics seismograms was taken from Der et al. (1986) as used by Priestley et al. (1994). Due to the long extent of the seismic line (2400 km) we have also applied the Earth flattening transformation described by Chapman (1973). The final inversion results for the velocity model for the 410–km and 660–km discontinuities are shown in Figs. 6a and 7a, respectively. In order to evaluate the effect of the 2–D crustal velocity model and upper mantle velocity model on our final models, a 1–D crustal velocity model and a smoothed version of model–T (Fig. 5, thick line) were considered. The resulting velocity models for the 410–km and 660–km discontinuities with a 1–D crustal velocity model and a smoothed version of model–T are shown in Figs. 6a and 7a, respectively.

Merely fitting the data by an inversion scheme method is not sufficient for estimating model parameters; measurement of resolution and uncertainty are required. Therefore, we have evaluated the binned PPD function, where we have assumed a constant travel–time variance of $\sigma = 0.5$ s for all models. The binary coding requires that the number of velocity

intervals for each node is an integral power of two. Thus, during the GA optimization procedure we set a fixed velocity interval $\Delta V = 0.1$ km/s, which is within the expected accuracy. In Figs. 6b and 7b we have also plotted the PPD's (dashed lines), calculated using eq. (3), at each node depth point.

In Figs. 6b and 7b, we show the data (solid curve) and the synthetics for the final model (dashed curve) for the arrivals from the 410–km and 660–km discontinuities, respectively. Figure 6c shows the data (solid curve) and the synthetic waveforms for our "best–fit" preferred model, a two–step gradient (dotted–dashed curve), a simple (one step) gradient (dotted curve) and a simple sharp discontinuity (dashed curve), for the 410–km discontinuity for stations located at 1803 km and 1982 km away from SP245. In order to quantify the goodness of fit between observed and synthetic seismograms, we have used the misfit function $\phi(j)$ defined as

$$\phi(j) \;=\; \frac{\sum_{t=t_0}^{t_0\,+\,Kdt} \left|U_{\mathrm{obs}}(j,t) \,-\, U_{\mathrm{syn}}(j,t)\right|^2}{\sum_{t=t_0}^{t_0\,+\,Kdt} \left(U_{\mathrm{obs}}(j,t)\right)^2} \qquad (4)$$

where $U_{\mathrm{obs}}(j,t)$ are the observed data, $U_{\mathrm{syn}}(j,t)$ are the synthetic seismograms for station j, and t is the time. The computation of $\phi(j)$ is done within a time window Kdt starting from the traveltime t_0 estimated from the inversion. For the 410–km discontinuity (Fig. 6(c)) the values of ϕ(j=1803 km) for the sharp, one–step gradient and two–step are 0.33, 0.19 and 0.11, respectively. The values of ϕ(j=1982 km) for the sharp, one–step gradient and two–step gradient are 0.38, 0.24 and 0.16, respectively. At both locations, the misfit is the lowest for the two–step gradient model.

DISCUSSION

The synthetic seismograms obtained from our final velocity models for the 410–km and 660–km discontinuities adequately fit the general features of the observed data. Our model for the transition zone near 410 km depth (Fig. 6a) consists of a two–stage velocity gradient. This model has produced the best–fit (Fig. 6c). The first stage extends from 400 to 415 km depth with P–wave velocity increasing from 8.70 to 9.25 km/s with a high velocity gradient

of 0.0433 s^{-1}. The second stage extends from 415 to 435 km depth with P–wave velocity increasing from 9.25 to 9.60 km/s and a low velocity gradient of 0.0175 s^{-1}. The PPD's curves clearly show this bimodal velocity structure, which suggests that long period seismic data are more (or may be only) sensitive to this first step gradient, where there is a greater velocity variation at around 415 km depth. This may explain observations of Benz & Vidale (1993). In a mineral physics context, this would imply that the transformation from olivine to β–spinel is not linear in the 410–km transition zone, and it is faster for the first 15 km. For mineral physics models, a thickness of 35 km might be postulated when the transformation from olivine to β–spinel has taken place completely (Ita & Stixrude, 1992).

Although our model and the model–T for the 410–km discontinuity shows the same shape (two–step velocity gradient), our velocity model is faster (up to 0.2 km/s). However, Priestley et al. (1994) have adopted a broad transition region for the 410–km discontinuity.

The PPD plot in Fig. 6b shows clearly that model–T might result from a secondary optimum. With error analysis used here, we can distinguish various possible models.

Our model for the 660–km discontinuity (Fig. 7a) is consistent with previous seismological models, such as the model–T. We estimate this transition zone as 5 km thick over the depth range 655–660 km, with velocity ranging from 10.15 and 10.70 km/s and have a velocity gradient of 0.055 s^{-1}. The PPD plots are more complex than the one from Fig. 6b, which could be due to low signal–to–noise ratio for these later arrivals. It should be noted that we have assumed a 1–D model in the upper mantle although the earth is truly 3–D. For low frequency waves this is a good approximation, but this limits our power of spatial depth and lateral resolution, which means that lateral heterogeneity can be mapped into a 1–D velocity model (Kennett & Bowman, 1990). This may explain some small discrepancies between the data and synthetic seismograms.

CONCLUSIONS

The main points of this study are :

(1) Our proposed inversion method approach which combines 2–D forward modeling with dynamic raytracing for the crust and 1–D inversion for the upper mantle is relevant. The

error–analysis using a graph–binning technique has shown the existence of local optima where solutions associated with previous velocity models derived from forward modeling schemes might get trapped.

(2) We presented a 1–D compressional velocity model for the 410–km and 660–km upper mantle discontinuities beneath the Siberian Platform that is derived from non–linear global inversion applied to the deep seismic data recorded along the RIFT profile. However, we still consider this a preliminary model since we have analyzed data from only one shot point of the RIFT profile.

The major features of our model are : (a) a two–stage velocity gradient for the transition zone near the 410 km depth. The first one is a high velocity gradient zone ranging from 400 to 415 km depth and the second one is a low velocity gradient zone ranging from 415 to 435 km depth, (b) a simple and narrow high gradient zone between 655 and 660 km depth.

(3) We also suggest that the phase transformation from olivine to β–spinel is not linear for the shallower transition zone, which in turn generates the two–step velocity gradient pattern observed for this region. This result is independently confirmed by Stixrude (1995)

REFERENCES

Basu, A. & Frazer, L. N., 1990. Rapid determination of the critical temperature in simulated annealing inversion, Science, 249, 1409–1412.

Belousov, B., Pavlenkova, N. I. & Kvyatkovskaya, G. N., 1991. Crustal structure of the territory of the USSR (in Russian), Nauka, Moscow.

Benz, H. M. & Vidale, J. E., 1993. Sharpness of upper–mantle discontinuities determined from high–frequency reflections, Nature, 365, 147–150.

Benz, H. M., Unger, J. D., Leith, W. S., Mooney, W. D., Solodilov, L., Egorkin, A. V. & Ryaboy, V. Z., 1992. Deep seismic sounding in Northern Eurasia, EOS, Trans. Am. geophys. Un., 73, 297–300.

Chapman, C. H., 1973. The Earth flattening transformation in body wave theory, Geophys.

J. R. astr. Soc., 35, 55–70.

Chapman, C. H., 1978. A new method for computing synthetic seismograms, Geophys. J. R. astr. Soc., 54, 481–518.

Chapman, C. H. & Drummond, R., 1982. Body wave seismograms in inhomogeneous media using Maslov asymptotic theory, Bull. seism. Soc. Am., 72, 277–317.

Chapman, C. H., Jen–Yi, C. & Lyness, D. G., 1988. The WKBJ seismogram algorithm, In Seismological Algorithms: Computational Methods and Computer programs, 47–74; Academic Press Ltd., London.

Chichinin, I. S., Yegorov, G. V., Yemelianov, A. V. & Bochanov, A. J., 1969. Portable Telemonitored Seismic Equipment Taiga, Methods of Seismic Research, 95–119; Nauka, Moscow.

Cipar, J. J., Priestley, K. F., Egorkin, A. V. & Pavlenkova, N. I., 1993. The Yamal Peninsula–Lake Baikal deep seismic sounding profile, Geophys. Res. Lett., 20, 1631–1634.

Der, Z., Lees, A. & Cormier, V., 1986. Frequency dependence of Q in the upper mantle underlying the shield areas of Eurasia, Part III: The Q model, Geophys. J. R. astr. Soc., 87, 1103–1112.

Evernden, J. F., Archambeau, C. B. & Cranswick, E., 1986. An evaluation of seismic decoupling and underground nuclear test monitoring using high–frequency seismic data, Rev. Geophysics, 24, 143–215.

Frazer, L. N. & Basu, A., 1990. Freeze–bath inversion, 60th Ann. Internat. Mtg., Soc. Expl. Geophys., Expanded Abstracts, 1123–1125.

Goldberg, D. E., 1989. Genetic Algorithms in Search, Optimization and Machine Learning, Addison–Wesley, Reading, MA.

Helffrich, G. & Bina, C. R., 1994. Frequency dependence of the visibility and depths of mantle seismic discontinuities, Geophys. Res. Lett., 24, 2613–2616.

Ita, J. & Stixrude, L., 1992. Petrology, elasticity, and composition of the mantle transition

zone, J. geophys. Res., 97, 6849–6866.

Ito, E. & Takahashi, E., 1989. Postspinel transformations in the system Mg2SiO4–Fe2SiO4 and some geophysical implications, J. geophys. Res., 94, 10637–10646.

Kennett, B. L. N. & Bowman, J. R., 1990. The velocity structure and heterogeneity of the upper mantle, Phys. Earth planet. Inter., 59, 134–144.

Lees, A. C., Bukowinski, M. S. T. & Jeanloz, R. J., 1983. Reflection properties of phase transition and compositional change models of the 670–km discontinuity, J. geophys. Res., 88, 8145–8159.

Landa, E., Beydoun, W. & Tarantola, A., 1989. Reference velocity model estimation from prestack waveforms : coherency optimization by simulated annealing, Geophysics, 54, 984–990.

Nolte, B. & Frazer, L. N., 1994. Vertical seismic profile inversion with genetic algorithms, Geophys. J. Int., 117, 162–178.

Mechie, J., Egorkin, A. V., Fuchs, K., Ryberg, T., Solodilov, L. & Wenzel, F., 1993. P–wave mantle velocity structure beneath northern Eurasia from long–range recordings along the profile Quartz, Phys. Earth planet. Inter., 33, 180–193.

Priestley, K. F., Cipar, J. J., Egorkin, A. V. & Pavlenkova, N.I., 1994. Upper–mantle velocity structure beneath the Siberian platform, Geophys. J. Int., 108, 369–378.

Sambridge, M. & Drijkoningen G., 1992. Genetic algorithms in seismic waveform inversion, Geophys. J. Int., 109, 323–342.

Scheimer, J. F. & Borg, I. Y., 1984. Deep seismic sounding with nuclear explosives in the Soviet Union, Science, 226, 787–792.

Stixrude, L., 1995. Mantle composition and structure of mantle discontinuities, IUGG XXI General Assembly, Abstract, B383.

Figure Captions

Figure 1. A schematic illustration of the operators employed by the genetic algorithm. The selection operator chooses the models from the initial population (in this example four models) with a probability of selection proportional to the maximum of the objective function (E). Model 1, with the highest E, was selected twice while model 4, with the lowest E, was rejected for the next generation. The crossover operator randomly chooses pairs of models and exchanges their portions (three parameter models in this example) at a point selected at random along the length of the model to produce two new off–spring. The mutation operator is shown operating on a single velocity of parameter 4. The colors represent different parameter values.

Figure 2. Simplified tectonic map of central Asia. The RIFT profile is the straight solid line and the large solid dots show the location of the nuclear explosion for the shot points 245, 173 and 35.

Figure 3. Recorded, unfiltered SP245 seismic section reduced at 8.2 km/s. The seismograms are trace normalized. The arrivals labeled are : (a) Pg, (b) Pn, (c) reflection/refraction from the 410–km discontinuity and (d) reflection/refraction from the 660–km discontinuity.

Figure 4. Smoothed 2–D crustal P–wave velocity model derived from chemical explosions along profile (Pavlenkova, personal communication). Numbers within the plot are velocities in km/s. Velocities vary linearly with distance and depth.

Figure 5. P–wave upper–mantle velocity–depth function (thin solid line) for SP245 model–T (Priestley et al., 1994). Thick solid line is a smoothed version of model–T.

Figure 6.(a) P–wave velocity–depth function for the 410–km discontinuity estimated from inversion with a 2–D crustal velocity structure (thick dark solid line), with a 1–D crustal velocity structure (thin solid line), with a smoothed model–T velocity structure (thick grey line) and model–T (dotted–dashed line). The crossed circles are the depth points where velocities were computed. The Posteriori Probability Density functions (PPDs) are shown by the dashed lines. (b) Comparison between synthetic seismograms (dashed

curve) filtered in the same frequency bandwidth and data (solid curve) for the 410–km discontinuity at reduced velocity of 8.2 km/s. The arrows show estimated traveltime from inversion and the dots those computed for model–T. (c) Comparison between data (solid curve) and the synthetic waveforms for a two–step gradient (dotted–dashed curve), a simple (one step) gradient (dotted curve) and a simple sharp discontinuity (dashed curve), for the 410–km discontinuity for the stations located at 1803 km and 1982 km away from SP245.

Figure 7. (a) P–wave velocity depth function for the 660–km discontinuity estimated from inversion with a 2–D crustal velocity structure (thick dark solid line), with a 1–D crustal velocity structure (thin solid line), with a smoothed model–T velocity structure (thick light solid line) and model–T (dotted–dashed line). The crossed circles are the depth points where velocities were computed. The Posteriori Probability Density functions (PPDs) are shown by the dashed lines.

(b) Comparison between synthetic seismograms (dashed curve) filtered in the same data frequency bandwidth and data (solid curve) for the 660–km discontinuity at reduced velocity of 8.2 km/s. The arrows show estimated traveltime from inversion and the dots those computed from model–T.

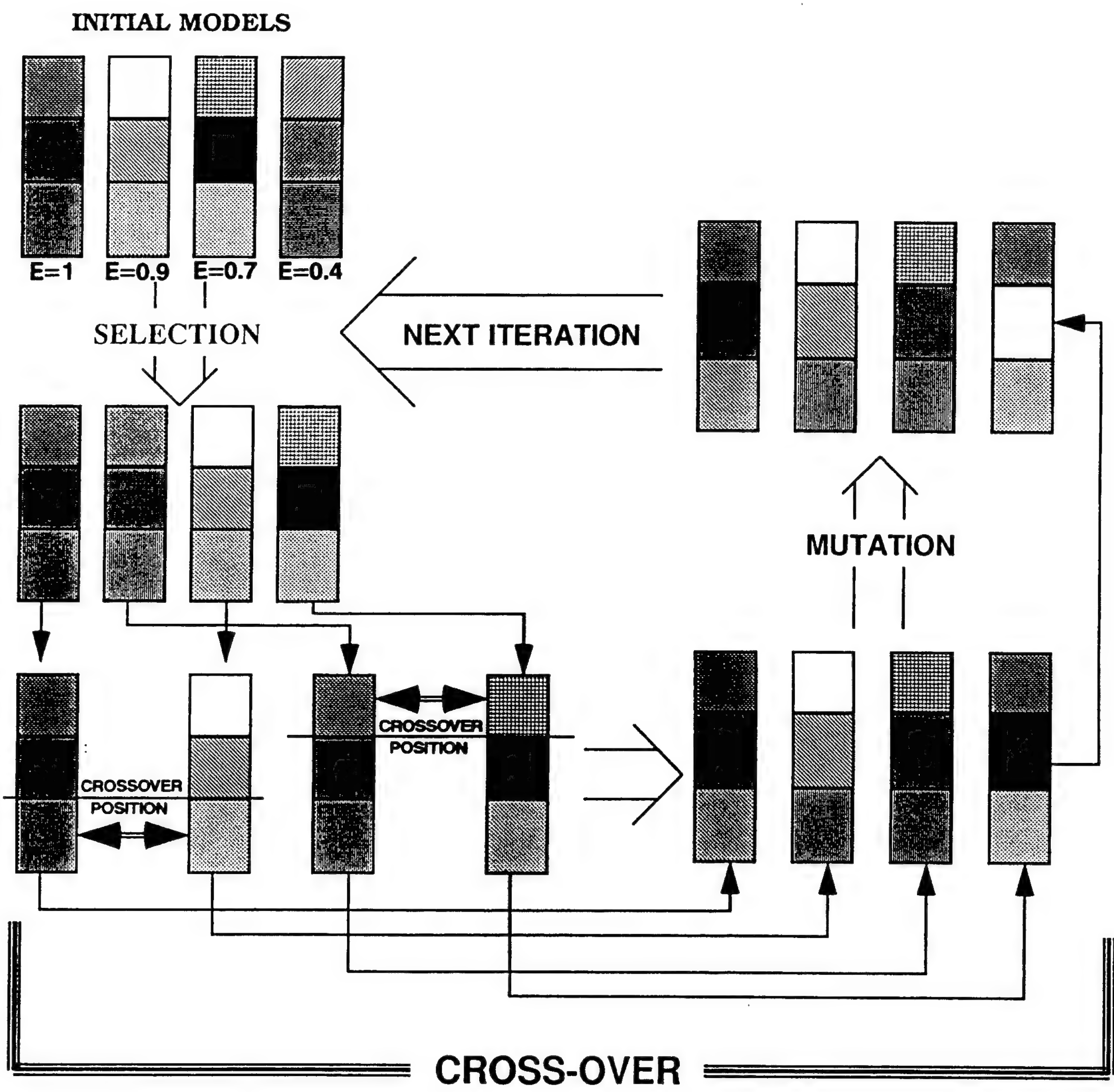
INITIAL MODELS
E=1
E=0.9
E=0.7
E=0.4
SELECTION
NEXT ITERATION
MUTATION
CROSSOVER
POSITION
CROSSOVER
POSITION
CROSS-OVER

FIGURE 1

FIGURE 2

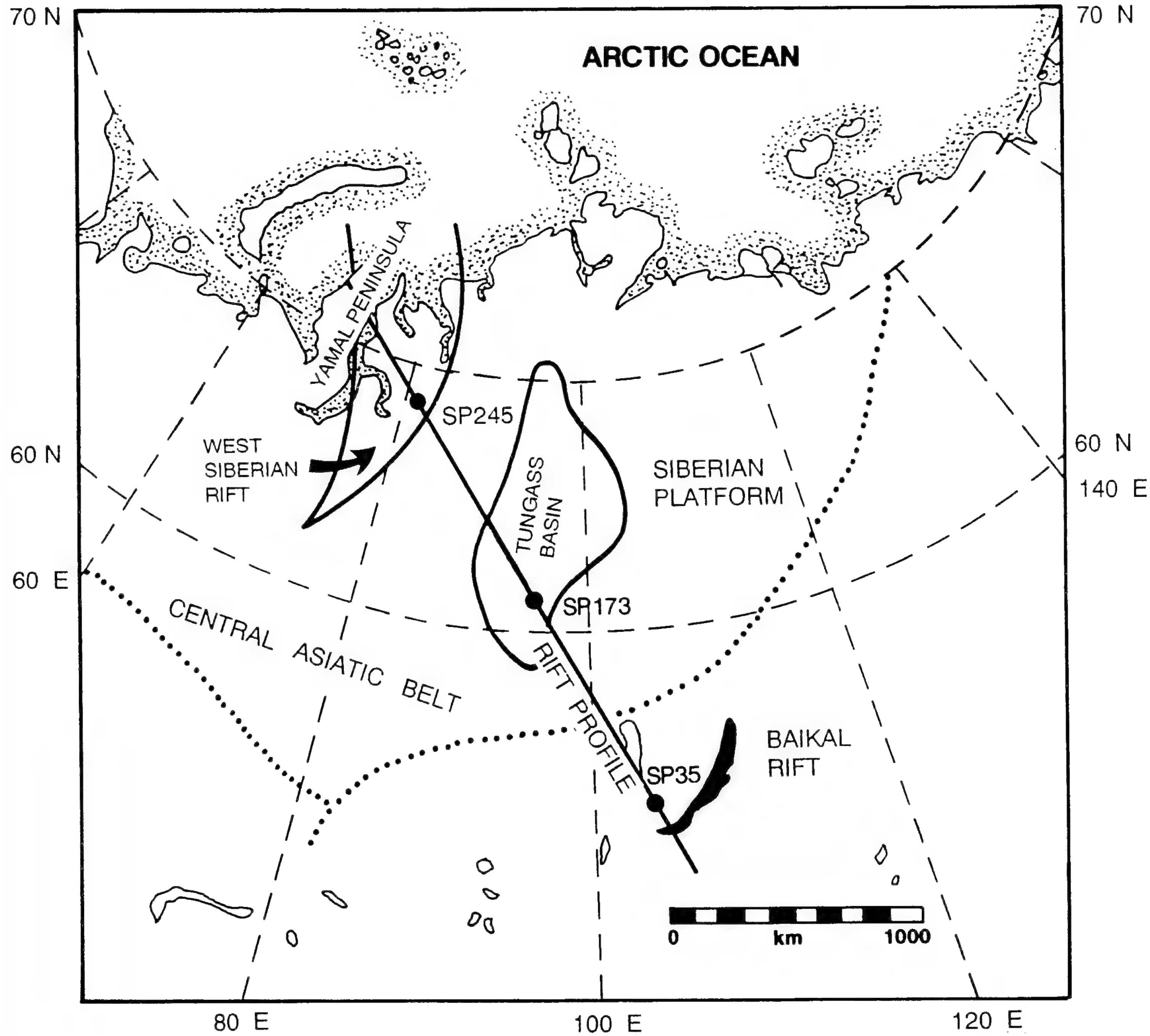

70 N
70 N
ARCTIC OCEAN
YAMAL PENINSULA
SP245
WEST
SIBERIAN
RIFT
60 N
60 N
140 E
SIBERIAN
PLATFORM
TUNGASS
BASIN
60 E
SP173
CENTRAL ASIATIC BELT
RIFT PROFILE
BAIKAL
RIFT
SP35
0
km
1000
80 E
100 E
120 E

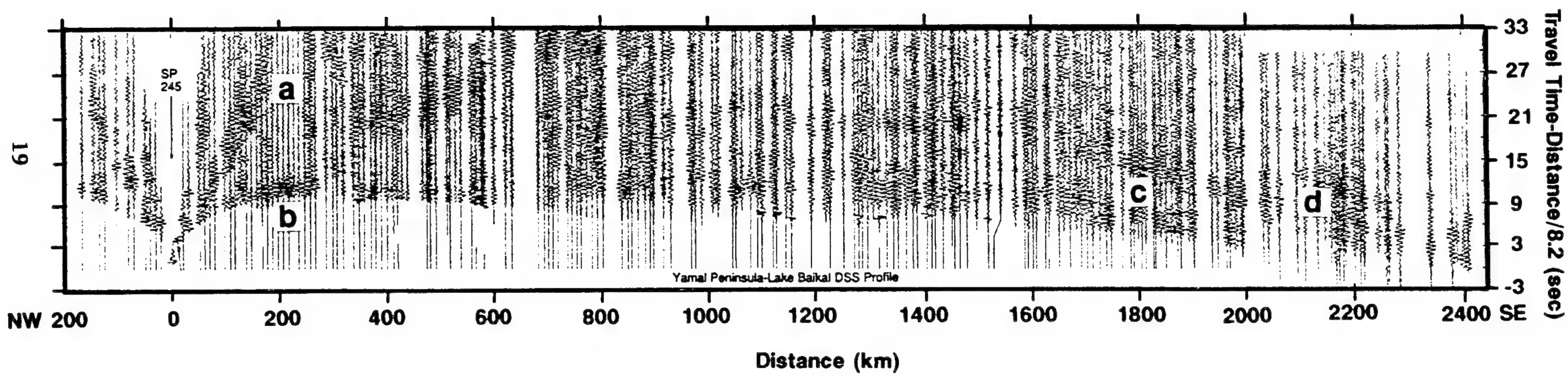
Travel Time-Distance/8.2 (sec)
33
27
21
15
9
3
-3
SP
245
a
b
c
d
Yamal Peninsula-Lake Baikal DSS Profile
NW 200
0
200
400
600
800
1000
1200
1400
1600
1800
2000
2200
2400 SE
Distance (km)

FIGURE 3

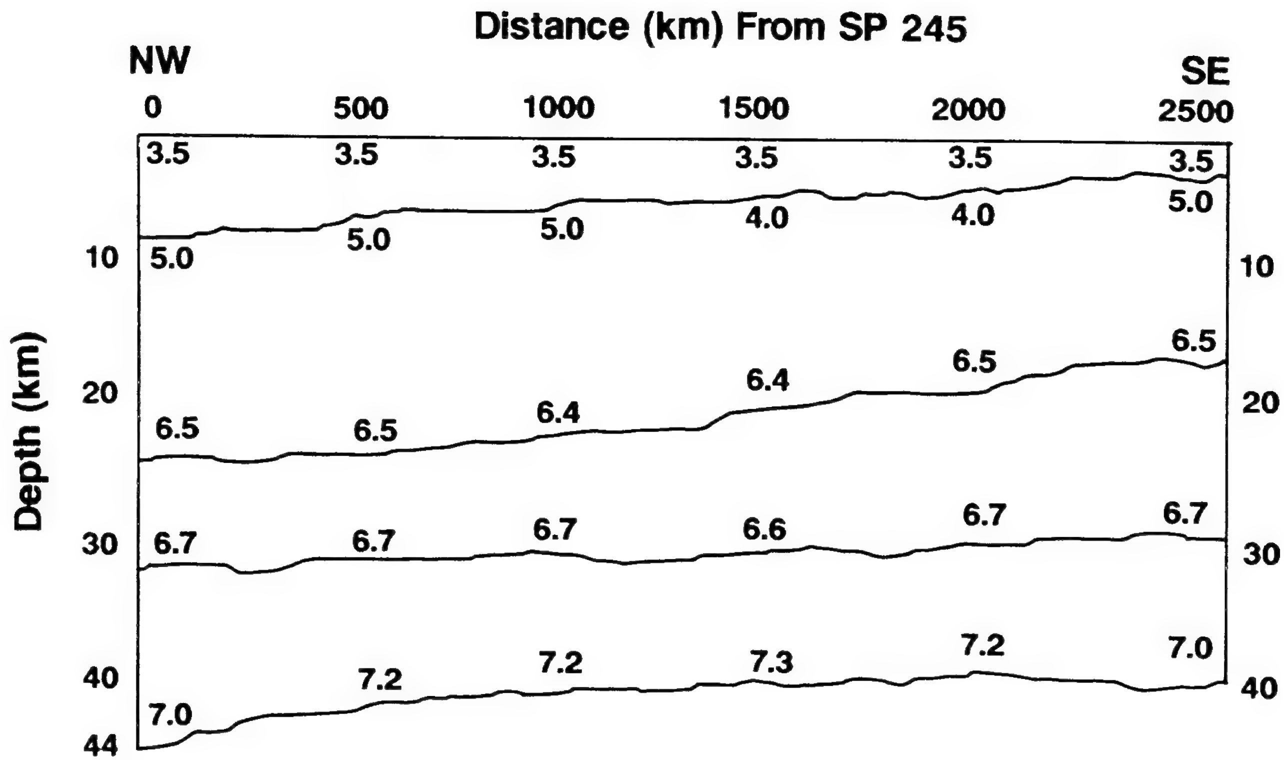

Distance (km) From SP 245
NW
SE
0
500
1000
1500
2000
2500
Depth (km)
10
20
30
40
44
3.5
5.0
4.0
6.5
6.4
6.7
6.6
7.0
7.2
7.3

FIGURE 4

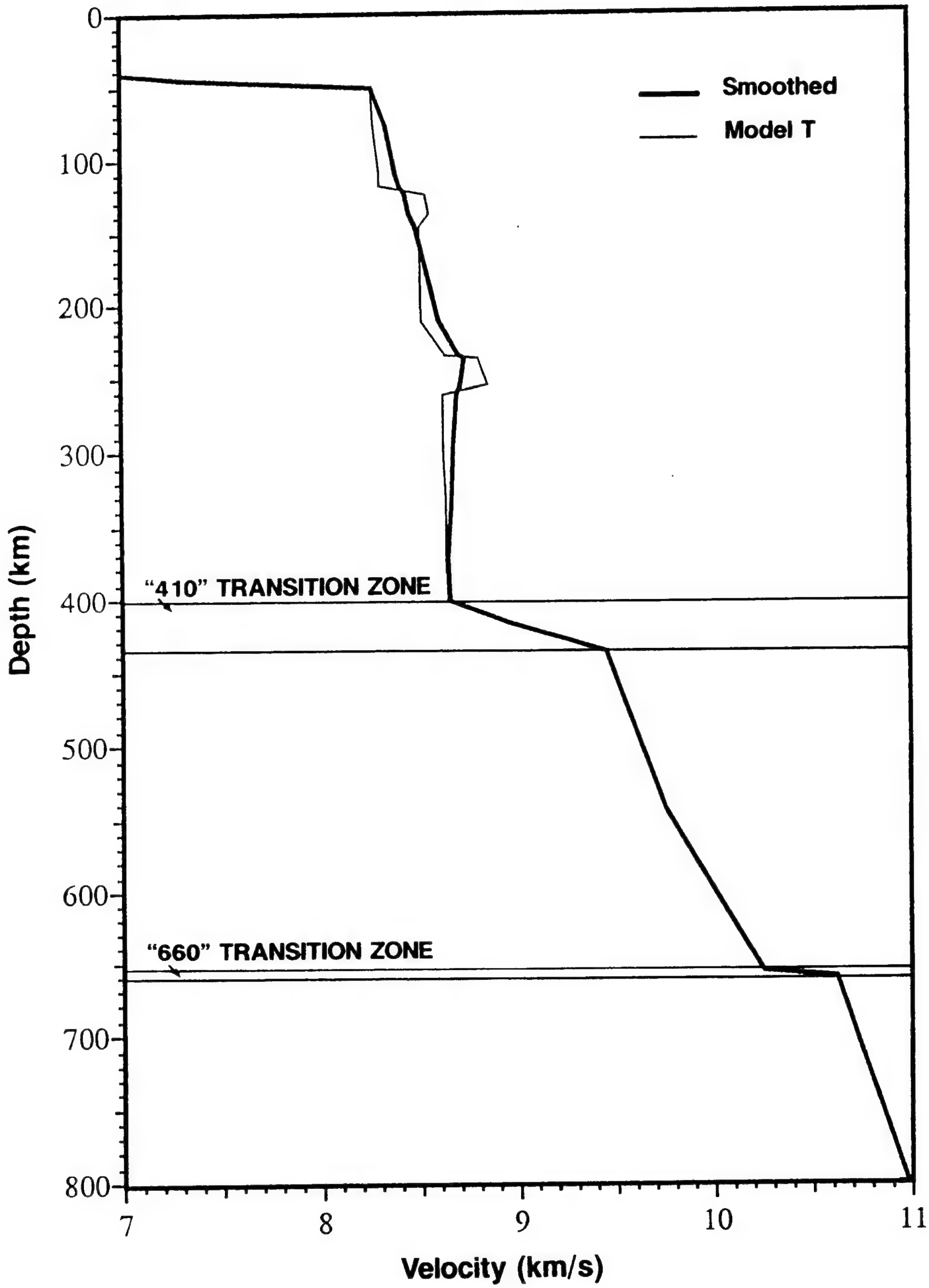

Smoothed
Model T
"410" TRANSITION ZONE
"660" TRANSITION ZONE
Depth (km)
Velocity (km/s)
0
100
200
300
400
500
600
700
800
7
8
9
10
11

FIGURE 5

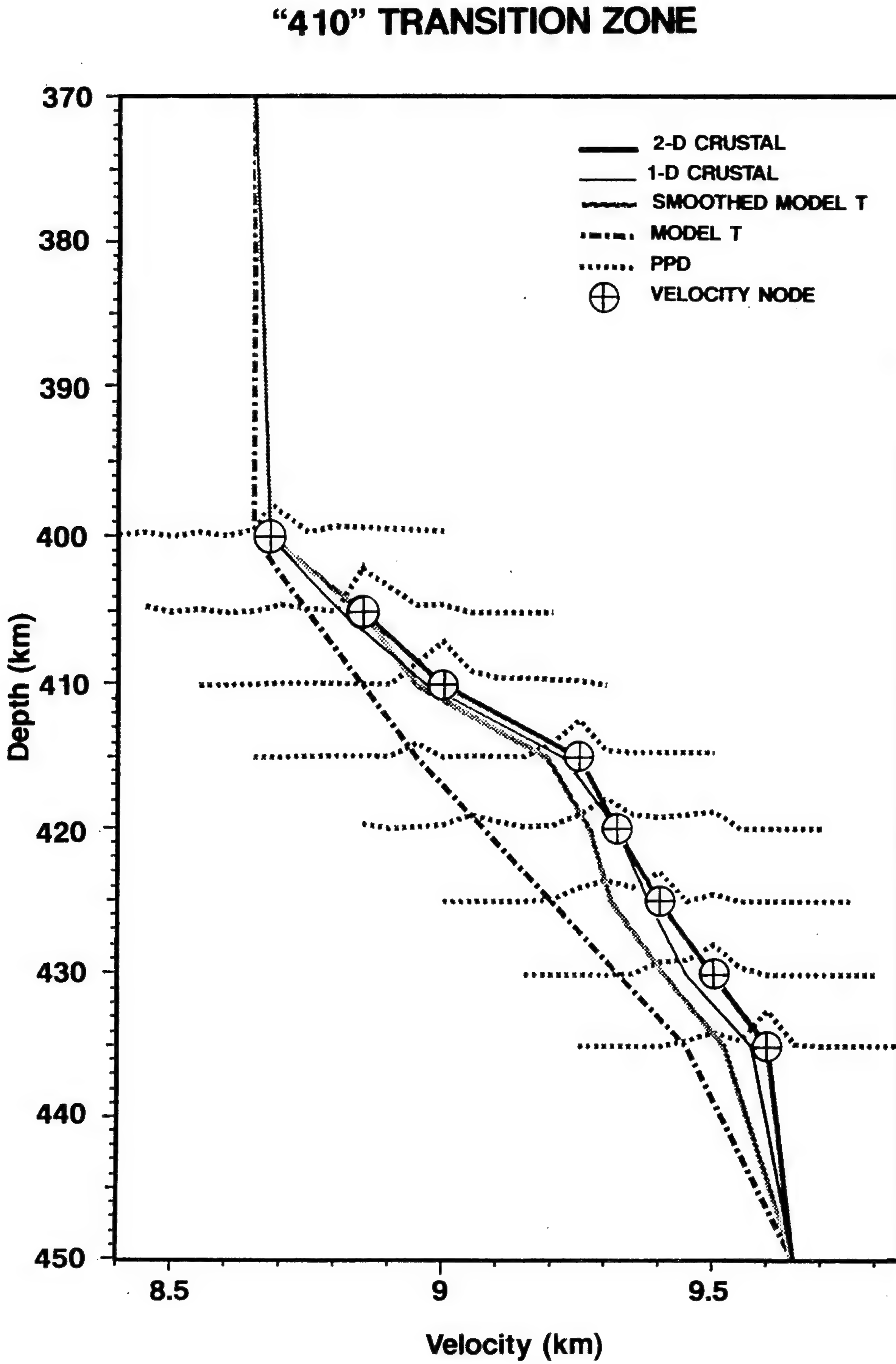

"410" TRANSITION ZONE
370
380
390
400
410
420
430
440
450
Depth (km)
2-D CRUSTAL
1-D CRUSTAL
SMOOTHED MODEL T
MODEL T
PPD
VELOCITY NODE
8.5
9
9.5
Velocity (km)

FIGURE 6a

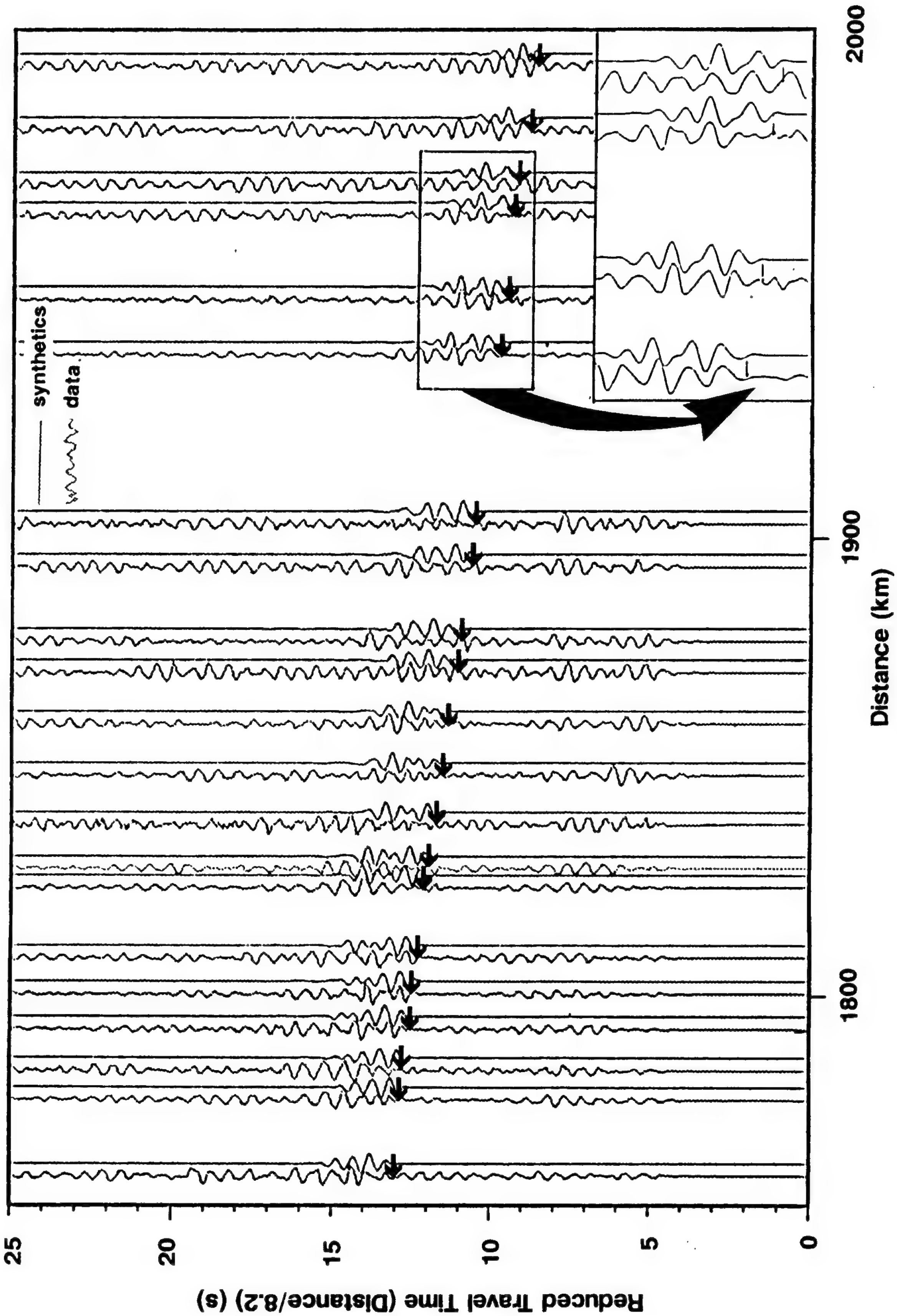
synthetics
data
25
20
15
10
5
0
Reduced Travel Time (Distance/8.2) (s)
1800
1900
2000
Distance (km)

FIGURE 6b

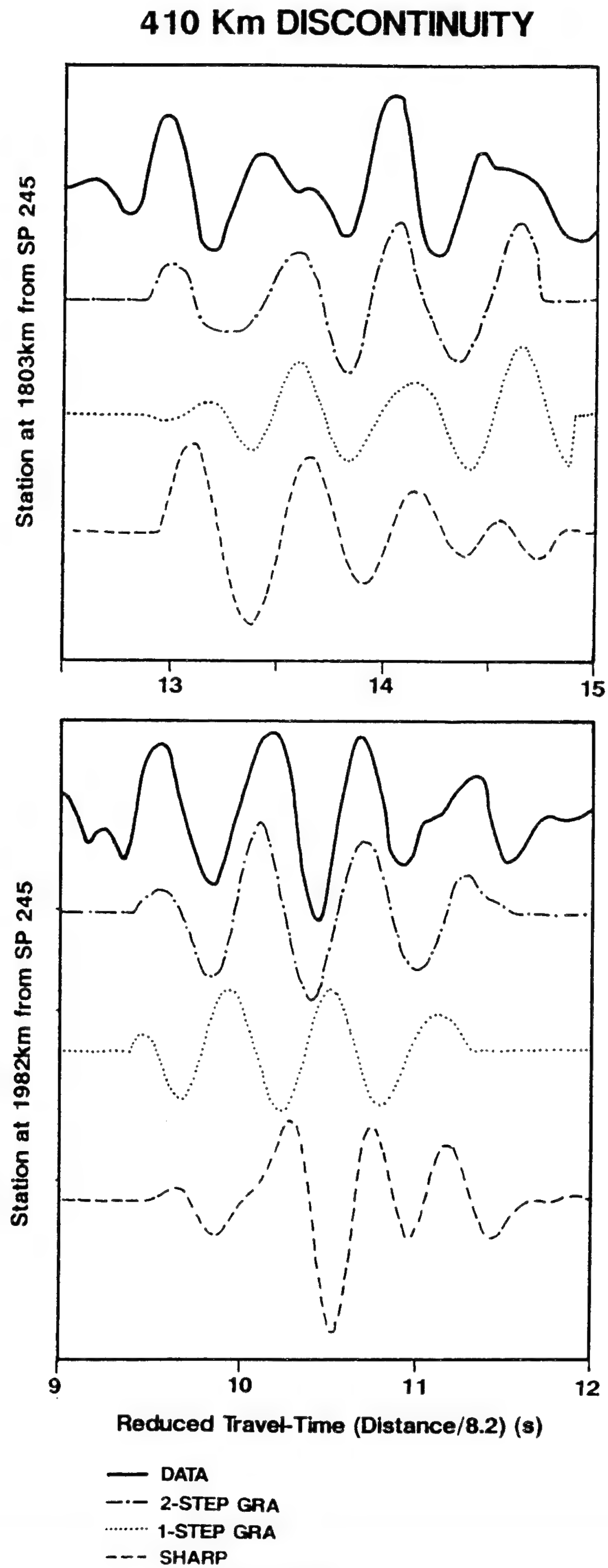
410 Km DISCONTINUITY
Station at 1803km from SP 245
13
14
15
Station at 1982km from SP 245
9
10
11
12
Reduced Travel-Time (Distance/8.2) (s)
DATA
2-STEP GRA
1-STEP GRA
SHARP

FIGURE 6c

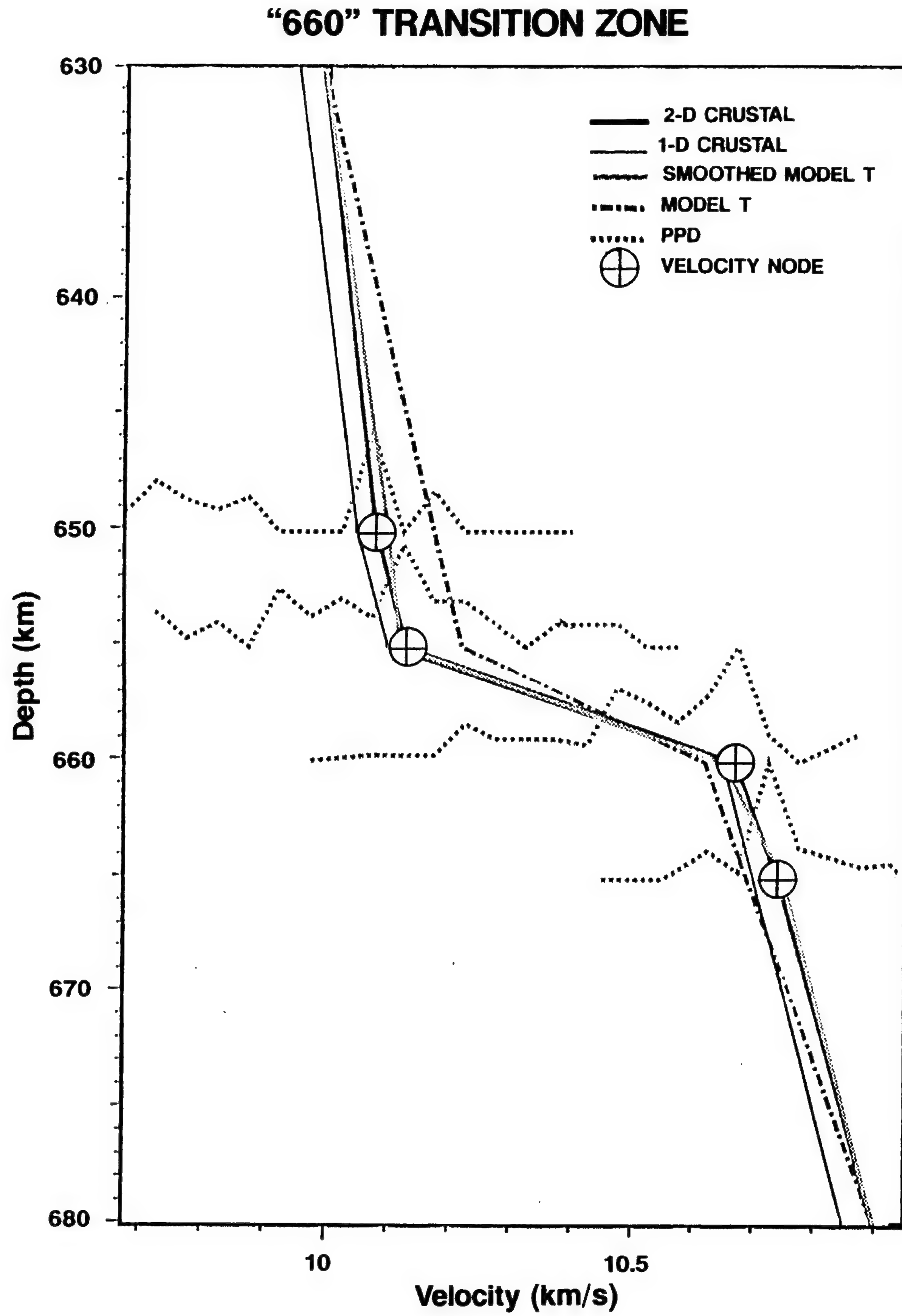
"660" TRANSITION ZONE
2-D CRUSTAL
1-D CRUSTAL
SMOOTHED MODEL T
MODEL T
PPD
VELOCITY NODE
630
640
650
660
670
680
Depth (km)
10
10.5
Velocity (km/s)

FIGURE 7a

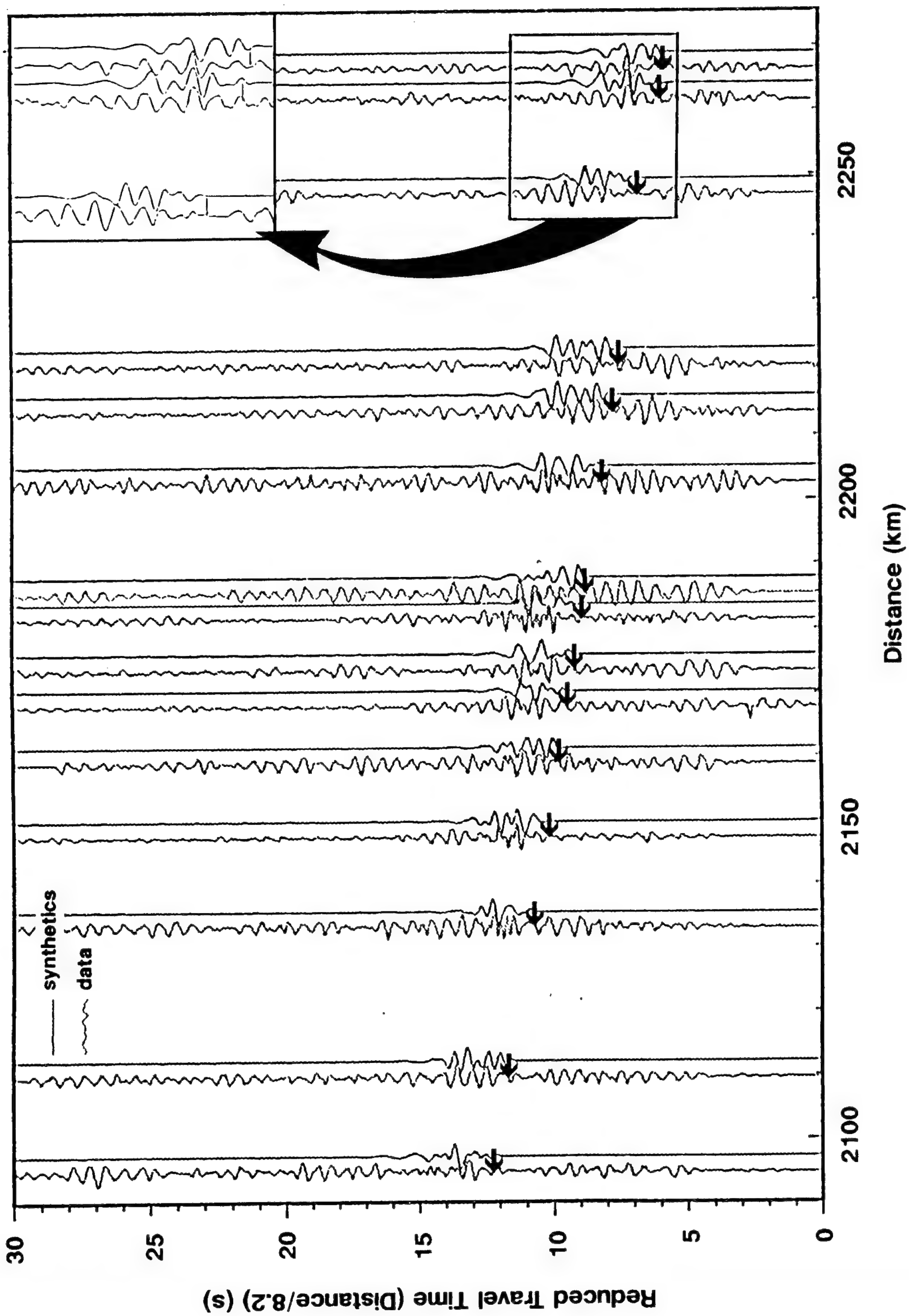
synthetics
data
Distance (km)
2100
2150
2200
2250
Reduced Travel Time (Distance/8.2) (s)
30
25
20
15
10
5
0

FIGURE 7b

Velocity Structure in the Region of the South Caspian Basin from Teleseismic Receiver Function Modeling

Stephen Mangino and Keith Priestley

Bullard Laboratories, Madingley Rise, Madingley Road, Cambridge CB3 0EZ, UK

SUMMARY

The crust and upper mantle structure of the south Caspian Basin and the Turkmenian Lowlands is enigmatic. From Soviet deep seismic sounding data collected in the 1960s, the crust appears to consist of two layers: a thick sedimentary section (15–25 km) with a low P–wave velocity (3.5–4.0 km/s) overlying a 12–18 km thick basaltic lower crust. It has been suggested that this basaltic lower crust is "oceanic–like" crust and that the south Caspian Basin represents a section of relic ocean from a Paleozoic – Triassic ocean or a Mesozoic – Paleogene marginal sea. Improved knowledge of the crust and upper mantle velocity structure of the south Caspian Basin is important in a seismic verification context because of the anomalous effect it has on regional seismic waveforms. To investigate the crust and upper mantle structure of the south Caspian Basin, we have installed six three–component seismograph stations within the former Soviet Republics of Turkmenia and Azerbaijan. Our objective is to determine the velocity structure of this region using both body wave receiver function and surface wave modeling techniques. We present receiver function inversion results for four sites and fundamental mode Rayleigh wave observations for two great circle paths across this region.

Key Words: South Caspian Basin, crust and upper mantle structure, receiver functions, surface wave dispersion

INTRODUCTION

The south Caspian Basin and the Turkmenian Lowlands form an anomalous aseismic depression that is bounded to the north by the Apsheron–Balkhan Sill, a narrow seismogenic zone extending from the Caucasus Mountains in Azerbaijan to the Kopet Dagh Mountains of Turkmenia; and to the west in Azerbaijan and to the south along the Iranian border by the

active fold and thrust belts of the Talesh and Alborz Mountains, respectively. The northward movement of the Iranian plate with respect to the Eurasian plate is causing compressional deformation throughout the Caspian region (Jackson and McKenzie, 1984). Mechanisms of earthquakes occurring within the bounding seismic belts of the south Caspian Basin suggest that the crust of the south Caspian Basin is being overriden by the continental crust of the Iranian plateau in the south, and to a lesser extent, by the northern Caspian continental crust (Priestley et al, 1994).

The crust and upper mantle velocity structure of the south Caspian Basin is poorly known. Deep seismic sounding data collected in the early 1960s suggest that the crust of the south Caspian Basin and west Turkmenian Lowlands consists of two layers: a thick sedimentary layer (15–20 km) with a P–wave velocity of 3.5–4.0 km/s which overlies a 12–18 km thick "basaltic" layer with a P–wave velocity of 6.6–7.0 km/s (Neprochnov 1968; Rezanov and Chamo, 1969). It has been suggested that the south Caspian Basin represents a section of "ocean–like" crust that may be either a relic of an older Paleozoic–Triassic ocean or a marginal sea which developed behind a Mesozoic–Paleogene ocean (Berberian and King 1981; Berberian 1983). The south Caspian Basin strongly affects the propagation of regional seismic waves. For example, the seismic phase Lg is blocked for paths crossing the south Caspian Basin (Kadinsky–Cade et al, 1981). This has important ramifications for seismic monitoring in the Middle East.

To develop better velocity models for the crust and upper mantle for the south Caspian Basin and the surrounding region, we have installed and operated a network of digital three–component seismic stations in Turkmenia and Azerbaijan. In this report we present our preliminary results from the analysis of teleseismic P–wave: (1) travel time residuals, (2) P–wave azimuthal anomalies, and (3) velocity models of the crust and upper mantle from the analysis of receiver functions. We also discuss observations of fundamental mode Rayleigh waves for two great circle paths across this region.

THE CASPIAN SEISMOGRAPH NETWORK

To better understand the crust and upper mantle structure in the south Caspian region and its effect on regional seismic wave propagation, we have installed a network of three–

component broadband digital seismographs around the south Caspian Sea in Turkmenia and Azerbaijan (Fig. 1). Not all stations have operated simultaneously. Five stations (BAK, KAT, KRV, LNK, and NBD) were installed in June, 1993. DTA was installed in December, 1993. BAK was found to be extremely noisy and was moved to SHE in June 1994. The highly unstable political climate in Azerbaijan due to war with Armenia coupled with the nearby fighting in Groznyy forced us to remove stations LNK and SHE in February, 1995. In June 1995 a new station was installed at KAR using the instruments previously deployed at LNK. Also shown in Figure 1 is the station ABKT which was installed in May, 1993 by the Incorporated Research Institutions for Seismology (IRIS).

Each of the Caspian Seismograph Network stations we operate consists of Refraction Technology 72a–02 16–bit data loggers with external hard disk drives and either Omega or GPS time code receivers. Stations DTA, KAR, KAT, KRV, and LNK have Guralp CMG–3T three–component broadband seismometers and stations BAK, NBD, and SHE have three–component Teledyne Geotech SL210/220 long period (15 sec free period) seismometers. Each seismograph was installed at a permanent seismograph site of either the Turkmenian Academy of Sciences or "Geoseism" (the equivalent Azerbaijan organization). The stations are permanently occupied by a station–keeper and family, which therefore contribute to the amount of noise generated at each site. All seismometers are installed on cement piers within vaults that are located either within a sub–basement or within a surface vault adjacent to the station keeper's house. To correct for seismometer drift we designed and installed a clock activated re–centering unit for each of the CMG–3T seismometers. This device issues a centering command to the CMG–3T at weekly intervals. The LP seismometers are manually re–centered by the station keeper. All stations record data continuously at 10 samples/sec. In addition, some stations have had a triggered data stream at 50 samples/sec. Every two months each stations' data is transferred from disk to either Exabyte or DAT tape and returned to the SYNAPSE Moscow Data Center (MDC). At the MDC an inspection of data quality is conducted and duplicate copies are made. The raw data files are then sent to the University of Cambridge, arriving between 5–8 months after initial collection. The IRIS station ABKT is equipped with Streckeisen STS–1 seismometers, a 24–bit Quantera digitizer, and a GPS clock. Data for ABKT is obtained from the IRIS Data Management Center in Seattle, Washington.

Parameters for each of these stations is given in Table 1.

We calibrate each station with a step function during each visit. More complete calibrations using a pseudo–random binary input and a sinusodial input are made on an annual basis. Analysis of the step calibrations indicate that the sensor characteristics have not deviated significantly during the deployment. Figure 2 shows the frequency response curves for the CMG–3T, the SL210/220, and STS–1 seismometers.

A catalogue of the recorded events recorded is given in Appendix 1.

TELESEISMIC BODY WAVEFORM MODELING

To determine the velocity structure of the crust and upper mantle beneath the seismographs shown in Figure 1 we model the teleseismic P–waveform using receiver function analysis (Owens et al, 1984). However, before we apply the receiver function method we use other information contained within teleseismic P–wave to determine more gross properties of the crust and upper mantle structure beneath each site. We first determine P–wave travel time residuals for the stations in the immediate vicinity of the south Caspian Basin relative to IASP91 and station ABKT. We then estimate the affects of scattering by examining P–wave azimuth anomalies. Finally, we model the P–waveforms using the receiver function technique.

P-wave Travel Time Residuals: To determine relative differences in crust and upper mantle structure in the south Caspian region we computed absolute P–wave travel time residuals with respect to the IASP91 earth model and relative travel time residuals of the south Caspian Basin stations compared to station ABKT. The relative residual is defined as

$$\mathrm{T_{resid}} = \left[\mathrm{T_{CSN}} - \mathrm{T_{IASP91(CSN)}}\right] - \left[\mathrm{T_{ABKT}} - \mathrm{T_{IASP91(ABKT)}}\right]$$

where T_{CSN} is the arrival time at the CSN station, T_{IASP91} is the predicted arrival time for the IASP91 model, and T_{ABKT} is the observed arrival time at ABKT.

The observed residuals are plotted for each of the sites in Figures 3–5 and summarized in Table 2 and 3. Arrivals at all stations are late with respect to those predicted by the IASP91 earth model. Stations NBD and KAT, both located in the Turkmenian Lowlands, show mean delays of 0.9 sec with respect to ABKT. These large delays are likely due to

the thick sedimentary section in the south Caspian Basin. The KRV residuals are negative with respect to ABKT with a mean advance of -0.28 sec for events to the northeast and a mean advance of -0.70 sec for events to the southeast. The change of -0.5 sec occurs over a fairly narrow range at an azimuth of about N80°E. Negative residuals at KRV with respect to ABKT suggest either a faster mantle, a thinner crust, or a thinner sedimentary section beneath KRV compared to that beneath ABKT.

P–wave azimuthal anomalies: The frequency dependence of backazimuth anomalies and the polarization characteristics can be indicative of the level of scattering in the P–wavefield due to inhomogeneities in the crust and upper most mantle beneath the recording site. It is important to assess the level of scattering and its frequency dependence before attempting to extract information on the crust and upper mantle structure using the receiver function technique. We have measured the polarization using a technique discussed discussed in Kanasewich (1981) and implemented by Harris (1980). For this, the rectilinearity of the particle motion over a specified time window can be obtained from the ratio of the principal axes of the diagonalized covariance matrix from the three component time series. The degree of rectilinearity can be determined by comparing the relative magnitude of the two largest eigenvalues; and the direction of polarization can be determined by considering the components of the eigenvectors associated with the largest eigenvalue with respect to the coordinate directions (Fig. 6).

We use this procedure to examine the polarization of teleseismic P–waves in the 0.07–0.2 Hz and 0.3–2.0 Hz bands. Assuming an average crustal P–wave velocity of 6.4 km/s these bands correspond to wavelengths of about 96 to 32 km or crustal dimensions and about 21 to 3 km or subcrustal dimensions. Figure 7 shows an example of the measurement made on a teleseismic P–wave for the lower of these frequency bands, and the associated particle motion plots.

The results of the polarization analysis in the two frequency bands are shown in Figures 8–10 and summarized in Table 4. The results are complex however some conclusions can be drawn from these plots. With the exception of station KRV the differences between the low frequency observed and the theoretical backazimuths are small. However, the highpass backazimuth anomalies are large indicating significant scattering.

At ABKT the lowpass measurements are essentially on azimuth while a pattern is present at higher frequencies. Arrivals from teleseismic sources northeast of ABKT are deflected to the north while arrivals from the southeast are deflected to the south. The division between this frequency dependent scattering is roughly parallel to the trend of the Main Fault of the Kopet Dag Mountains. Although the bearing results at station DTA are sparse, this pattern is not present 200 km east of ABKT. At station KRV both the low and highpass bearings are inconsistent with the expected azimuth of arrival. The mean difference between the expected and observed azimuth of arrival is 17.5 degrees, counterclockwise about the station. These differences point to a mis–aligned seismometer. Stations NBD, KAT and LNK located within the Basin and all show significant scattering at higher frequencies while the lowpass bearings are variable.

Receiver Functions: We computed receiver function Caspian station we isolated the P to S converted phases in the 30 seconds following the P–wave arrival using the source equalization method (Langston, 1979; Ammon, 1991). Most of the source regions are along the Circum Pacific Seismogenic Zone, hence most of the receiver functions sample the lithosphere to the east of each station. Only the most stable deconvolutions (those with averaging functions that approximate a narrow band Gaussian pulse) are used to infer structure. Events from common source regions are then stacked and the variance of the stacked data is used as a measure of coherence of individual Ps arrivals. We examined the radial and tangential receiver functions as a function of azimuth and determined 1–D estimates of the receiver structure using the inversion method of Ammon et al. (1990).

Figure 11 presents the receiver function inversion results for the northeast backazimuth of CSN station KRV. The synthetic waveform fits are compared to the +/- 1 STD bounds obtained from the variance of the stacked data. Also shown are the stacked radial and tangential receiver functions and the range model space examined. We believe this range adequately covers most known rock types found in the earths crust. The KRV-NE radial receiver function is dominated by two Ps arrivals at 7s and 9.5s. These arrivals are well above the scattered wave field indicated by the amplitude of the tangential receiver function. Particle motion of these arrivals is consistent with P to S converted energy generated at a

near horizontal interface. Rotation of the KRV receiver functions by 17.5 degrees (the mean observed in the bearing analysis) yields a radial receiver function that does not significantly differ from the amplitude and phase of the unrotated data. The KRV-NE solution models indicate a 3-4 Km thick gradational shallow crust over a relatively constant upper crustal layer between 4-16 Km depth. A step in velocity of 1.5 Km/s is present between 16-18 Km. Beneath this step from 20 to 36 km depth the average P-wave velocity is between 6.5-7.0 km/s. From 36 to 46 km velocities range from 6.8-7.3 km/s. The crust-mantle boundary is gradational and velocities greater than 8 Km/s are first encountered at 52-54 Km depth.

Figure 12 presents a summary of the receiver function models obtained at the CSN stations and at station ABKT. Although these 1-D models represent only several data points across a complex region, some of the gross structural differences between the south Caspian Basin and adjacent Kopet Dag Mtns are clear. The models for stations KAT and LNK indicate the presence of a 10-12 km thick sedimentary layer in the upper crust. Both of these stations are located in the southern portion of the south Caspian Basin. The thickness of this layer is consistent with but less than the previously reported sedimentary thickness of 15-25 Km. It is important to note that our stations are located along the perimeter of the Basin and the previous DSS estimates are for the center of the Basin. Beneath the sedimentary layer at station LNK the mid-crustal velocities are high and are consistent with an ultra-mafic material, perhaps basalt, while at KAT a broad shallow low-velocity zone is present. The KRV-NE solutions and the ABKT-NE solutions both show a similar upper crustal velocity profile and include a step in velocity near 20 km depth. The crust-mantle boundary is gradational for all models and and occurs between 50-55 Km depth around the perimeter of the Basin and between 44-46 km depth beneath station ABKT. We are currently examining 1-D velocity estimates of the crust and upper mantle to depths approaching 150 km.

SURFACE WAVE OBSERVATIONS

The study of Kadinsky–Cade et al. (1981) demonstrated that the seismic phase Lg is largely blocked for paths crossing the south Caspian Basin and this is also apparent in the data we have collected in the region immediately surrounding the Caspian. However, Figure

13 shows that the south Caspian Basin also severely disrupts low frequency fundamental mode surface wave trains. Figure 13a compares long period seismograms for a mid–Atlantic ridge earthquake propagating along a great circle path between LNK and KAT. The LNK seismogram shows a dispersed fundamental mode wave train ($\sim$ 2400–3000 seconds) followed by scattered surface wave arrivals. The lowest frequency fundamental mode surface wave arrival seen in the LNK seismogram is clear in the KAT seismogram ($\sim$2600–2700 seconds) but the dispersed wave train observed at LNK is largely missing from the KAT seismogram and the overall surface wave amplitude has decreased significantly. Figure 13b compares seismograms for a north Mulucca Sea earthquake propagating along a great circle path between KAT and LNK, i.e., reversing the path of the event in Figure 13a. These seismograms exhibit the same degradation of the surface wave train and show that this is not, for example, an instrumental effect. We have observed this phenomenon for all events propagating along great circle paths across the central portion of the south Caspian Basin.

Surface waves propagating along the KRV–KAT great circle path across the Turkmenian Lowlands do not show the same disruption (Fig. 14) as those propagating across the main part of the basin (Fig. 13). Russian earth scientists have suggested that this region is structurally part of the south Caspian Basin and that the crust in the region consists of 10–15 km of sediment lying on "ocean–like" crust. The deep thickness of sediments is verified from well logs (Sengor, personal communications, 1995). The two upper seismograms in Figure 14a show one of four great circle path Rayleigh wave pairs recorded at stations KRV and KAT that are used to determine the dispersion curve. The comparison of the two wave trains in the lower part of the upper plot shows the match of the original KAT Rayleigh wave with the KRV Rayleigh wave after being filtered with the dispersion transfer function.

Figure 14b shows the fundamental mode Rayleigh wave phase velocity dispersion curve for this path. This curve was computed from four seismogram pairs using a constrained least–squares algorithm (Gomberg et al, 1988). The KRV–KAT phase velocity curve is compared with observed dispersion curves for several other possibly analogous regions; an ocean basin structure (Kuo et al, 1962), a continental tectonic structure (Knopoff et al, 1966), and the Bay of Bengal [curves A to D] (Brune and Singh, 1986). The main difference between curves A to D is due to an increase of sedimentary layer thickness from south to north in the Bay

of Bengal as one gets closer to the mouth of the Ganges River. The dispersion curve for the western Turkmenian Lowlands is most similar to curve "D" for the Bay of Bengal observed by Brune and Singh (1986). They suggest that a thick sedimentary section introduces a blanketing effect which results in an increase in temperature causing in the serpentinization of oceanic crust into a more "continental–like" crust. A similar blanketing process might be affecting the crust in the south Caspian Basin.

DISCUSSION AND CONCLUSIONS

This study has shown that the south Caspian has an anomalous crustal structure which has a pronounced effect on not only higher frequency regional seismic waveforms but also on lower frequency surface waves. The velocity structures from body wave modeling provide some insight into the effects of crustal structure on regional seismic waves propagating across the south Caspian Basin. It is clear from the Caspian data that both longer and shorter period surface wave trains are greatly scattered or attenuated for travel paths across the Caspian Sea, and to a lesser degree for paths across the Turkmenian Lowlands. The Lg phase is blocked for travel paths across the oceanic crust as well as in regions where the crustal structure includes rapid changes in thickness. If we consider the Lg phase to consist of multiple reflected S waves trapped within the crustal wave guide, then the receiver function modeling results suggest that the blockage is due to the abrupt change in crustal structure from a relatively simple model beneath ABKT to complex models beneath KAT and LNK. Although these are 1–D models and the basin is a 3–D structure, these observations support a scattering mechanism. Recent analysis of the logarithmic rms amplitude ratio of Sn/Lg (Zhang and Lay 1994) has shown that this ratio can be linearly related to changes in surface topography. The southern margins of the Basin and the eastern margin of the Turkmenian Lowlands range from below sea level at LNK up to 2 km in the Alborz Mountains. These features probably contribute to the Lg blockage, but these effects have not yet been examined.

Acknowledgements: Installation and the first year and a half of station operation in the Caspian was funded by the Phillips Laboratory. Operation of the stations in the second and third years was funded by USAF EOARD and INTAS grants. Station installation and main-

tenance in the Caspian region was made possible by the support of Drs. M. Roshkov and V. Kiseleivich, SYNAPSE Moscow Data Center; Drs. T Ashirov and B. Karryev, Institute of Seismology of Turkmenia; and Drs. A. Gasanov and S. Agamirzoev of the Geophysical Expedition of Azerbaijan. Throughout network operations indispensable technical support and software was obtained from the Program of Array Seismic Studies of the Continental Lithosphere (PASSCAL) Instrument Center at Lamont–Doherty Geological Observatory (LDGO) and from Refraction Technology.

References

Ammon, C. J., The isolation of receiver effects from teleseismic P waveforms, *Bull. Seism . Soc. Am.*, **81**, 2504–2510, 1991.

Ammon, C. J., G. E. Randall and G. Zandt, On the resolution and non–uniqueness of receiver function inversions, *J. Geophys. Res.*, **95**, 15303–15318, 1990.

Berberian, M., The southern Caspian: A compressional depression floored by trapped, modified oceanic crust, *Can. J. Earth Sci.*, **20**, 163–183, 1983.

Berberian, M. and G. C. P. King, Towards a paleogeography and tectonic evolution of Iran, *Can. J. Earth Sci.*, **18**, 210–265, 1981.

Gomberg, J.S., K.F. Priestley, T.G. Masters, and J.N. Brune, The structure of the crust and upper mantle of northern Mexico, *Geophys. J.*, **94**, 1–20.

Harris, D.B., Comparison of the direction estimation performance of high–frequency seismic arrays and three–component stations, *Bull. Seis. Soc. Am., 80*, 1951–1968, 1990.

Jackson, J. A., and D. McKenzie, Active tectonics of the Alpine–Himalayan Belt between western Turkey and Pakistan, *Geophys. J. R. Astr. Soc.*, **77**, 185–264, 1984.

Kadinsky–Cade, K., M. Barazangi, J. Oliver, and B. Isacks, Lateral variations of high–frequency seismic wave propagation at regional distances across the Turkish and Iranian Plateaus, *J. Geophys. Res.*, **86**, 9377–9369, 1981.

Knopoff, L., S. Mueller, and W.L. Pilant, Structure of the crust and upper mantle in the Alps

from the phase velocity of Rayleigh waves, *Bull. Seis. Soc. Am.*, *56*, 1009–1044, 1966.

Kuo, J., J. Brune, and M. Major, Rayleigh wave dispersion in the Pacific Ocean for the period range 20 to 140 seconds, *Bull. Seis. Soc. Am.*, *52*, 338–357, 1962.

Langston, C. A., Structure under Mount Rainier, Washington inferred from teleseismic body waves, *J. Geophys. Res.*, **84**, 4749–4762, 1979.

Neprochnov, Y. P., Structure of the earth's crust of epi–continental seas: Caspian, Black, and Mediterranean, *Can. J. Earth Sci.*, **5**, 1037–1043, 1968.

Park, J., F. Vernon and C. R. Lindberg, Frequency dependent polarization analysis of high–frequency seismograms, *J. Geophys. Res.*, **92**, 12,664–12,674, 1987.

Priestley, K., C. Baker and J. Jackson, Implications of earthquake focal mechanism data for the active tectonics of the south Caspian Basin and surrounding regions, *Geophys. J. Int.*, **118**, 111–141, 1994.

Rezanov, I. A. and S. S. Chamo, Reasons for absence of a granitic layer in basins of the South Caspian and Black Sea type, *Can. J. Earth Sci.*, **6**, 671–678, 1969.

Zhang, T., and T. Lay, Analysis of short period regional phase path effects associated with topography in Eurasia, *Bull. Seis. Soc. Am.*, *84*, 119–132, 1994.

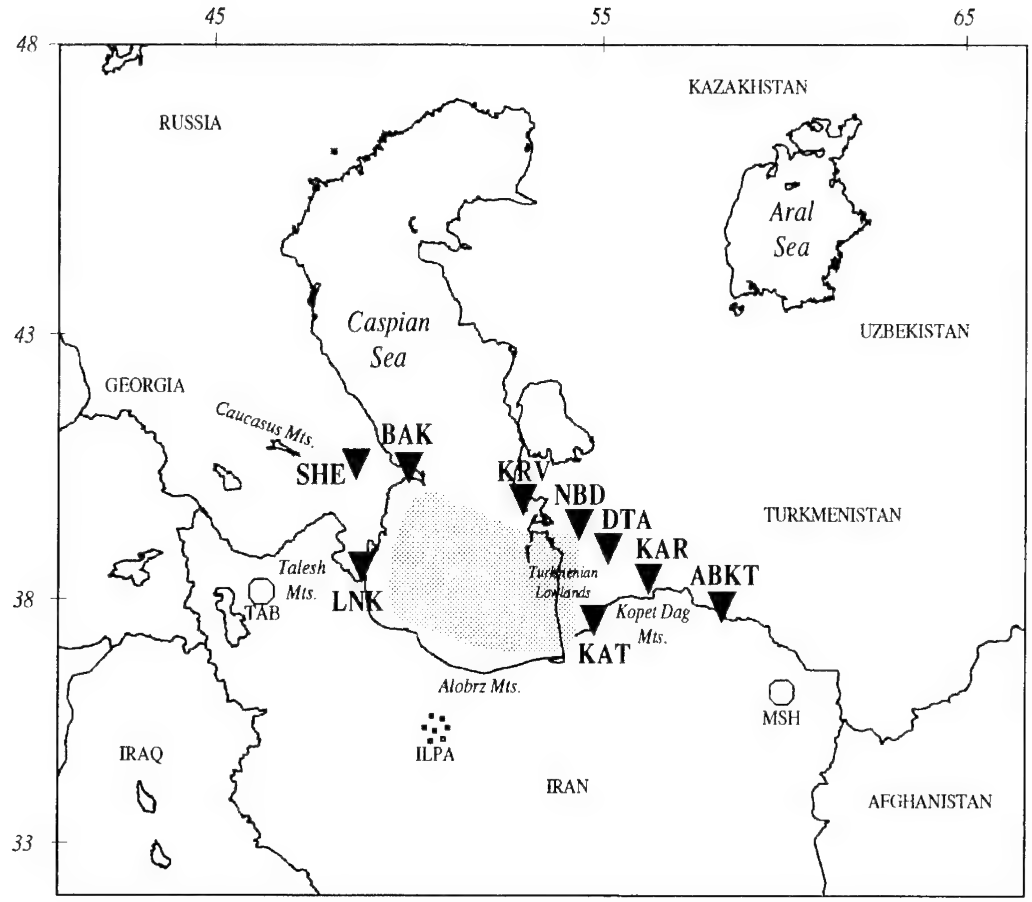

Figure 1. Map of the Caspian Sea and surrounding regions. Caspian Seismograph Network stations are located in Turkmenistan near Krasnovosdk (KRV), Nebit Dag (NBD), Kizyl Atrek (KAT), Dana Tag (DTA), Kala Kara (KAR), and in Azerbaijan near Lenkoran (LNK), Baku (BAK) and Shemaha (SHE). Also shown are WWSSN stations Tabriz (TAB) and Mashad (MSH), the Iranian Long Period Array (ILPA) and IRIS station Alibek (ABKT). The shaded region denotes the subsurface lateral extent of the suspected "oceanic" crust.

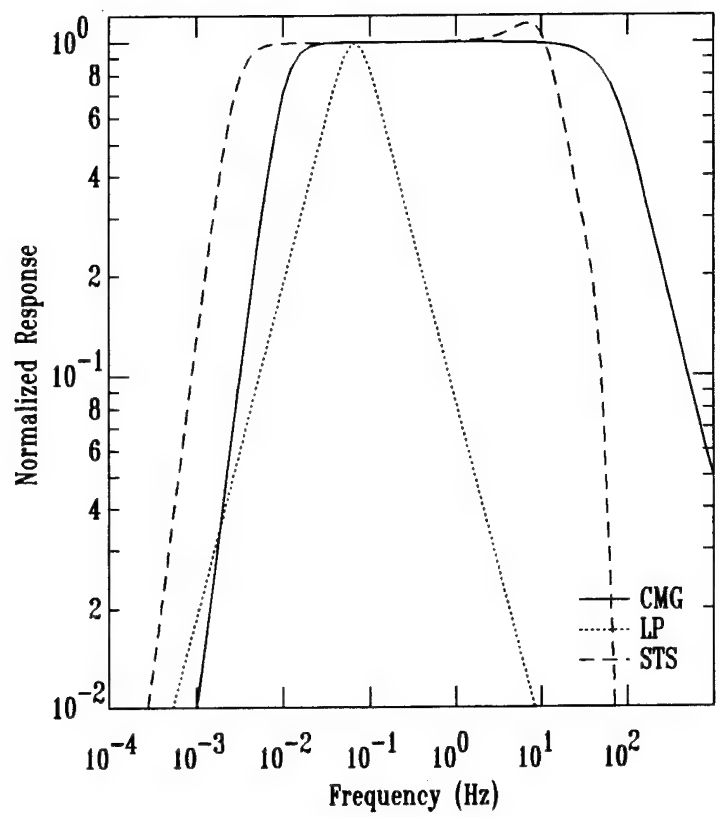

Figure 2. Instrument response characteristics for the CMG-3T, LP and STS-1 seismometers.

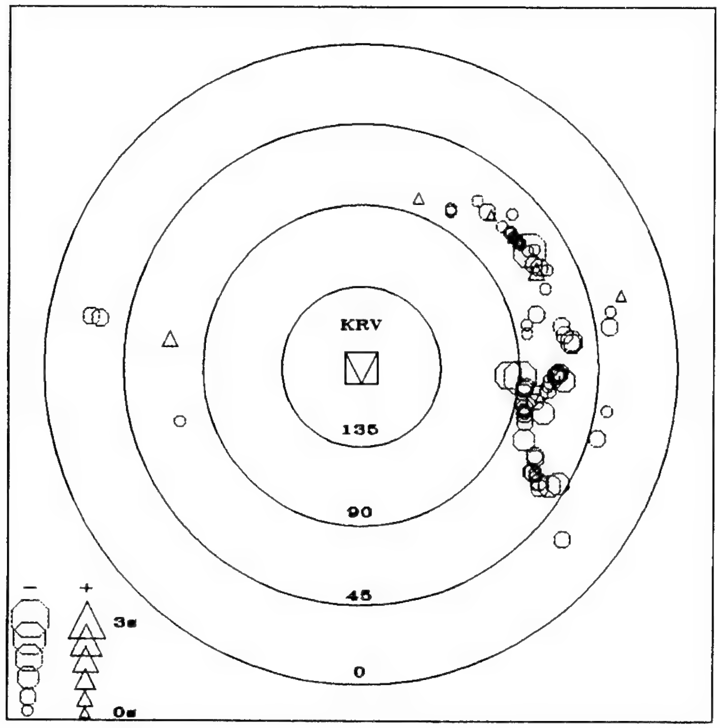

Figure 3. P-wave traveltime residuals for station KRV. Symbol size is scaled at 0.5s intervals, circles are fast and triangles are slow with respect to standard station ABKT. Concentric circles indicate epicentral distance in degrees and residuals are plotted as a function of azimuth.

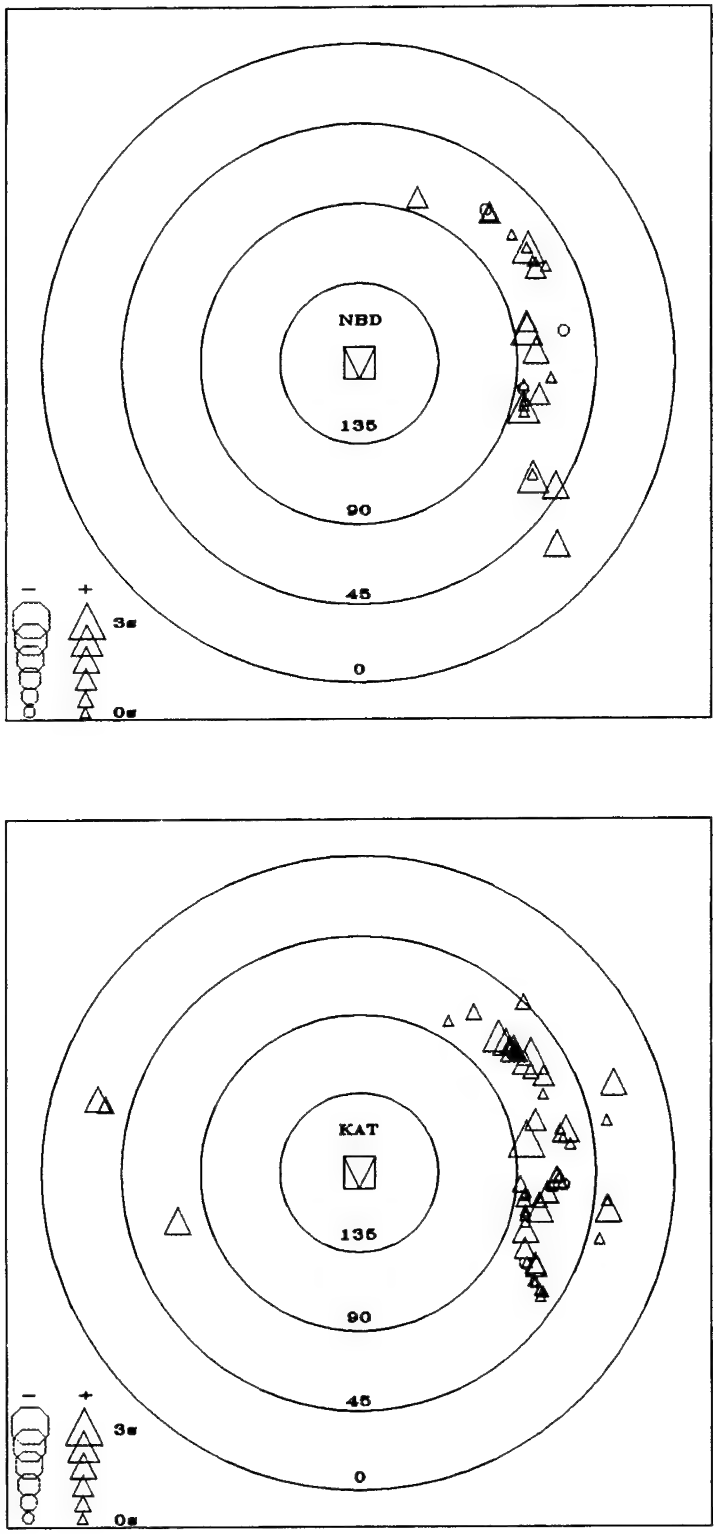

Figure 4. P-wave traveltime residuals for stations NBD (top) and KAT (bottom) relative to ABKT. Format is the same as in Figure 3.

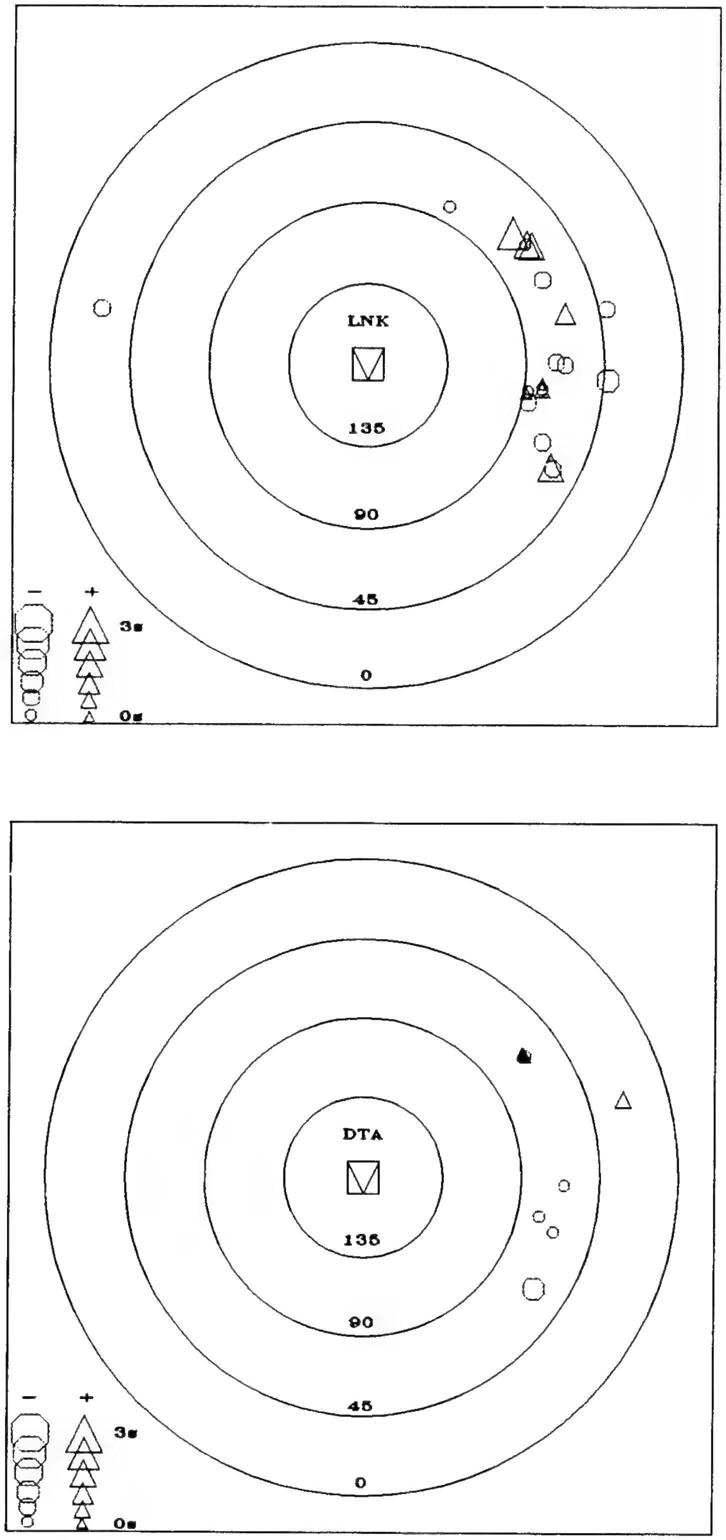

Figure 5. P-wave traveltime residuals for stations LNK (top) and DTA (bottom) relative to ABKT. Format is the same as in Figure 3.

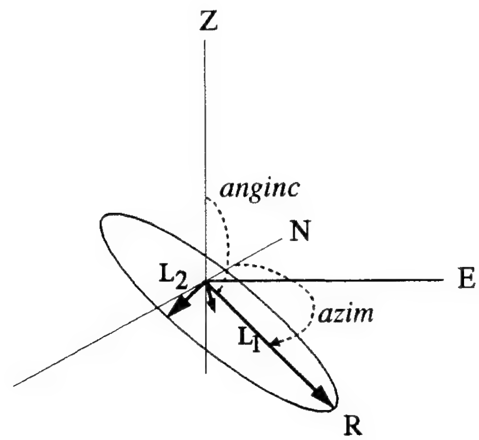

Figure 6. A perspective diagram of the three eigenvectors associated with the covariance matrix for a P-wave. The largest eigenvector extends through the center of the ellipse drawn above in 2 dimensions and defines the radial (R) direction.

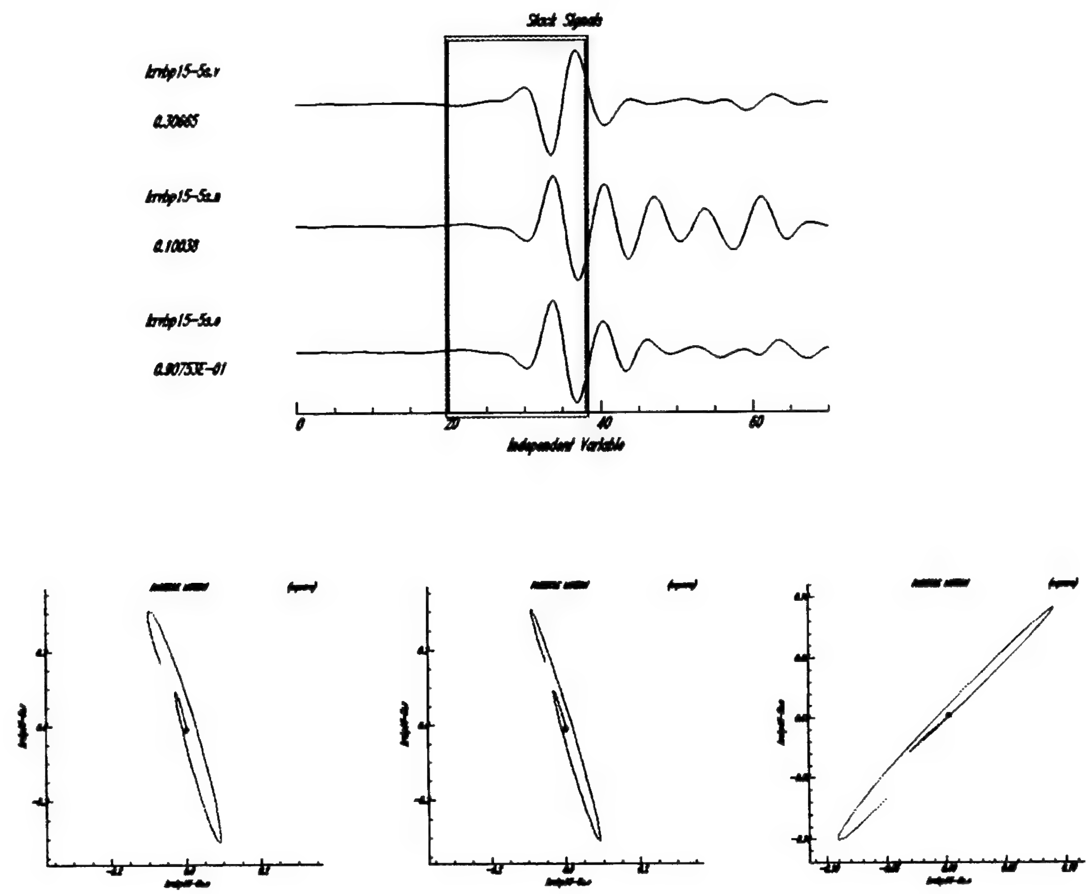

Figure 7. Sample P-wave polarization analysis window (top) and corresponding particle motion in the three orthogonal planes between the source and receiver.

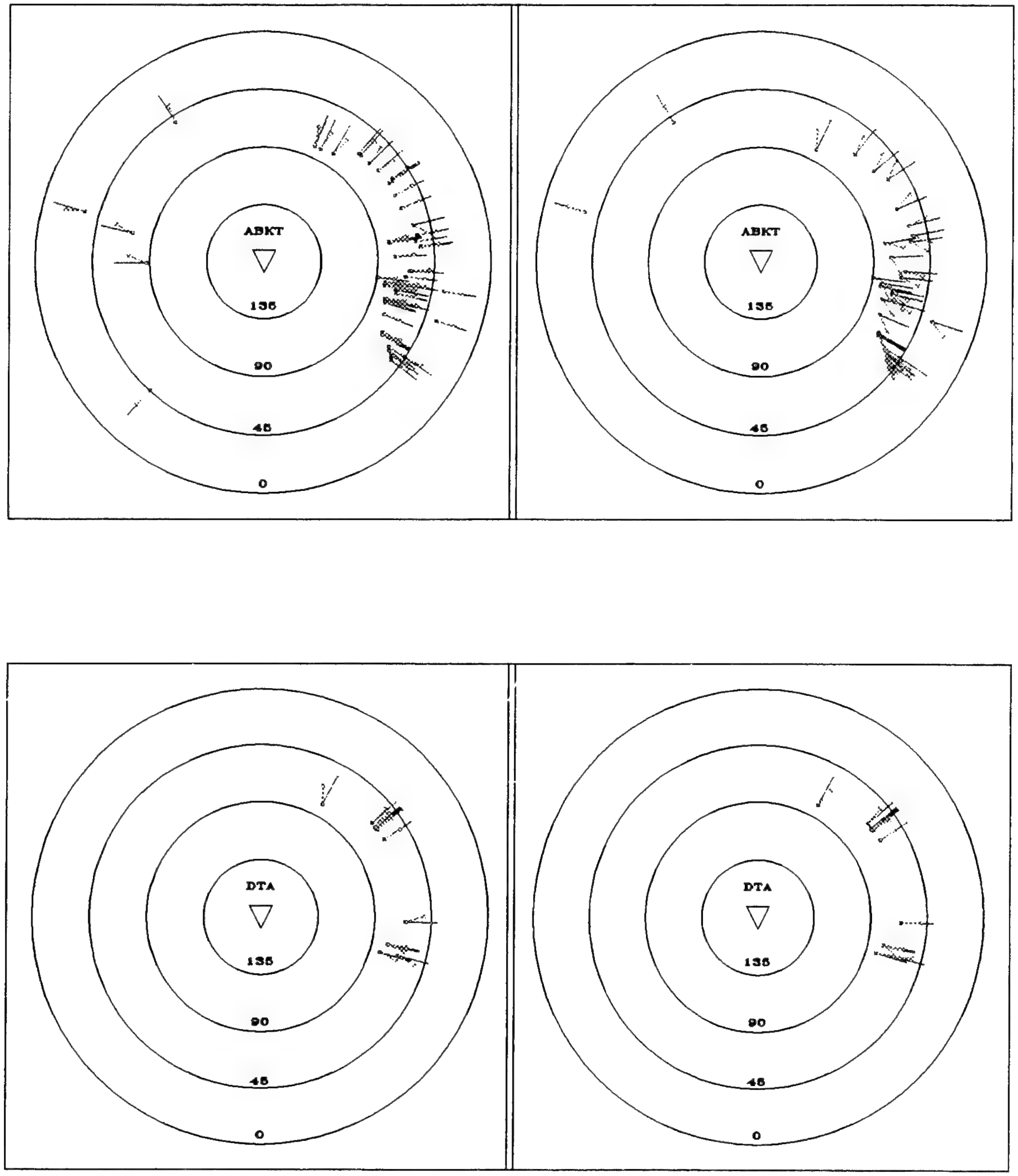

Figure 8. Stations ABKT (top) and DTA (bottom) expected (solid line) compared to the observed P-wave bearing (dashed line) for the lowpass 15s to 5s (left) and highpass 3s-2Hz filtered data (right). Concentric circles indicate epicentral distance from the station.

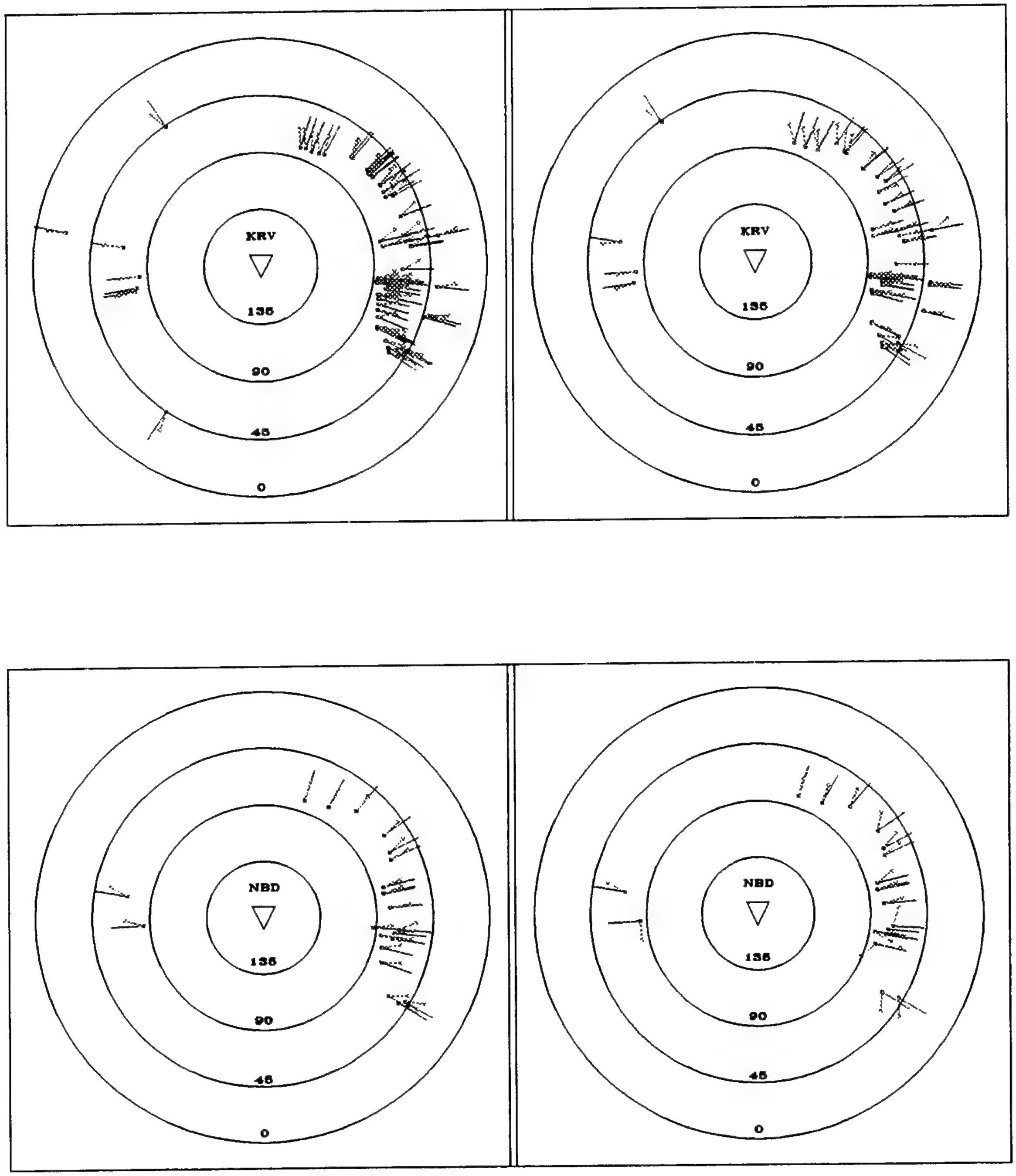

Figure 9. Stations KRV (top) and NBD (bottom) expected compared to the observed P-wave bearing . Format is the same as in Figure 8.

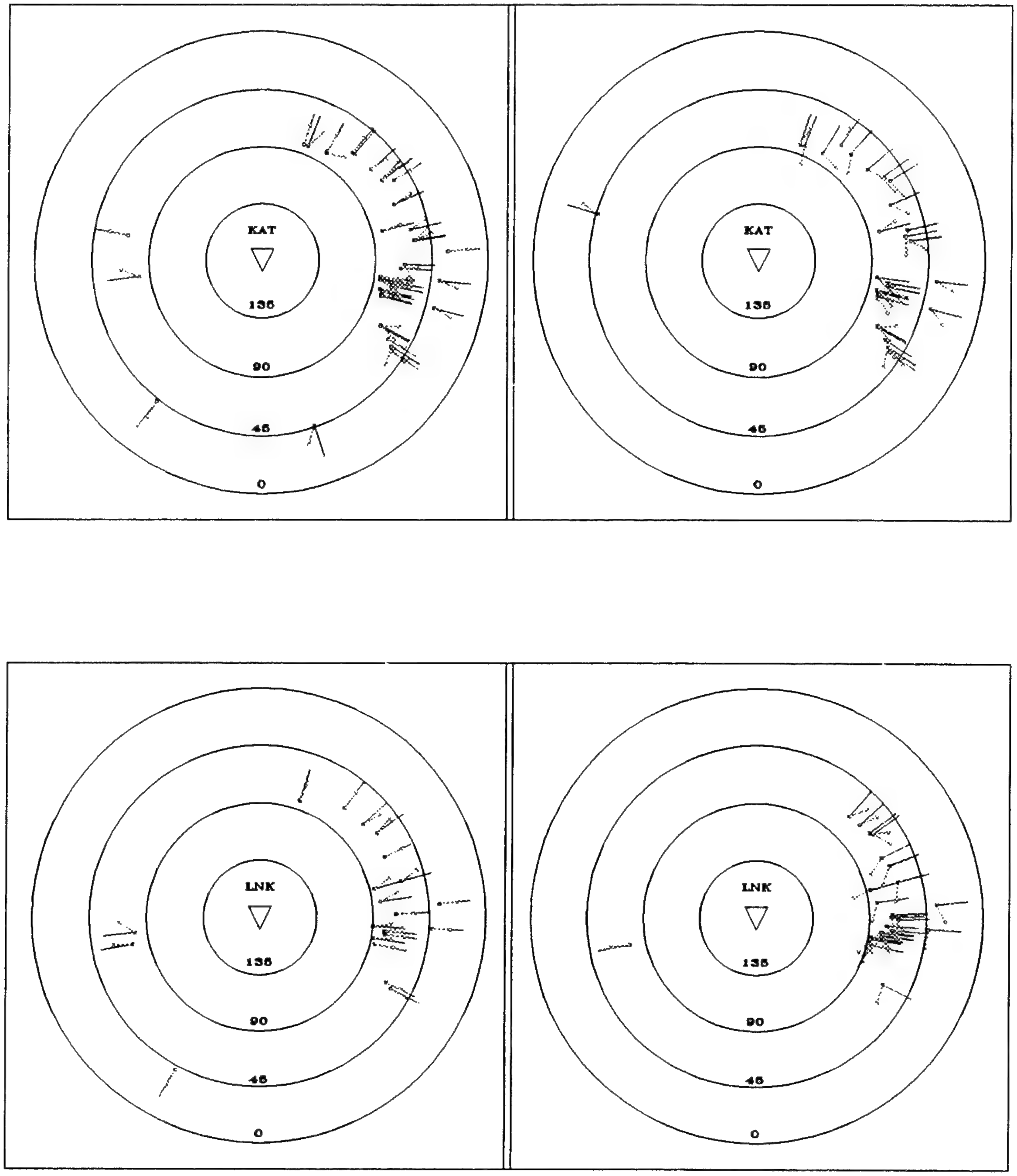

Figure 10. Stations KAT (top) and LNK (bottom) expected compared to the observed P-wave bearing . Format is the same as in Figure 8.

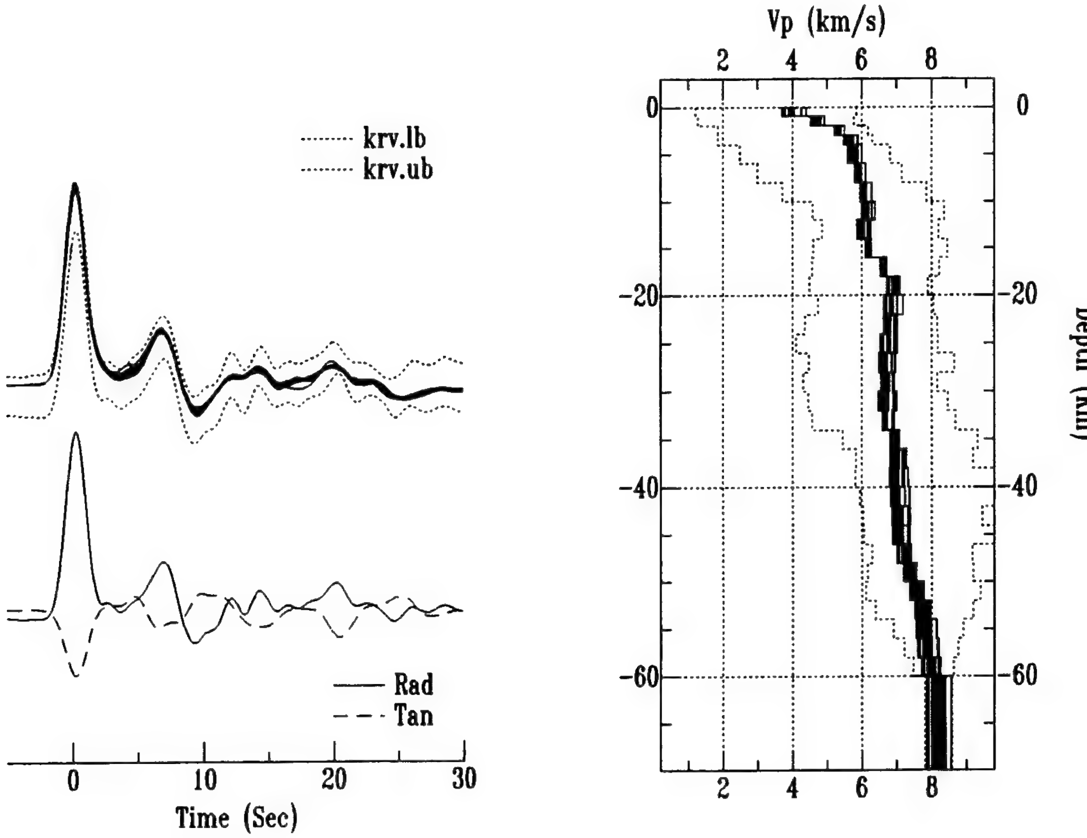

Figure 11. CSN station KRV-NE synthetic waveform fits compared to the +/- 1 STD bounds (top left), the stacked radial and tangential receiver functions (bottom left) and the corresponding solution models (right).

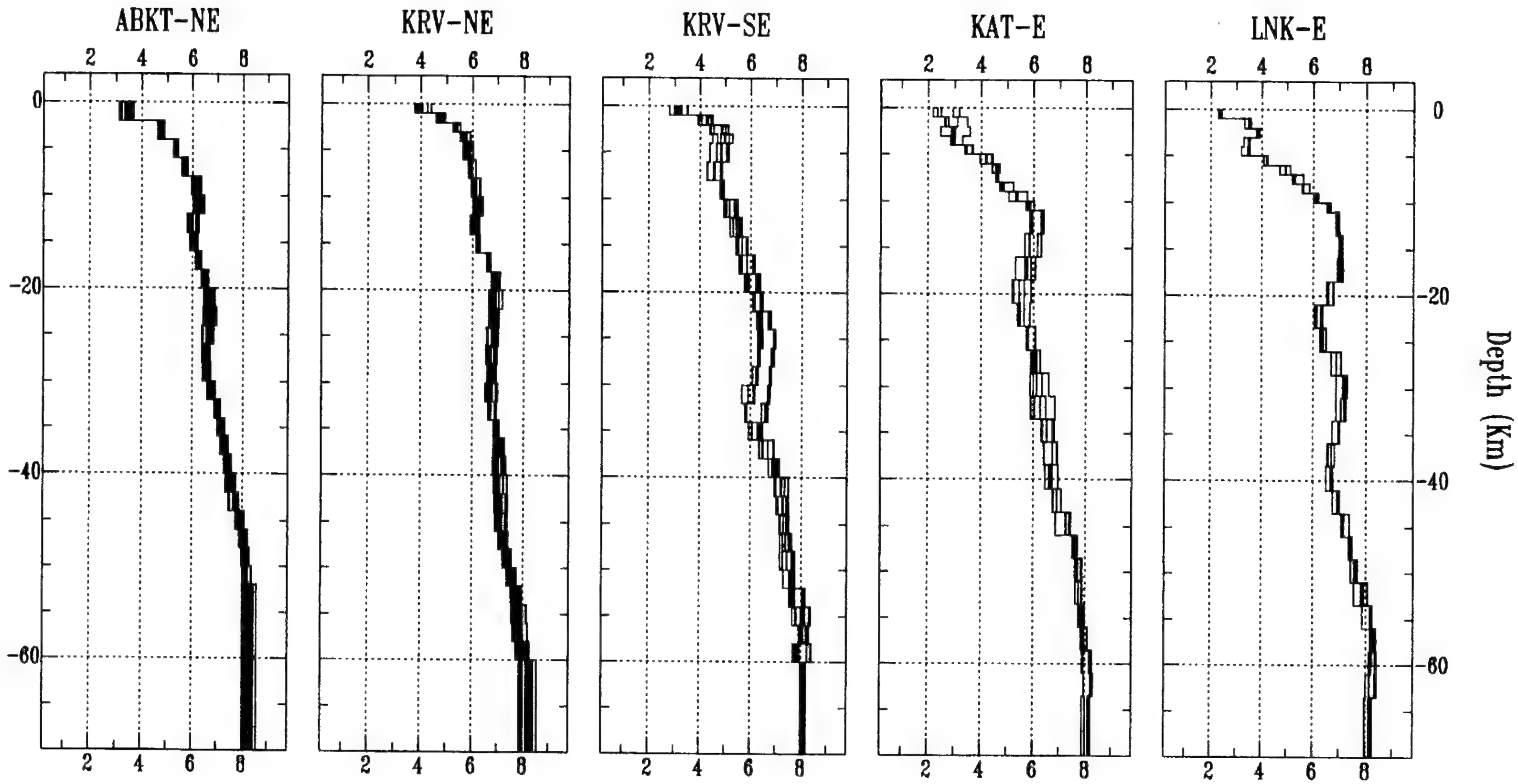

Figure 12. P-wave velocity receiver function modeling results for stations ABKT, KRV, KAT and LNK.

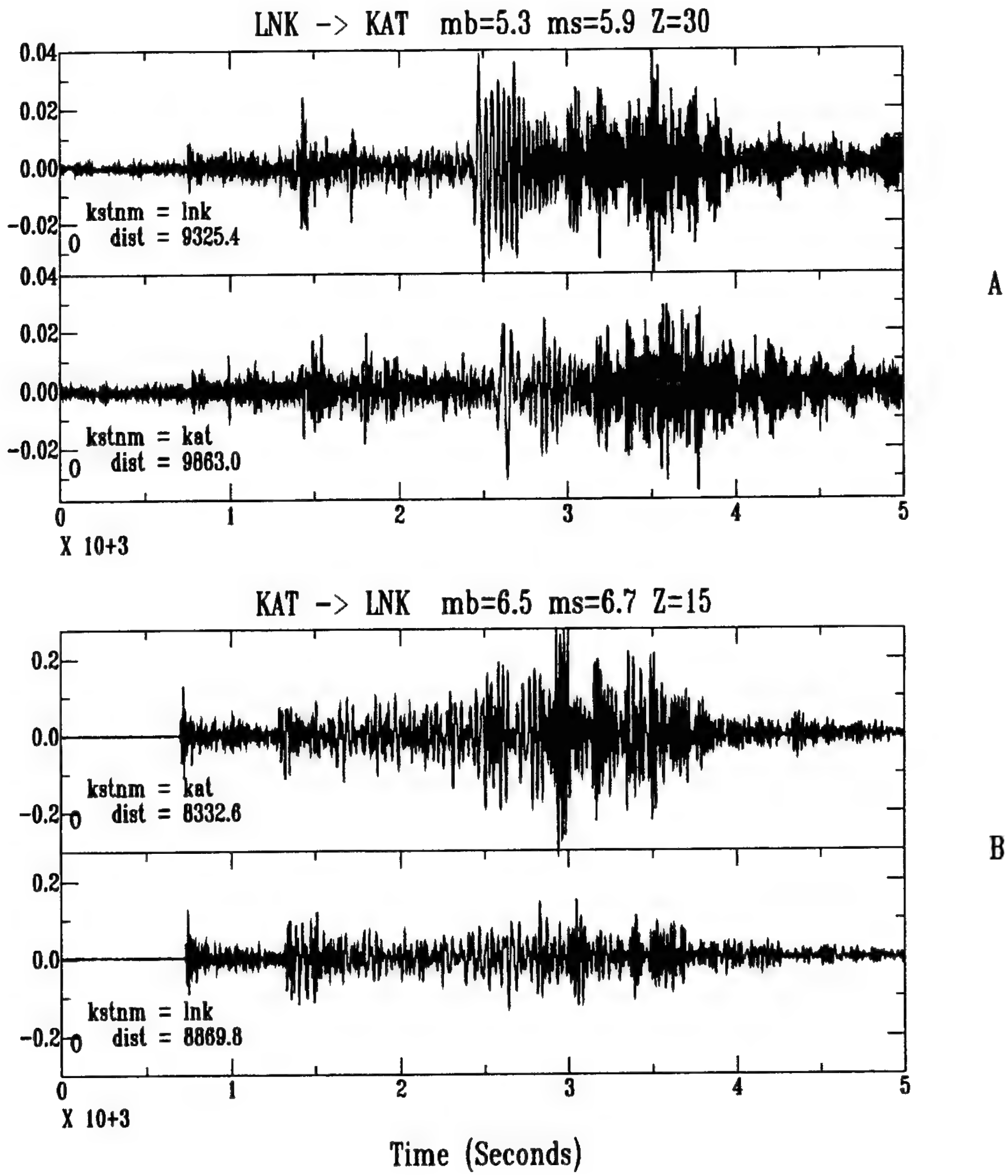

Figure 13. Reversed, great circle path vertical component seismograms recorded at CSN stations LNK and KAT. The upper pair (A) is a record of a mid-Atlantic ridge earthquake propagating from west to east across the south Caspian Basin, while the lower pair (B) is a larger event from the Mulucca Sea which propagates across the Basin from east to west. Both pairs show considerable degradation of the surface wave train after propagating across the south Caspian Basin. These seismograms are characteristic of all great circle path events across the central portion of the south Caspian Basin.

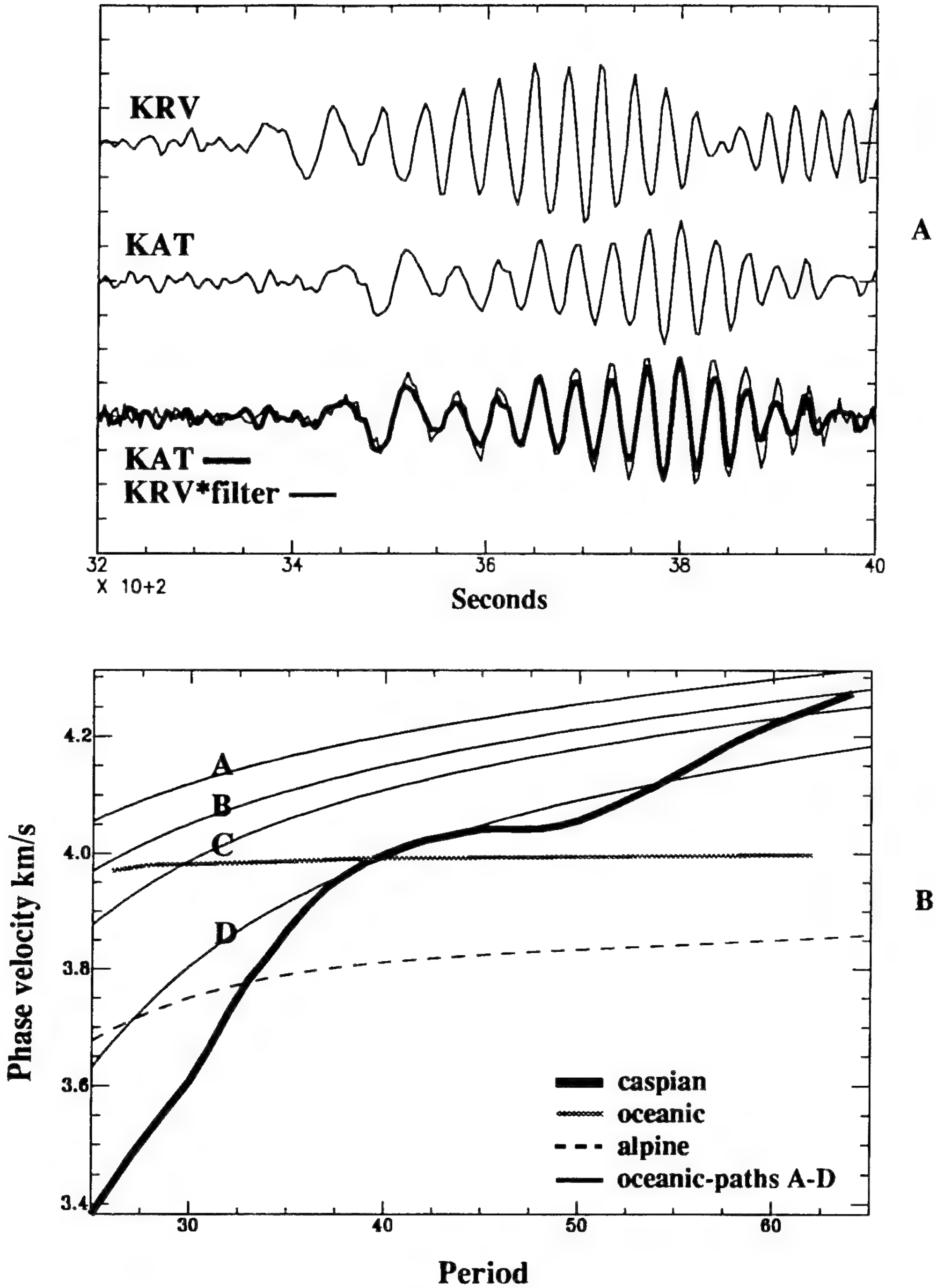

Figure 14. Fundamental mode Rayleigh wave phase velocity dispersion curve for the KRV-KAT path. This curve was computed from four seismogram pairs using a constrained least-squares alogrithm (Gomberg et al. 1988). The KRV-KAT phase velocity curve is compared with observed dispersion curves for an ocean basin (Kuo et al. 1962), a continental tectonic region (Knopoff et al. 1966), and the Bay of Bengal (Brune and Singh 1988) region. The primary differences in paths "A" to "D" is an increase in thickness of the near surface sedimentary layer and an increase in Moho depth from "A" to "D".

Table 1

Caspian Seismograph Network

STATION ID # KEY	STATION LAT, LON ELEV	AZIMUTH +°N +°E	DAS# CLOCK SENSOR	FIELD NOTES
KRV #1	40.0063° N 52.9575° E +4 m	184.8° 274.8°	580 GPS CMG-3T	Installed 5/93 CMG#357, 3Km east of Caspian Sea sub-basement vault overlies bedrock. Topography varies up to 100m, Edge of Krasnovosdk Plateau, Turkmenistan.
NBD #2	39.5077° N 54.3872° E +18 m	4.6° 94.6°	458 Ω CMG-3T/ LP	Installed 5/93 CMG #360; 12/93-present: LPZ=186 LPN=048, LPE=050; Sub-basement vault overlies unconsolidated sands and clay; Relatively flat topography; Turkmenian Lowlands.
KAT #3	37.6697° N 54.7766° E +84 m	4.1° 94.1°	454 Ω CMG-3T	Installed 5/93 CMG#363; 12/93-present CMG#360 Sub-basement vault overlies alluvium. Topography is ±10m; Turkmenian Lowlands, 3 Km north of Iraian Border, 20 Km north of Alborz Mtns.
LNK #4	38.7100° N 48.7788° E -2 m	4.4° 94.4°	450 Ω CMG-3T	Installed 6/93 CMG #364; Removed 5/95. Surface vault overlies bedrock. Topography ±50m. Foothills of Talesh Mts., 10Km west of Caspian Sea; Azerbaijan.
BAK #5	40.5813° N 49.9869° E -27 m	4.8° 94.8°	456 Ω LP	Installed 6/93 LPZ=077 LPN=043 LPE=039 Removed 6/94; 1Km west of Caspian Sea. Surface vault overlies unconsolidated sands and clay. Apsheron Peninsula, Azerbaijan.
DTA #6	39.0755° N 55.1663° E +319 m	4.5° 94.5°	582 GPS CMG-3T	Installed 12/93 CMG #363; Surface vault overliies silt stone and shale, Topography ± 200m Kopet Dag Mtns., Turkmenistan
SHE #7	40.6433° N 48.6394° E +829 m	184.8° 274.8°	456 Ω LP	Installed 6/94 LPZ=077, LPN=043, LPE=039 Removed 5/95; Surface vault overlies carbonates. Topography ±100. Eastern Caucasus, Azerbaijan.
ABKT #8	37.9304° N 58.1189° E +678 m	0° 90°	IRIS GPS STS-1	Operated by IRIS, installed 4/93, Sensors in tunnel within silt stone and carbonates. Kopet Dag Mtns., Turkmenistan.
KAR #9	38.4357° N 56.2709° E +304 m	184.3° 274.3°	456 Ω CMG-3T	Installed 6/95 CMG #364, Sensors in sub-basement vault, Kopet Dag Mtns., Turkmenistan

Table 2

Teleseismic P-wave residuals computed with respect to IASP91. BAZ= azimuthal search range, Mean= mean residual over the specified BAZ, STD= standard deviation and # Ev's= number of events used in calculation and all times are in seconds.

STATION	BAZ	MEAN	STD	# EV'S
DTA	0-360°	1.78	0.523	36
KRV	0-360°	1.38	0.807	113
NBD	0-360°	2.80	1.289	29
KAT	0-360°	2.96	0.888	99
LNK	0-360°	1.94	0.870	25
ABKT	0-360°	1.85	0.885	147

Table 3

Teleseismic P-wave residuals computed with respect to 'standard-station' ABKT. BAZ= azimuthal search range, Mean= mean residual over the specified BAZ, STD= standard deviation and # Ev's= number of events used in calculation, and all times are in seconds.

STATION	BAZ	MEAN	STD	# EV'S
DTA	0-360°	0.06	0.433	17
KRV	0-360°	-0.51	0.472	94
KRV	0-70°	-0.28	0.411	39
KRV	70-180°	-0.70	0.412	51
NBD	0-360°	0.89	0.825	26
KAT	0-360°	0.87	0.691	72
LNK	0-360°	0.06	0.998	22

Table 4

Summary of P-wave bearing analysis where BAZ is range of search, MEAN = average difference between observed and expected P-wave azimuth computed over the specified BAZ; STD=standard deviation; and # EV's = number of events.

	Lowpass results				Highpass results			
Station	BAZ	MEAN	STD	# EV's	BAZ	MEAN	STD	# EV's
ABKT	0-360°	1.89°N	8.41	61	0-80° 80-180°	22.66°N 31.85°S	7.57 12.43	6 27
DTA	0-360°	2.28°S	11.56	17	0-80° 80-180°	6.90°S 1.39°S	7.92 13.64	10 6
KRV	0-360° 0-180°	16.67°N 17.35°N	7.51 7.17	69 64	0-360° 0-180°	11.83°N 11.87°N	10.6 10.89	52 48
NBD	0-360°	8.26°N	12.22	24	0-360°	0.35°S	48.76	20
KAT	0-360°	7.74°S	25.45	42	0-360°	11.83°N	10.6	52
LNK	0-360°	1.74°N	12.14	23	0-360°	88.82°S	41.61	27

Appendix 1

Caspian Seismograph Network Event Index

Events are indexed by YR:Day:HR:MN:SS according to the Preliminary Determination of Epicenter monthly (1993-1994) and weekly (1995) bulletins. The station lookup key is equal to 1 if archived, 0 if not, and the stations are numbered as: KRV=1, NBD=2, KAT=3, LNK=4, BAK=5, DTA=6, SHE=7, ABKT=8 and KAR=9.

EventID	Lat	Lon	Z	Mb	Ms	Location	Key 123456789
93143161830	46.564	153.267	21	5.1	4.9	KURIL ISLANDS	011000010
93144235120	-23.238	-66.631	221	6.2		JUJUY PROVINCE, ARGENTINA	111000010
93145183825	37.557	45.961	33	4.1		NORTHWESTERN IRAN	111000000
93145231643	55.021	-160.513	37	6.2	5.8	ALASKA PENINSULA	111000010
93148094903	62.354	-147.732	51	4.0		CENTRAL ALASKA	111000000
93148155527	55.862	-155.171	33	5.0	5.0	SOUTH OF ALASKA	111000010
93148173110	37.031	68.067	33	4.4		AFGHANISTAN-USSR BORDER REGION	111000000
93149065013	19.072	-26.476	12	5.9	6.2	NORTH ATLANTIC OCEAN	111000010
93149105036	33.978	59.859	33	4.7		IRAN	111000000
93150141220	-3.674	142.703	6	5.9	5.6	NEAR N COAST OF PAPUA NEW GUINEA	111100000
93150170853	1.546	127.207	81	6.0		HALMAHERA	111100010
93150223403	-0.621	124.208	75	5.6		MOLUCCA SEA	111100000
93151000527	28.713	55.561	33	4.1		SOUTHERN IRAN	111100000
93151083422	-72.448	174.838	10	5.3	5.1	ROSS SEA	111100010
93151133812	37.767	66.581	50	4.1		AFGHANISTAN-USSR BORDER REGION	111100000
93151195329	36.599	71.626	33	4.8	3.4	AFGHANISTAN-USSR BORDER REGION	111000000
93152094529	34.352	26.184	47	4.9	4.2	CRETE	111000010
93152155347	-45.711	-77.211	33	5.3	5.4	OFF COAST OF SOUTHERN CHILE	111000010
93152195110	46.166	16.467	30	4.9		YUGOSLAVIA	111000000
93153030018	-46.471	33.954	10	5.6	5.5	PRINCE EDWARD ISLANDS REGION	111000010
93153082719	51.513	-178.744	33	5.6	5.4	ANDREANOF ISLANDS, ALEUTIAN IS.	111000010
93153161512	32.407	48.669	53	4.2		WESTERN IRAN	111000000
93153220148	28.940	47.606	10	4.7		EASTERN ARABIAN PENINSULA	111000000
93154074647	40.896	35.964	10	4.3		TURKEY	110000000
93154093825	-14.841	167.299	152	5.9		VANUATU ISLANDS	110000000
93155030635	11.799	142.493	25	5.6	5.5	SOUTH OF MARIANA ISLANDS	111000010
93155104933	3.734	128.497	20	5.9	5.8	NORTH OF HALMAHERA	111000010
93155215625	42.969	43.613	33	4.2		WESTERN CAUCASUS	111000000
93157110500	36.377	71.333	33	4.6		AFGHANISTAN-USSR BORDER REGION	111000000
93157132320	15.823	146.595	14	6.0	6.6	MARIANA ISLANDS	111000010
93158071427	39.924	46.273	36	4.4		N.W. IRAN-USSR BORDER REGION	111000000
93158074935	35.972	141.529	36	5.6	5.5	NEAR EAST COAST OF HONSHU, JAPAN	111000010
93158131438	35.286	141.900	11	5.3	4.9	NEAR EAST COAST OF HONSHU, JAPAN	111000010
93159130336	51.218	157.829	71	6.4	7.3	NEAR EAST COAST OF KAMCHATKA	111000010
93159143037	33.585	72.746	33	4.8		PAKISTAN	111000000
93159231741	-31.560	-69.234	113	6.5		SAN JUAN PROVINCE, ARGENTINA	111000010
93160040740	32.026	49.278	33	4.4		WESTERN IRAN	111000000
93160173336	34.763	53.276	30	5.0		IRAN	111000010
93161054938	39.383	67.665	33	4.6		SOUTHEASTERN UZBEK SSR	111000000
93161120456	51.170	159.097	21	5.5	5.2	OFF EAST COAST OF KAMCHATKA	111000010
93161125859	51.115	159.272	16	5.8	5.1	OFF EAST COAST OF KAMCHATKA	111000000
93161174838	-24.353	-176.082	34	5.7	5.4	SOUTH OF FIJI ISLANDS	111000000
93162095529	39.547	68.939	33	4.1		TAJIK SSR	111000000
93162130903	35.508	26.603	28	4.5		CRETE	111000000
93162132255	36.800	71.651	33	4.8		AFGHANISTAN-USSR BORDER REGION	111000000
93163054521	-11.140	162.937	15	5.5	6.1	SOLOMON ISLANDS	111000010
93163085826	40.624	35.792	10	4.6		TURKEY	111000000
93163182642	-4.375	135.118	10	5.8	6.1	WEST IRIAN REGION	111000010
93163203325	51.259	157.692	44	5.9	6.0	NEAR EAST COAST OF KAMCHATKA	111000010
93164232640	39.363	20.495	20	5.3	4.9	GREECE-ALBANIA BORDER REGION	111000010
93165073017	35.568	78.407	33	5.1	4.4	EASTERN KASHMIR	111000010
93165195942	39.624	38.410	26	5.0	4.5	TURKEY	111000010
93166044257	34.868	141.683	47	5.4	5.3	OFF EAST COAST OF HONSHU, JAPAN	111000010

Appendix 1 (continued)

EventID	Lat	Lon	Z	Mb	Ms	Location	Key 123456789
93166231224	35.629	77.788	33	4.9		EASTERN KASHMIR	111000000
93168204452	36.168	71.236	104	5.2		AFGHANISTAN-USSR BORDER REGION	110000000
93169115251	-29.053	-176.753	16	6.2	6.7	KERMADEC ISLANDS REGION	110000000
93169175746	-28.678	-176.893	11	5.9	6.7	KERMADEC ISLANDS REGION	110000000
93170170156	36.807	54.904	33	4.6		IRAN	110000000
93171020924	-6.262	130.092	152	5.3		BANDA SEA	110000000
93171172630	-6.946	155.776	38	5.5	5.6	SOLOMON ISLANDS	110000000
93172003251	39.200	40.401	10	4.2		TURKEY	110000000
93172161555	37.605	72.638	33	4.3		TAJIK SSR	110000000
93173123345	64.624	-17.543	5	5.1	4.8	ICELAND	110000000
93173163243	30.149	50.814	33	5.5	4.8	IRAN	110000000
93174112919	-60.549	-56.376	10	6.2	5.4	SOUTH SHETLAND ISLANDS	110000000
93175165339	38.911	71.230	33	4.5		AFGHANISTAN-USSR BORDER REGION	110000000
93176100429	33.315	93.306	33	4.8	4.3	QINGHAI PROVINCE, CHINA	100000000
93186005241	-24.886	-112.393	10	5.2	5.6	EASTER ISLAND REGION	000100010
93186080221	37.164	71.379	33	4.5		AFGHANISTAN-USSR BORDER REGION	000100000
93187194809	37.891	39.315	47	4.8		TURKEY	100100000
93187025303	-24.601	-111.888	10	5.5	6.1	EASTER ISLAND REGION	000100010
93188111053	27.887	127.992	35	5.1	4.9	RYUKYU ISLANDS	100100010
93189103549	-20.832	169.294	34	5.5	5.3	VANUATU ISLANDS	100100000
93189104625	51.218	159.151	36	5.4	5.3	OFF EAST COAST OF KAMCHATKA	100100010
93189182217	-20.858	172.317	33	5.4	5.9	VANUATU ISLANDS REGION	101100010
93189233106	37.337	69.983	33	4.5		AFGHANISTAN-USSR BORDER REGION	101100000
93190102921	28.416	55.369	23	5.3	4.8	SOUTHERN IRAN	101100010
93190153753	-19.782	-177.486	398	6.0		FIJI ISLANDS REGION	101100010
93190230605	36.853	55.230	61	4.6		IRAN	101100000
93192133621	-25.304	-70.166	48	6.2	6.1	NEAR COAST OF NORTHERN CHILE	101000010
93192174811	47.626	154.156	28	5.6	5.3	KURIL ISLANDS	101000010
93193050531	72.175	1.071	10	5.1	4.9	NORWEGIAN SEA	101000010
93193131711	42.851	139.197	17	6.6	7.6	HOKKAIDO, JAPAN REGION	101000010
93193144505	43.124	139.183	33	6.0	6.3	EASTERN SEA OF JAPAN	101000000
93194083553	-3.372	145.633	24	5.3	5.6	NEAR N COAST OF PAPUA NEW GUINEA	101000010
93194142253	37.032	55.310	26	4.6		IRAN-USSR BORDER REGION	101000010
93195123149	38.224	21.756	23	5.3	5.5	GREECE	101000000
93195173833	43.181	139.124	20	5.5		EASTERN SEA OF JAPAN	101000000
93196005113	46.679	152.577	32	5.7	5.0	KURIL ISLANDS	101000000
93196193737	42.670	139.016	20	5.3	4.7	HOKKAIDO, JAPAN REGION	101000000
93198094634	28.011	99.636	31	5.3	4.8	YUNNAN PROVINCE, CHINA	101000000
93198184819	29.880	51.489	33	4.4		SOUTHERN IRAN	101000000
93200193504	34.465	141.339	46	5.2	5.1	OFF EAST COAST OF HONSHU, JAPAN	101000000
93201132604	27.374	139.990	465	5.4		BONIN ISLANDS REGION	101000000
93201165044	-52.917	27.174	10	5.1	5.2	SOUTH OF AFRICA	101000000
93203015456	39.533	40.116	11	4.6		TURKEY	101000000
93203045707	6.470	-71.210	20	6.1	5.9	NORTHERN COLOMBIA	101000010
93203121536	21.760	144.261	127	5.6		MARIANA ISLANDS REGION	101000010
93204115006	36.437	70.416	272	5.2		HINDU KUSH REGION	101000000
93205020156	5.070	127.714	116	5.7		PHILIPPINE ISLANDS REGION	101000000
93205102656	51.509	-176.879	33	5.2	4.4	ANDREANOF ISLANDS, ALEUTIAN IS.	101000010
93205125603	39.087	138.636	14	5.1	4.6	EASTERN SEA OF JAPAN	101000000
93205202450	-13.060	167.056	194	5.8		VANUATU ISLANDS	101000000
93205213205	36.443	70.604	223	4.6		HINDU KUSH REGION	101000000
93206150519	-17.844	-13.431	10	5.2	4.7	SOUTH ATLANTIC RIDGE	101000000
93207093130	29.960	66.626	33	4.1	4.9	PAKISTAN	101000000
93208194449	34.442	141.591	25	5.3	5.0	OFF EAST COAST OF HONSHU, JAPAN	001000000
93209031024	36.676	71.171	265	4.1		AFGHANISTAN-USSR BORDER REGION	001000000
93209033238	36.639	70.785	33	4.1		HINDU KUSH REGION	001000000
93209171640	46.361	150.971	86	5.0		KURIL ISLANDS	001000000
93209180748	-5.573	154.132	26	5.6	5.9	SOLOMON ISLANDS	001000000
93211142551	45.684	26.568	148	4.7		ROMANIA	001000000
93211233410	28.864	34.821	18	4.7		ARAB REPUBLIC OF EGYPT	001000000

Appendix 1 (continued)

EventID	Lat	Lon	Z	Mb	Ms	Location	Key 123456789
93212023245	-4.397	28.361	10	5.0		LAKE TANGANYIKA REGION	001000000
93212175301	29.394	34.475	10	4.4		ARAB REPUBLIC OF EGYPT	001000000
93212192921	27.976	91.944	33	4.4		BHUTAN	001000000
93212231316	56.210	112.476	10	4.8		LAKE BAIKAL REGION	001000010
93213002040	15.385	31.690	13	5.2	5.1	SUDAN	001000010
93213141928	-43.824	-16.235	10	5.0	4.9	SOUTH ATLANTIC RIDGE	001000000
93214031321	30.828	131.418	33	5.4	5.4	KYUSHU, JAPAN	001000010
93214160059	30.914	51.839	39	4.9	4.2	IRAN	001000000
93214164815	36.992	71.341	115	4.6		AFGHANISTAN-USSR BORDER REGION	001000010
93214230455	37.482	70.947	33	4.7		AFGHANISTAN-USSR BORDER REGION	001000000
93215061555	85.253	91.728	10	4.9	4.5	NORTH OF SEVERNAYA ZEMLYA	001000000
93215071959	51.188	-130.797	10	5.5	6.1	QUEEN CHARLOTTE ISLANDS REGION	001000010
93215104327	85.294	91.440	10	4.8		NORTH OF SEVERNAYA ZEMLYA	001100000
93215123120	28.549	34.608	10	4.5		ARAB REPUBLIC OF EGYPT	001100000
93215124305	28.729	34.553	10	5.9	5.8	ARAB REPUBLIC OF EGYPT	001100010
93216075943	30.105	51.392	33	4.6		IRAN	001100000
93216113118	-1.629	99.615	32	5.9	6.3	SOUTHERN SUMATERA	001100010
93216194609	37.008	57.936	33	4.4		IRAN-USSR BORDER REGION	001100000
93217070533	72.219	1.514	10	4.6	4.5	NORWEGIAN SEA	001100010
93217115319	-5.430	151.700	61	5.2	5.1	NEW BRITAIN REGION	001100000
93219000037	26.585	125.612	155	6.0		NORTHEAST OF TAIWAN	001100010
93219175324	-23.866	179.846	523	6.0		SOUTH OF FIJI ISLANDS	001100010
93219194241	41.985	139.839	14	6.2	6.1	HOKKAIDO, JAPAN REGION	001100010
93220083424	12.982	144.801	59	7.1	8.0	SOUTH OF MARIANA ISLANDS	001100000
93220200314	13.483	145.657	56	5.3	5.7	MARIANA ISLANDS	001100000
93220224143	38.662	70.447	16	5.1	4.8	AFGHANISTAN-USSR BORDER REGION	001100000
93221124248	36.379	70.868	215	6.2		HINDU KUSH REGION	011000000
93221060503	28.737	34.704	10	4.6		ARAB REPUBLIC OF EGYPT	001100000
93221113830	36.436	70.711	204	5.8		HINDU KUSH REGION	001000000
93222005153	-45.277	166.927	28	6.2	7.0	OFF W. COAST OF S. ISLAND, N.Z.	111000010
93222055822	40.201	22.978	15	4.6		GREECE	111000010
93222094635	-38.520	177.553	14	6.0	6.0	NORTH ISLAND, NEW ZEALAND	111000010
93222193620	83.066	-27.533	10	5.4	5.0	NEAR NORTH COAST OF GREENLAND	111000010
93223141737	13.178	145.651	22	5.9	6.1	MARIANA ISLANDS	111000010
93225003143	28.561	34.716	9	4.7		ARAB REPUBLIC OF EGYPT	111000000
93225004341	32.465	49.537	16	4.6		WESTERN IRAN	111000000
93225110220	-35.989	178.510	95	5.8		OFF E. COAST OF N. ISLAND, N.Z.	111000010
93226035242	37.542	70.714	64	4.5		AFGHANISTAN-USSR BORDER REGION	111000010
93226143004	25.440	101.545	33	4.9	4.8	YUNNAN PROVINCE, CHINA	111000010
93227031021	0.711	-25.956	15	5.3	5.3	CENTRAL MID-ATLANTIC RIDGE	111000010
93228043348	12.966	144.972	18	5.6	6.0	SOUTH OF MARIANA ISLANDS	111000010
93230120921	34.969	26.016	29	4.5		CRETE	110000000
93231080322	13.169	145.531	61	5.5		MARIANA ISLANDS	110000010
93231100428	35.089	52.094	18	4.6		IRAN	110000000
93231142656	33.204	71.983	33	4.7		PAKISTAN	110000000
93231152138	7.197	126.807	31	5.4	5.5	MINDANAO, PHILIPPINE ISLANDS	110000010
93231215205	7.167	126.743	31	5.3	4.8	MINDANAO, PHILIPPINE ISLANDS	110000010
93232050653	-5.997	142.743	15	6.0	6.0	PAPUA NEW GUINEA	110000010
93232101020	28.127	53.879	65	4.1		SOUTHERN IRAN	110000000
93232115204	21.686	143.064	288	5.3		MARIANA ISLANDS REGION	110000000
93232185710	-25.991	-175.261	22	5.5	5.1	SOUTH OF TONGA ISLANDS	110000000
93232231000	28.764	34.687	10	4.5		ARAB REPUBLIC OF EGYPT	110000000
93233080749	-46.404	96.032	10	5.2	5.5	SOUTHEAST INDIAN RISE	110000000
93233154114	27.359	55.922	33	4.3		SOUTHERN IRAN	110000000
93234015304	14.255	56.262	10	4.8	3.8	ARABIAN SEA	110000000
93235052143	30.035	67.921	25	5.0	4.6	PAKISTAN	110000010
93235120740	36.401	141.994	35	5.1	4.7	NEAR EAST COAST OF HONSHU, JAPAN	110000000
93235195110	30.045	67.891	32	4.8		PAKISTAN	110000000
93236174730	20.641	71.365	25	5.0	4.7	INDIA	110000010
93237052532	-44.718	-79.958	10	5.6	5.4	OFF COAST OF SOUTHERN CHILE	110000010

Appendix 1 (continued)

EventID	Lat	Lon	Z	Mb	Ms	Location	Key 123456789
93237225704	36.070	31.018	66	4.4		TURKEY	110000000
93238013000	-35.899	178.265	33	5.5	5.4	OFF E. COAST OF N. ISLAND, N.Z.	110000010
93238100357	36.736	28.051	33	5.3	4.5	DODECANESE ISLANDS	110000010
93238213233	45.727	26.565	136	5.0		ROMANIA	110000010
93240042623	17.173	73.672	5	4.9	4.5	INDIA	110000000
93240201445	6.571	94.668	133	5.8		NICOBAR ISLANDS REGION	110000010
93241095754	-7.005	129.560	147	5.8		BANDA SEA	110000010
93242121231	48.508	143.326	18	5.2	4.3	SAKHALIN ISLAND	110000000
93243065532	41.878	49.466	85	5.3		CASPIAN SEA	110000010
93244004123	31.712	141.611	46	5.4	5.7	SOUTH OF HONSHU, JAPAN	110000010
93244033527	31.859	141.641	44	5.1	4.9	SOUTH OF HONSHU, JAPAN	110000000
93244114838	-4.331	102.567	71	5.8		SOUTHERN SUMATERA	110000010
93244140319	2.986	96.122	34	5.9	6.2	NORTHERN SUMATERA	110000010
93246123500	14.523	-92.713	27	5.8	6.8	NEAR COAST OF CHIAPAS, MEXICO	110000010
93247061137	13.862	145.003	26	5.5	4.6	MARIANA ISLANDS	110000000
93247113838	36.429	70.812	195	5.9		HINDU KUSH REGION	110000010
93247172510	30.340	94.831	10	5.1		TIBET	110000000
93247213933	-9.571	122.528	33	5.8	5.8	SAVU SEA	110000010
93249035600	-4.641	153.231	49	6.2	6.6	NEW IRELAND REGION	110000000
93250024850	-31.635	-179.440	10	5.9	6.5	KERMADEC ISLANDS REGION	110000010
93251113837	29.987	52.028	31	4.9	4.4	SOUTHERN IRAN	110100010
93251195441	40.191	52.490	82	4.5		TURKMEN SSR	110100010
93253160232	35.039	12.366	10	5.0	4.9	MEDITERRANEAN SEA	110100000
93253191254	14.717	-92.645	34	6.2	7.3	NEAR COAST OF CHIAPAS, MEXICO	110100010
93254045533	42.003	142.581	58	5.7		HOKKAIDO, JAPAN REGION	110100010
93254173646	20.113	121.446	42	5.4	5.4	PHILIPPINE ISLANDS REGION	100100010
93255032238	13.826	-90.429	68	5.4	5.5	NEAR COAST OF GUATEMALA	000100000
93255082234	-29.608	-177.279	33	5.6	5.8	KERMADEC ISLANDS	000100000
93256052207	-6.072	149.908	30	5.3	5.4	NEW BRITAIN REGION	000100000
93256123751	-29.492	-177.136	20	5.8	6.2	KERMADEC ISLANDS	000100000
93257052112	14.410	53.566	10	4.7	4.3	ARABIAN SEA	000100000
93258150813	33.322	75.740	33	5.0		EASTERN KASHMIR	100100000
93259005926	44.533	149.036	33	5.8	5.1	KURIL ISLANDS	100100010
93261002747	1.632	126.770	40	5.5	5.1	MOLUCCA PASSAGE	111100000
93261050227	36.421	71.592	113	6.1		AFGHANISTAN-USSR BORDER REGION	111100000
93262041836	-60.079	-26.967	46	5.4	5.4	SOUTH SANDWICH ISLANDS REGION	110100010
93262141056	14.362	-93.325	18	5.7	6.4	NEAR COAST OF CHIAPAS, MEXICO	110100010
93263101742	0.750	-29.354	10	5.8	6.0	CENTRAL MID-ATLANTIC RIDGE	110100010
93264032855	42.314	-122.012	11	5.7	5.8	OREGON	110100010
93264054533	42.358	-122.045	5	5.6	5.8	OREGON	110100000
93264191135	11.478	39.638	15	5.4	5.0	ETHIOPIA	110100010
93265123703	-6.470	154.901	28	6.1	6.0	SOLOMON ISLANDS	110100010
93268044419	38.167	73.002	103	4.4		TAJIK-XINJIANG BORDER REGION	110100010
93269022934	36.253	71.219	106	4.6		AFGHANISTAN-USSR BORDER REGION	110100000
93269033114	9.997	138.222	10	6.1	6.0	WEST CAROLINE ISLANDS	110100010
93269115552	13.009	145.016	64	5.8		MARIANA ISLANDS	110100010
93270044355	30.678	132.121	38	5.5	5.3	SOUTHEAST OF SHIKOKU, JAPAN	110100010
93270133732	-53.651	-51.621	33	6.2	6.6	SOUTH ATLANTIC OCEAN	110100010
93272093920	-18.966	167.667	35	5.5	5.2	VANUATU ISLANDS	110000000
93272111603	0.494	121.528	97	6.1		MINAHASSA PENINSULA	110000010
93272141801	36.421	70.886	188	4.6		HINDU KUSH REGION	110000010
93272182620	-42.677	-18.385	10	5.9	5.9	SOUTH ATLANTIC RIDGE	110000000
93272222548	18.066	76.451	7	6.3	6.2	INDIA	110000010
93273170445	11.815	92.529	23	5.4	4.7	ANDAMAN ISLANDS REGION	110000000
93273182750	15.417	-94.698	19	5.8	6.4	NEAR COAST OF OAXACA, MEXICO	110000000
93274035933	36.637	23.967	88	4.9		SOUTHERN GREECE	110000000
93275011730	39.066	69.966	14	5.0	4.4	TAJIK SSR	110000000
93275084232	38.190	88.663	14	6.2	6.3	SOUTHERN XINJIANG, CHINA	100000010
93275094319	38.169	88.605	14	5.8	5.3	SOUTHERN XINJIANG, CHINA	100000000
93275172333	38.171	88.690	14	5.6	5.0	SOUTHERN XINJIANG, CHINA	100000000

Appendix 1 (continued)

EventID	Lat	Lon	Z	Mb	Ms	Location	Key 123456789
93277205438	-21.437	-174.301	34	5.8	5.7	TONGA ISLANDS	101000010
93278015956	41.667	88.695	0	5.9	4.7	SOUTHERN XINJIANG, CHINA	101000010
93278050945	-6.130	128.965	13	5.9	6.1	BANDA SEA	101000010
93278183539	36.649	29.792	37	4.1		TURKEY	101000000
93278212806	77.727	126.454	33	5.0		LAPTEV SEA	101000010
93280032658	38.214	88.726	11	5.0		SOUTHERN XINJIANG, CHINA	100000000
93280175938	36.443	70.628	216	4.9		HINDU KUSH REGION	100000010
93281182347	46.505	150.037	172	5.5		KURIL ISLANDS	100000010
93282222421	11.712	57.660	10	5.2	4.7	ARABIAN SEA	100000000
93284130729	-17.845	-178.726	555	5.8		FIJI ISLANDS REGION	101100010
93284155421	32.020	137.832	351	6.4		SOUTH OF HONSHU, JAPAN	101100010
93285023500	-33.913	94.278	10	5.2	4.8	SOUTH INDIAN OCEAN	101100000
93285210452	13.048	51.063	10	5.0	4.8	EASTERN GULF OF ADEN	101110010
93286005233	7.576	121.484	44	5.3	4.8	MINDANAO, PHILIPPINE ISLANDS	101110010
93286020600	-5.889	146.020	25	6.4	7.0	EAST PAPUA NEW GUINEA REGION	101110010
93286030730	-5.932	146.153	33	6.1	6.7	EAST PAPUA NEW GUINEA REGION	101100000
93286233421	28.629	103.419	33	5.0		SICHUAN PROVINCE, CHINA	101110010
93287120235	-50.436	139.904	10	5.4	5.7	SOUTH OF AUSTRALIA	100110010
93288223719	40.744	48.105	56	4.8		EASTERN CAUCASUS	100110000
93289030530	-5.898	146.202	27	6.2	6.4	EAST PAPUA NEW GUINEA REGION	100110010
93289105225	7.472	123.447	31	5.5	5.4	MINDANAO, PHILIPPINE ISLANDS	100110010
93291012822	36.443	53.950	33	4.4		IRAN	100110000
93291135714	22.133	62.861	10	5.2	4.7	ARABIAN SEA	100110010
93291205115	28.896	34.570	9	4.8		ARAB REPUBLIC OF EGYPT	100110010
93292040221	-22.378	-65.971	272	5.9		JUJUY PROVINCE, ARGENTINA	100110010
93292153137	38.791	73.242	33	4.8		TAJIK-XINJIANG BORDER REGION	100110010
93292225038	35.140	25.888	83	4.3		CRETE	100110000
93293101103	36.827	71.651	33	4.1		AFGHANISTAN-USSR BORDER REGION	100110000
93294073655	-56.497	-138.909	10	5.4	5.4	SOUTH PACIFIC CORDILLERA	100110010
93294215220	30.154	51.235	15	5.2		IRAN	101110010
93295084216	-54.835	-26.557	33	5.5	5.5	SOUTH SANDWICH ISLANDS REGION	101110010
93296132642	29.773	51.103	33	4.3		SOUTHERN IRAN	100110000
93297055329	11.327	125.396	49	5.8	5.2	SAMAR, PHILIPPINE ISLANDS	100110010
93297075215	16.755	-98.717	21	6.3	6.7	NEAR COAST OF GUERRERO, MEXICO	100110010
93298100711	-5.882	145.933	18	5.7	5.6	EAST PAPUA NEW GUINEA REGION	100110010
93298102704	-5.909	145.990	30	6.3	7.0	EAST PAPUA NEW GUINEA REGION	100110010
93298143319	41.336	49.478	33	4.7		CASPIAN SEA	100110010
93299113821	38.477	98.655	8	5.9	5.4	QINGHAI PROVINCE, CHINA	100110010
93299202503	37.225	70.192	10	4.5		AFGHANISTAN-USSR BORDER REGION	100110000
93301015206	41.604	142.024	67	5.2		HOKKAIDO, JAPAN REGION	101110010
93301111357	34.390	26.203	47	4.6		CRETE	101110000
93302040905	51.509	-178.184	34	5.8	5.3	ANDREANOF ISLANDS, ALEUTIAN IS.	101110010
93303001607	11.249	57.597	10	4.7		ARABIAN SEA	101110000
93303083033	15.437	121.785	39	5.3	5.1	LUZON, PHILIPPINE ISLANDS	101110010
93303175902	-31.704	-68.232	107	5.9		SAN JUAN PROVINCE, ARGENTINA	101110010
93303230553	30.405	67.651	10	4.7	4.5	PAKISTAN	101110010
93305064631	28.244	57.569	10	4.7		SOUTHERN IRAN	101110000
93305181722	38.950	29.947	13	4.7		TURKEY	101110000
93306071450	42.812	131.129	546	4.9		E. USSR-N.E. CHINA BORDER REG.	101110010
93307131810	-7.123	67.916	10	5.4	5.4	MID-INDIAN RISE	101110010
93307183933	28.654	34.650	13	4.9	4.6	ARAB REPUBLIC OF EGYPT	101110010
93308003240	31.985	59.969	33	4.5		IRAN	101110000
93308051837	38.372	22.002	17	5.0	5.2	GREECE	101110010
93309070206	-7.033	106.101	75	5.4		JAVA	101110010
93309223720	-3.188	148.339	14	5.7	6.2	BISMARCK SEA	101110000
93311082951	34.494	70.671	33	4.7	3.9	AFGHANISTAN	101110000
93312010602	28.698	34.673	14	4.9	4.3	ARAB REPUBLIC OF EGYPT	101110010
93312204854	36.183	141.669	33	5.4	4.9	NEAR EAST COAST OF HONSHU, JAPAN	101110010
93313021403	14.353	53.744	10	5.3	5.1	ARABIAN SEA	101110010
93314214501	-22.583	179.169	613	5.2		SOUTH OF FIJI ISLANDS	101110010

Appendix 1 (continued)

EventID	Lat	Lon	Z	Mb	Ms	Location	Key 123456789
93315002833	50.200	-177.446	19	6.3	5.6	ANDREANOF ISLANDS, ALEUTIAN IS.	101110010
93315101355	-4.543	153.147	46	5.7	5.5	NEW IRELAND REGION	101110010
93316111633	51.414	-177.976	33	5.2	5.1	ANDREANOF ISLANDS, ALEUTIAN IS.	101110010
93316134923	40.929	51.907	33	4.4		CASPIAN SEA	101110000
93317001649	16.288	-98.638	20	5.7	5.3	NEAR COAST OF GUERRERO, MEXICO	101110010
93317011804	51.934	158.647	34	6.5	7.0	NEAR EAST COAST OF KAMCHATKA	101110010
93318082438	36.306	71.310	111	4.5		AFGHANISTAN-USSR BORDER REGION	001110000
93319224519	-18.559	167.637	48	5.2	4.8	VANUATU ISLANDS	101100000
93320155248	30.798	67.219	27	5.4	5.6	PAKISTAN	101100010
93321111851	51.816	158.659	33	6.1	5.6	NEAR EAST COAST OF KAMCHATKA	101100010
93323014323	54.287	-164.164	30	6.1	6.4	UNIMAK ISLAND REGION	101100010
93323090539	7.317	-34.703	10	5.7	5.6	CENTRAL MID-ATLANTIC RIDGE	101100010
93324192453	60.025	-153.003	116	5.6		SOUTHERN ALASKA	101100010
93326030055	5.877	126.229	38	5.7	5.1	MINDANAO, PHILIPPINE ISLANDS	101110010
93329083114	-22.035	170.094	32	5.6	5.6	LOYALTY ISLANDS REGION	101110010
93329202400	-0.963	-13.264	10	5.7	5.5	NORTH OF ASCENSION ISLAND	101110010
93330232004	-9.597	158.148	17	5.9	6.2	SOLOMON ISLANDS	101110010
93331061122	38.625	141.164	104	5.9		NEAR EAST COAST OF HONSHU, JAPAN	101110010
93332105027	-5.599	110.267	569	5.6		JAVA SEA	101110010
93332205927	36.474	71.309	108	5.1		AFGHANISTAN-USSR BORDER REGION	101110010
93334045926	-59.047	-18.158	33	5.2	5.5	SOUTHWESTERN ATLANTIC OCEAN	101110010
93334075830	36.537	71.050	170	4.3		AFGHANISTAN-USSR BORDER REGION	101110000
93334203712	39.263	75.533	18	5.2	5.6	SOUTHERN XINJIANG, CHINA	101110010
93335005901	-57.475	-25.685	33	5.5	5.3	SOUTH SANDWICH ISLANDS REGION	101110010
93336143917	36.405	70.394	220	4.8		HINDU KUSH REGION	101110010
93337054108	51.204	179.308	33	5.2	5.0	RAT ISLANDS, ALEUTIAN ISLANDS	101110010
93337123625	-60.353	-20.446	10	5.5	5.2	SOUTHWESTERN ATLANTIC OCEAN	101110010
93338233411	28.886	34.903	10	4.4	4.5	ARAB REPUBLIC OF EGYPT	101110000
93339001056	27.931	55.269	10	4.4		SOUTHERN IRAN	101110000
93340025821	35.748	71.027	130	4.1		PAKISTAN	101110000
93340104203	-6.360	154.916	48	5.6	5.7	SOLOMON ISLANDS	101110010
93340125019	37.737	72.332	33	4.9		TAJIK SSR	101110000
93340142535	39.201	30.189	33	4.1		TURKEY	101110000
93340205445	6.818	78.301	10	5.2	4.7	LACCADIVE SEA	101110010
93343043219	0.486	125.995	15	6.5	6.7	MOLUCCA PASSAGE	101110010
93343113827	0.425	125.891	16	6.3	6.4	MOLUCCA PASSAGE	101110010
93344085935	20.912	121.282	12	5.8	5.8	PHILIPPINE ISLANDS REGION	101110010
93346170319	0.317	125.939	23	5.8	5.5	MOLUCCA PASSAGE	111110010
93346172126	41.514	28.823	28	4.8		TURKEY	111110000
93346182628	0.344	125.925	33	5.6	5.5	MOLUCCA PASSAGE	111110010
93346204130	36.445	140.962	43	5.4	4.9	NEAR EAST COAST OF HONSHU, JAPAN	111110010
93347114344	-20.422	-173.839	33	5.8	5.9	TONGA ISLANDS	111110010
93348063119	-20.704	-173.451	31	5.5	6.1	TONGA ISLANDS	101110000
93348071214	37.963	72.732	134	5.0		TAJIK SSR	101110000
93348074959	-13.624	168.939	21	5.4	5.4	VANUATU ISLANDS	101110000
93349214942	23.184	120.574	17	5.5	5.2	TAIWAN	111110010
93350092215	41.473	23.079	10	4.5		GREECE-BULGARIA BORDER REGION	111110000
93350114818	37.422	20.806	33	4.4		IONIAN SEA	111110010
93350201121	53.804	171.382	9	5.8	5.7	NEAR ISLANDS, ALEUTIAN ISLANDS	111110010
93351031903	39.186	142.182	54	5.4		NEAR EAST COAST OF HONSHU, JAPAN	111110010
93351174228	36.669	71.053	204	4.1		AFGHANISTAN-USSR BORDER REGION	111110000
93352224420	-20.477	-173.883	33	5.7	5.7	TONGA ISLANDS	111110010
93353114530	25.210	62.603	24	5.1	5.0	PAKISTAN	111110010
93353175313	36.532	71.421	33	4.2		AFGHANISTAN-USSR BORDER REGION	111110000
93354135614	-6.876	131.340	8	6.4	5.7	TANIMBAR ISLANDS REGION	111110010
93354194538	36.330	71.086	33	4.6		AFGHANISTAN-USSR BORDER REGION	111110000
93356103517	-4.938	132.083	33	5.4		WEST IRIAN REGION	111110010
93356194013	38.395	21.759	20	4.3		GREECE	111110010
93357142235	36.756	-2.937	27	5.0	4.9	STRAIT OF GIBRALTAR	111110010
93358051834	-21.853	-178.646	445	5.6		FIJI ISLANDS REGION	111110010

Appendix 1 (continued)

EventID	Lat	Lon	Z	Mb	Ms	Location	Key 123456789
93358215319	40.158	19.815	25	5.2	4.6	ALBANIA	111110010
93359100222	36.590	70.613	195	4.4		HINDU KUSH REGION	111110010
93359101527	34.921	24.217	37	4.8		CRETE	111110000
93359153335	37.467	68.253	33	4.5		AFGHANISTAN-USSR BORDER REGION	111110000
93360084548	38.628	68.926	19	5.0		TAJIK SSR	111110010
93362032943	12.519	125.267	40	5.6	5.6	SAMAR, PHILIPPINE ISLANDS	111110010
93362043521	12.470	125.288	24	5.3	4.8	SAMAR, PHILIPPINE ISLANDS	111110010
93363074814	-20.230	169.789	33	6.1	6.7	VANUATU ISLANDS	111110010
93363083944	-19.990	169.857	33	6.1	6.5	VANUATU ISLANDS	111110010
93363125719	32.003	49.029	79	4.2		WESTERN IRAN	111110000
93364142404	44.735	78.793	15	5.7	5.2	EASTERN KAZAKH SSR	111110010
93365033030	40.169	63.304	33	4.3		UZBEK SSR	111110000
94001051051	28.048	55.565	55	4.8		SOUTHERN IRAN	111110000
94002041211	37.291	71.435	101	5.0		AFGHANISTAN-USSR BORDER REGION	111110010
94003055227	36.028	100.104	8	5.8	5.5	QINGHAI PROVINCE, CHINA	111110010
94003132413	-49.265	164.222	16	6.0	6.0	AUCKLAND ISLANDS REGION	111110010
94003210031	37.002	35.842	26	5.0	4.8	TURKEY	111110010
94004092938	29.188	51.442	30	4.8		SOUTHERN IRAN	111110000
94004193159	-4.301	135.145	11	5.8	6.0	WEST IRIAN REGION	111110010
94005132409	39.085	15.145	273	5.7		SOUTHERN ITALY	111100010
94006022922	37.110	72.005	33	4.8		TAJIK SSR	111100000
94007034242	52.028	159.019	55	5.6		OFF EAST COAST OF KAMCHATKA	111100010
94007092546	34.761	71.211	37	4.7	4.0	PAKISTAN	111100000
94007192353	-0.591	98.601	30	5.6	5.3	SOUTHERN SUMATERA	111100010
94008060411	36.006	70.712	98	4.8		HINDU KUSH REGION	111100000
94009212901	48.482	154.491	65	5.9		KURIL ISLANDS	111100010
94010155350	-13.339	-69.446	596	6.4		PERU-BOLIVIA BORDER REGION	111100010
94011005156	25.231	97.203	10	6.0	5.9	BURMA-CHINA BORDER REGION	111100010
94011021805	25.223	97.128	32	4.6		BURMA-CHINA BORDER REGION	111100000
94011072251	35.959	21.945	33	5.4	5.4	MEDITERRANEAN SEA	111100010
94012010024	30.511	131.637	45	5.0	4.6	KYUSHU, JAPAN	111100010
94012105045	34.797	23.099	10	4.6		CRETE	111100010
94013094306	-17.350	-14.486	10	5.7		SOUTH ATLANTIC RIDGE	111100010
94013235551	37.463	72.083	89	4.7		TAJIK SSR	111100000
94014060748	37.571	20.942	31	4.8		IONIAN SEA	111100000
94015165541	36.659	71.145	210	4.3		AFGHANISTAN-USSR BORDER REGION	111110000
94015170331	-20.849	-173.926	36	5.5	5.6	TONGA ISLANDS	111110010
94016165813	49.106	103.276	12	4.8	4.7	MONGOLIA	111110010
94017123055	34.213	-118.537	18	6.4	6.8	SOUTHERN CALIFORNIA	111110010
94017233330	34.326	-118.698	10	5.7	5.9	SOUTHERN CALIFORNIA	111110010
94019015334	-3.176	135.970	23	6.1	6.8	WEST IRIAN REGION	111110010
94019162648	-17.584	-178.495	533	5.4		FIJI ISLANDS REGION	111110010
94020055010	23.976	121.811	36	5.4	5.3	TAIWAN	111110010
94020090652	-6.002	-77.052	123	5.8		NORTHERN PERU	111110010
94021022429	1.015	127.733	20	6.2	7.2	HALMAHERA	111110010
94021180017	-4.859	103.664	90	6.1		SOUTHERN SUMATERA	111110010
94024195437	44.977	149.791	50	5.4		KURIL ISLANDS	111100010
94025071244	10.601	-41.715	30	5.3	5.9	NORTH ATLANTIC RIDGE	111100010
94025213148	36.421	71.111	223	4.9		AFGHANISTAN-USSR BORDER REGION	111100010
94026100351	41.728	143.669	32	5.5	5.1	HOKKAIDO, JAPAN REGION	111100010
94028115209	38.719	38.688	17	4.4		TURKEY	111100000
94028154524	38.693	27.493	5	5.2	5.1	TURKEY	111100010
94030205743	-29.184	-177.589	61	5.6		KERMADEC ISLANDS	111110010
94031095735	-37.132	52.395	10	5.2	4.8	SOUTH INDIAN OCEAN	111110010
94032093055	17.228	73.523	10	5.0		INDIA	111110010
94032224428	24.778	122.525	133	5.4		TAIWAN REGION	111100010
94033162011	36.363	71.349	75	4.6		AFGHANISTAN-USSR BORDER REGION	111100010
94034102330	-15.413	166.961	23	5.6	5.2	VANUATU ISLANDS	111110010
94034154343	-41.886	84.490	10	5.4	5.4	SOUTHEAST INDIAN RISE	111110010
94036233409	0.593	30.037	14	5.8	6.0	UGANDA	111100010

Appendix 1 (continued)

EventID	Lat	Lon	Z	Mb	Ms	Location	Key 123456789
94039032754	66.512	-19.220	10	5.3	5.3	ICELAND REGION	111100010
94040192708	-21.126	-174.091	26	5.7	5.2	TONGA ISLANDS	111100010
94041022435	39.121	71.580	24	4.7	4.1	TAJIK SSR	111100010
94041061518	36.969	35.828	17	4.9	4.3	TURKEY	111100010
94042174007	42.478	43.726	16	4.5		WESTERN CAUCASUS	111100000
94042211731	-18.773	169.169	206	6.4		VANUATU ISLANDS	111100010
94043041626	-10.786	-128.798	15	6.3	6.6	SOUTH PACIFIC OCEAN	111100010
94043175823	-20.553	169.361	28	6.4	7.1	VANUATU ISLANDS	111100010
94045111427	51.920	158.894	51	5.6	5.5	NEAR EAST COAST OF KAMCHATKA	111100010
94046150817	-20.563	169.393	30	5.8	5.7	VANUATU ISLANDS	111110010
94046170743	-4.967	104.302	23	5.9	7.0	SOUTHERN SUMATERA	111110010
94046210939	36.104	100.164	20	5.6	5.5	QINGHAI PROVINCE, CHINA	111110010
94046222927	44.208	39.427	33	4.6		WESTERN CAUCASUS	111110000
94047064657	-20.094	168.906	13	5.7	6.3	LOYALTY ISLANDS	111110010
94047220308	-20.230	168.925	11	5.7	5.8	LOYALTY ISLANDS	111110010
94048215247	-9.506	152.083	20	5.5	5.6	DENTRECASTEAUX ISLANDS REGION	111110010
94048194156	9.891	125.838	35	5.4	5.0	MINDANAO, PHILIPPINE ISLANDS	011110000
94049041907	-45.330	96.232	10	5.6	6.1	SOUTHEAST INDIAN RISE	111110010
94049125332	14.290	56.233	10	5.0	4.5	ARABIAN SEA	111110000
94049161940	14.133	56.248	10	5.2	4.8	ARABIAN SEA	111110010
94050031308	29.991	67.845	33	4.6		PAKISTAN	111110010
94051015435	2.059	126.475	28	5.6	5.6	MOLUCCA PASSAGE	111110010
94051214812	13.691	120.787	207	5.6		MINDORO, PHILIPPINE ISLANDS	111110010
94054080204	30.853	60.596	6	6.1	6.1	IRAN	111110010
94054115433	30.765	60.519	10	5.3	4.9	IRAN	111110010
94054224517	30.767	60.480	10	5.4		IRAN	111110010
94055001112	30.775	60.495	10	6.1	6.1	IRAN	111110010
94055004500	30.869	60.510	10	4.5		IRAN	111110000
94055100922	36.488	70.014	193	4.8		HINDU KUSH REGION	111110010
94055152535	-17.421	-174.287	124	5.7		TONGA ISLANDS	111110000
94055205131	30.924	60.446	10	4.7	4.4	IRAN	111110010
94056004029	-17.420	-174.271	121	5.6		TONGA ISLANDS	111110000
94056023051	38.854	20.532	36	5.3	5.1	GREECE	111110010
94057023111	30.897	60.549	9	5.8	6.0	IRAN	111110010
94057180228	30.825	60.376	10	4.5		IRAN	111110000
94058090427	30.832	131.427	40	4.9	5.0	KYUSHU, JAPAN	111110010
94059111354	30.805	60.562	10	5.5	5.5	IRAN	111110010
94060034900	29.096	52.617	13	5.8	6.0	SOUTHERN IRAN	111110010
94060190132	28.941	52.855	33	4.4		SOUTHERN IRAN	111110000
94061130009	36.434	69.826	24	4.8	4.2	HINDU KUSH REGION	111110010
94061145722	30.844	60.460	33	4.6		IRAN	111110000
94062145648	27.920	57.234	33	4.7		SOUTHERN IRAN	111110000
94062151048	33.134	48.394	33	4.3	4.1	WESTERN IRAN	111110000
94062235401	28.900	52.465	33	4.9	3.9	SOUTHERN IRAN	111110000
94064040352	36.579	68.659	27	5.1	4.4	HINDU KUSH REGION	111110010
94065080143	-21.556	-113.701	10	5.6	5.7	EASTER ISLAND CORDILLERA	111110010
94066105457	33.146	48.033	26	4.8	4.2	WESTERN IRAN	111110000
94066172900	36.475	71.075	194	4.4		AFGHANISTAN-USSR BORDER REGION	111110010
94068061337	32.625	47.150	10	4.5		IRAN-IRAQ BORDER REGION	111110000
94068120834	-9.580	154.986	38	5.7	5.6	DENTRECASTEAUX ISLANDS REGION	111110010
94068165837	-9.444	159.604	10	5.6	5.4	SOLOMON ISLANDS	111110000
94068232806	-18.039	-178.413	563	6.6		FIJI ISLANDS REGION	111110010
94069122543	-18.058	-178.260	600	5.2		FIJI ISLANDS REGION	111110000
94072031128	51.343	-178.231	33	5.3	4.4	ANDREANOF ISLANDS, ALEUTIAN IS.	111110010
94073043007	-1.083	-23.929	10	6.0		CENTRAL MID-ATLANTIC RIDGE	111110000
94073205124	15.994	-92.428	164	5.8	6.2	MEXICO-GUATEMALA BORDER REGION	111110010
94074033619	11.110	-88.083	15	5.8	5.6	OFF COAST OF CENTRAL AMERICA	111110010
94074214615	36.800	54.780	33	4.4		IRAN	111010000
94076080616	28.941	52.536	33	4.8		SOUTHERN IRAN	111010000
94077035110	29.035	52.491	33	4.4		SOUTHERN IRAN	111010000

EventID	Lat	Lon	Z	Mb	Ms	Location	Key 123456789
94078012444	51.500	159.290	33	5.3	5.2	OFF EAST COAST OF KAMCHATKA	111010010
94078045400	28.633	53.129	33	4.4		SOUTHERN IRAN	111010000
94078055704	28.727	52.588	33	4.4		SOUTHERN IRAN	111010000
94082171445	28.874	52.596	33	4.7		SOUTHERN IRAN	111010010
94085152224	39.506	55.155	33	4.3		TURKMEN SSR	111010000
94085215101	33.437	141.289	38	5.4		OFF EAST COAST OF HONSHU, JAPAN	111010000
94086134512	-10.326	161.153	54	5.4	5.2	SOLOMON ISLANDS	111010000
94088075653	29.096	51.256	33	5.4		SOUTHERN IRAN	111010010
94088112041	30.695	70.385	33	4.6		PAKISTAN	111010000
94089132911	9.003	126.254	40	5.9	5.3	MINDANAO, PHILIPPINE ISLANDS	111010010
94089195546	28.994	52.745	54	5.5		SOUTHERN IRAN	111010010
94090224052	-22.057	-179.533	580	6.1		SOUTH OF FIJI ISLANDS	101010010
94091142459	28.823	52.650	33	4.6		SOUTHERN IRAN	101010000
94093065157	28.821	52.745	23	5.2	4.8	SOUTHERN IRAN	101010010
94093071936	28.887	52.705	33	4.7		SOUTHERN IRAN	101010000
94093130351	30.134	68.015	33	4.4		PAKISTAN	101010000
94093224937	36.420	67.212	21	4.8	4.7	HINDU KUSH REGION	101010010
94094013702	-15.468	-173.014	24	5.7	5.5	TONGA ISLANDS	101010010
94094152833	36.194	66.826	33	4.5		HINDU KUSH REGION	101010010
94094183547	37.017	71.382	80	4.7		AFGHANISTAN-USSR BORDER REGION	101010000
94095093544	51.296	-178.152	20	5.8	6.0	ANDREANOF ISLANDS, ALEUTIAN IS.	101010010
94096070327	26.188	96.867	33	5.6	5.6	BURMA	101010010
94096121344	-17.371	167.816	17	5.6	5.9	VANUATU ISLANDS	101010010
94096211832	28.740	34.645	10	4.6		ARAB REPUBLIC OF EGYPT	101010000
94098011040	40.608	143.683	13	6.0	6.3	OFF EAST COAST OF HONSHU, JAPAN	101010010
94100134047	43.049	46.180	86	4.7		EASTERN CAUCASUS	101010010
94100194620	39.982	23.620	20	4.7	4.6	AEGEAN SEA	101010010
94100234555	23.710	126.852	10	5.9	5.8	RYUKYU ISLANDS REGION	101010010
94101112021	11.735	42.859	16	5.6	5.7	ETHIOPIA	101010010
94102001717	44.515	146.612	123	5.4		KURIL ISLANDS	101010010
94102111442	34.956	24.074	13	4.7		CRETE	101010000
94103040047	22.775	123.628	10	5.7	5.6	SOUTHEAST OF TAIWAN	101010010
94103141923	-33.975	-108.801	10	5.0	5.5	EASTER ISLAND CORDILLERA	101010010
94103222229	-3.136	135.968	29	6.0	6.3	WEST IRIAN REGION	101010010
94104032826	-6.587	129.771	166	5.8		BANDA SEA	101010010
94104100805	29.158	51.592	33	4.5		SOUTHERN IRAN	111010000
94104110340	28.290	55.340	22	5.2		SOUTHERN IRAN	111010010
94104112637	28.237	55.288	20	4.6		SOUTHERN IRAN	111010000
94104201539	-7.015	155.885	40	5.7	5.1	SOLOMON ISLANDS	111010000
94107054651	37.042	71.485	129	4.5		AFGHANISTAN-USSR BORDER REGION	111010010
94107080232	41.948	46.317	33	5.0	4.6	EASTERN CAUCASUS	111010010
94108162955	-34.531	-71.897	5	0.0		NEAR COAST OF CENTRAL CHILE	111010000
94108172954	-6.470	154.934	26	6.6	6.7	SOLOMON ISLANDS	111010010
94108200735	36.319	70.922	134	5.0		HINDU KUSH REGION	111010010
94109161455	31.432	49.536	17	4.8	4.4	WESTERN IRAN	111010000
94110000508	28.294	55.326	24	4.8		SOUTHERN IRAN	111010010
94110233530	-17.800	-178.404	543	5.6		FIJI ISLANDS REGION	111010010
94111024215	-5.617	154.067	38	5.5	5.5	SOLOMON ISLANDS	111010010
94111035144	-5.702	154.120	28	5.9	6.6	SOLOMON ISLANDS	111010010
94111115032	27.477	54.385	33	4.6		SOUTHERN IRAN	111010000
94113150052	-14.175	167.537	11	6.0	6.0	VANUATU ISLANDS	111010000
94114025710	11.604	43.014	10	5.3	4.9	ETHIOPIA	111010000
94115001905	60.899	-151.142	68	5.4		KENAI PENINSULA, ALASKA	111010000
94116185927	56.727	117.867	18	5.3	5.4	EAST OF LAKE BAIKAL	111010010
94117092326	-21.515	-173.667	28	6.2	6.1	TONGA ISLANDS	111010010
94117141145	13.074	119.545	10	5.8	5.8	PHILIPPINE ISLANDS REGION	111010010
94118164454	-39.312	-74.756	27	5.7	5.0	OFF COAST OF CENTRAL CHILE	111010010
94119071129	-28.299	-63.252	562	6.3		SANTIAGO DEL ESTERO PROV., ARG.	111010010
94120032838	31.420	131.292	26	5.7	5.6	KYUSHU, JAPAN	111010000
94121120035	36.901	67.163	19	6.0	6.3	HINDU KUSH REGION	111010000

Appendix 1 (continued)

EventID	Lat	Lon	Z	Mb	Ms	Location	Key 123456789
94121211720	39.126	71.621	33	5.2	4.6	TAJIK SSR	111010000
94122171400	-1.116	97.487	15	6.2	5.8	SOUTHWEST OF SUMATERA	111010010
94122181405	40.306	43.130	59	4.5		TURKEY-USSR BORDER REGION	111010000
94123163643	10.241	-60.758	36	5.8	5.8	TRINIDAD	111010010
94123202018	33.501	47.384	33	4.4		WESTERN IRAN	111010000
94124063736	-17.047	168.265	206	5.8		VANUATU ISLANDS	101010010
94124114721	51.518	-168.518	33	5.5	4.7	FOX ISLANDS, ALEUTIAN ISLANDS	101010010
94125051449	64.578	-17.482	9	5.7	5.2	ICELAND	101010010
94125111853	37.648	72.040	33	4.5		TAJIK SSR	101010000
94126042439	40.109	73.611	33	4.7		KIRGHIZ SSR	101010010
94126182037	-59.982	-18.550	10	5.4	5.7	SOUTHWESTERN ATLANTIC OCEAN	101010010
94126223926	-4.681	153.099	49	5.8	5.5	NEW IRELAND REGION	101010010
94127142444	30.329	50.586	54	4.7		IRAN	101010000
94128034825	-56.381	147.096	10	5.2	5.1	WEST OF MACQUARIE ISLAND	101010010
94129091411	40.263	78.938	46	4.8	4.7	SOUTHERN XINJIANG, CHINA	101010010
94129123637	-2.060	99.731	28	6.0	5.5	SOUTHERN SUMATERA	101010010
94130014903	-19.613	-69.792	52	5.8		NORTHERN CHILE	101010010
94130062653	5.234	125.971	111	4.6		MINDANAO, PHILIPPINE ISLANDS	101010010
94130181912	13.433	120.603	70	5.7		MINDORO, PHILIPPINE ISLANDS	101010000
94131081815	-2.008	99.770	21	6.0	6.3	SOUTHERN SUMATERA	101010010
94131114111	37.471	72.327	130	4.2		TAJIK SSR	101010000
94131211433	-2.056	99.669	28	5.9	5.9	SOUTHERN SUMATERA	101010010
94133201227	7.972	123.189	33	5.6	5.6	MINDANAO, PHILIPPINE ISLANDS	101010010
94134223434	15.207	42.055	10	5.0	4.7	WESTERN ARABIAN PENINSULA	101010010
94135034457	-48.993	73.666	10	5.8	5.7	KERGUELEN ISLANDS REGION	101010010
94137094613	-1.902	99.618	33	5.7	5.6	SOUTHERN SUMATERA	101010010
94138035400	44.727	149.401	26	6.0	5.9	KURIL ISLANDS	101010010
94138165609	29.038	142.295	33	5.3	5.1	SOUTH OF HONSHU, JAPAN	101010010
94138171852	41.133	43.982	10	4.5		TURKEY-USSR BORDER REGION	101010000
94139234143	-8.204	124.813	33	5.4		TIMOR	101010010
94140164000	25.099	128.829	37	5.7	5.1	RYUKYU ISLANDS	101010010
94142191233	12.405	57.834	10	4.5	4.7	ARABIAN SEA	101010000
94143014142	18.165	-100.527	55	6.0		GUERRERO, MEXICO	101010010
94143053601	24.166	122.535	20	5.7	6.0	TAIWAN REGION	101010000
94143064616	35.559	24.727	76	6.0		CRETE	101010000
94143150448	14.657	54.465	10	4.5		ARABIAN SEA	101010000
94143151657	24.065	122.560	26	6.0	5.8	TAIWAN REGION	101010010
94144020536	38.664	26.542	17	5.0	5.3	AEGEAN SEA	101010010
94144040042	23.959	122.448	16	6.2	6.7	TAIWAN REGION	101010010
94144211319	56.170	161.169	95	5.9		NEAR EAST COAST OF KAMCHATKA	101010010
94145040341	-4.199	135.489	33	6.0	6.4	WEST IRIAN REGION	101010010
94145074258	40.232	63.134	33	5.2		UZBEK SSR	101010010
94145111515	35.560	71.344	33	4.2	4.4	PAKISTAN	101010000
94145163653	-1.962	138.805	28	5.5	5.1	NEAR N. COAST OF WEST IRIAN	101010000
94145184219	7.646	94.279	25	5.7	5.5	NICOBAR ISLANDS REGION	101010000
94146034627	39.805	69.833	33	4.7		TAJIK SSR	101010000
94146082652	35.305	-4.103	10	5.7	5.8	STRAIT OF GIBRALTAR	101010000
94146233542	14.768	54.842	10	5.0		ARABIAN SEA	101010000
94147024952	15.119	57.771	10	4.6		ARABIAN SEA	101010000
94147044911	37.049	72.498	150	4.5		TAJIK SSR	101010000
94148080432	35.406	136.134	49	5.1	4.4	SOUTHERN HONSHU, JAPAN	101010010
94148090350	37.750	72.737	33	4.3		TAJIK SSR	101010000
94149141150	20.556	94.160	36	6.2	6.2	BURMA	101000010
94151174155	7.414	-72.033	12	6.3	5.6	NORTHERN COLOMBIA	101000010
94152113308	38.307	39.463	10	4.3		TURKEY	101000000
94153181734	-10.477	112.835	18	5.7	7.2	SOUTH OF JAVA	101000010
94154112506	3.524	-78.778	9	5.9	5.1	SOUTH OF PANAMA	101000010
94154155311	36.817	71.346	33	4.7		AFGHANISTAN-USSR BORDER REGION	101000000
94154210659	-10.362	112.892	26	6.1	6.4	SOUTH OF JAVA	101000010
94154224021	28.736	70.070	33	5.9	5.6	PAKISTAN	101000010

Appendix 1 (continued)

EventID	Lat	Lon	Z	Mb	Ms	Location	Key 123456789
94155005750	-10.777	113.366	11	6.0	6.3	SOUTH OF JAVA	101000010
94155103856	36.821	54.747	33	4.6		IRAN	101000000
94155113636	-10.831	113.225	34	5.6	5.1	SOUTH OF JAVA	101000010
94155200934	-10.826	113.199	30	5.7	5.1	SOUTH OF JAVA	101000010
94156010930	24.511	121.905	11	6.1	6.6	TAIWAN	101000010
94156014502	-10.349	113.398	26	5.8		SOUTH OF JAVA	101000000
94156165408	29.601	52.313	33	4.5		SOUTHERN IRAN	101000000
94157080238	36.333	71.413	33	4.7		AFGHANISTAN-USSR BORDER REGION	101000000
94157090300	28.598	129.099	60	5.8		RYUKYU ISLANDS	101000010
94157204740	2.917	-76.057	12	6.4	6.6	COLOMBIA	101000010
94157222223	38.849	71.581	33	4.5		AFGHANISTAN-USSR BORDER REGION	101000000
94158183142	-5.792	104.436	42	5.7		SOUTHERN SUMATERA	101000010
94160003316	-13.841	-67.553	631	7.0		NORTHERN BOLIVIA	101000010
94160011517	-14.365	-68.439	650	6.1		PERU-BOLIVIA BORDER REGION	101000000
94160162222	13.259	124.281	76	5.8		LUZON, PHILIPPINE ISLANDS	101000010
94160203650	36.945	71.325	87	5.4		AFGHANISTAN-USSR BORDER REGION	101000010
94161030044	38.560	70.629	33	5.4	4.6	AFGHANISTAN-USSR BORDER REGION	101000010
94161062557	41.527	88.710	0	5.8		SOUTHERN XINJIANG, CHINA	101000010
94161213950	27.995	140.700	28	5.4	5.0	BONIN ISLANDS REGION	101000000
94162093756	29.070	52.537	18	4.8	4.2	SOUTHERN IRAN	101000010
94162161903	36.223	70.229	133	4.7		HINDU KUSH REGION	101000010
94164100749	29.162	52.625	33	4.2		SOUTHERN IRAN	101000000
94164210409	-10.285	113.491	24	5.7	5.6	SOUTH OF JAVA	101000010
94166092257	-10.335	113.660	20	6.0	6.1	SOUTH OF JAVA	101000010
94166165301	37.596	30.075	8	4.4		TURKEY	101000000
94167101246	-7.391	128.125	109	6.0		BANDA SEA	101000010
94167184128	-15.250	-70.294	200	5.6		SOUTHERN PERU	101000000
94169032515	-42.963	171.658	14	6.2	7.1	SOUTH ISLAND, NEW ZEALAND	100000010
94169124200	28.971	52.673	11	5.1		SOUTHERN IRAN	101000010
94169223819	-10.150	113.632	46	5.6	5.0	SOUTH OF JAVA	101000010
94170134351	-43.273	171.611	10	5.7	5.9	SOUTH ISLAND, NEW ZEALAND	101000010
94171090902	28.968	52.614	9	5.9	5.7	SOUTHERN IRAN	101001010
94171104434	29.131	52.388	33	4.5		SOUTHERN IRAN	101001000
94172041552	29.021	52.596	41	4.7		SOUTHERN IRAN	011001010
94172031754	29.151	52.554	33	4.4	4.5	SOUTHERN IRAN	001001000
94173065858	28.754	53.051	10	4.3		SOUTHERN IRAN	111001000
94174201128	37.697	37.077	10	4.2		TURKEY	111001000
94175013236	30.252	52.006	33	4.0		IRAN	111001000
94176050046	41.777	43.697	33	4.4		TURKEY-USSR BORDER REGION	111100000
94176083806	43.883	147.213	66	5.3		KURIL ISLANDS	111100000
94176104416	39.386	72.707	33	4.7		KIRGHIZ SSR	111100000
94178120303	-16.122	67.484	10	5.1	4.5	MID-INDIAN RISE	111100100
94180182233	32.567	93.673	10	5.9	5.6	TIBET	111100110
94181092321	36.326	71.130	227	6.1		AFGHANISTAN-USSR BORDER REGION	111100110
94181095509	40.941	50.609	33	4.9		CASPIAN SEA	111100100
94182101241	40.232	53.383	41	6.0	5.2	TURKMEN SSR	111100110
94182130555	27.645	56.514	44	5.0	4.2	SOUTHERN IRAN	111100110
94182195004	40.219	53.391	44	5.6		TURKMEN SSR	111100110
94182200231	38.267	38.824	10	4.7		TURKEY	111100110
94183091443	-5.763	131.103	88	5.9		BANDA SEA	111100110
94183204532	36.714	68.707	33	4.8		HINDU KUSH REGION	111100110
94183210726	36.743	68.650	57	4.7		HINDU KUSH REGION	111100110
94184142641	28.742	34.573	15	4.3		ARAB REPUBLIC OF EGYPT	111100110
94184214444	-48.219	31.542	10	5.2	4.8	SOUTH OF AFRICA	111100100
94185213641	14.888	-97.322	15	6.1	6.1	OFF COAST OF OAXACA, MEXICO	111100110
94186100922	10.432	125.322	29	5.5	5.5	LEYTE, PHILIPPINE ISLANDS	111100110
94187091310	5.983	125.929	151	5.7		MINDANAO, PHILIPPINE ISLANDS	111100110
94187121925	37.024	71.645	33	4.8		AFGHANISTAN-USSR BORDER REGION	111100110
94188193126	44.359	79.130	33	4.4		EASTERN KAZAKH SSR	111100110
94189171014	0.256	66.740	10	5.1	4.8	CARLSBERG RIDGE	111100110

Appendix 1 (continued)

EventID	Lat	Lon	Z	Mb	Ms	Location	Key 123456789
94190155758	-37.217	-95.101	26	5.4	5.1	SOUTHERN PACIFIC OCEAN	111100110
94191231406	36.478	70.150	230	4.8		HINDU KUSH REGION	111100110
94192205737	37.541	54.474	29	4.8	4.3	IRAN-USSR BORDER REGION	111100110
94193001216	37.774	54.611	33	4.6		IRAN-USSR BORDER REGION	111100100
94193043505	36.411	71.056	248	4.6		AFGHANISTAN-USSR BORDER REGION	111100110
94194002514	-16.644	167.469	33	5.4	5.1	VANUATU ISLANDS	111100110
94194023556	-16.620	167.518	33	6.4	7.3	VANUATU ISLANDS	111100110
94194052343	29.875	51.195	33	4.5		SOUTHERN IRAN	111100100
94194114523	-7.532	127.770	159	6.5		BANDA SEA	111100110
94195000924	-16.582	167.452	20	5.6	5.9	VANUATU ISLANDS	111100110
94195201351	28.070	55.489	33	4.6		SOUTHERN IRAN	111100100
94197180505	-4.619	125.615	443	5.8		BANDA SEA	111100100
94199154416	38.713	20.435	10	4.8		GREECE	111000100
94199163359	-9.591	112.939	33	5.6	5.0	SOUTH OF JAVA	111000110
94200040549	37.563	71.958	33	4.8		AFGHANISTAN-USSR BORDER REGION	111000100
94200115944	-23.438	-175.470	50	5.3	5.7	TONGA ISLANDS REGION	111000110
94202183631	42.340	132.865	471	6.5		NEAR E. COAST OF EASTERN USSR	111000100
94203165748	-7.777	158.417	19	5.9	5.9	SOLOMON ISLANDS	111000100
94204070814	37.438	54.413	31	4.9		IRAN-USSR BORDER REGION	111000100
94204205759	31.068	86.549	16	5.1	5.0	TIBET	111000110
94205054710	40.402	63.680	33	4.1		UZBEK SSR	111000100
94205144748	37.006	71.662	120	5.6		AFGHANISTAN-USSR BORDER REGION	111000110
94205175540	-16.966	167.574	21	5.9	6.5	VANUATU ISLANDS	111000110
94205215727	-10.654	113.269	34	6.0		SOUTH OF JAVA	111000110
94206220022	-56.362	-27.365	81	6.3		SOUTH SANDWICH ISLANDS REGION	111000100
94207014633	-10.263	113.590	33	5.7		SOUTH OF JAVA	111000110
94207180141	28.481	52.122	33	4.2		SOUTHERN IRAN	111000100
94208133937	36.438	71.198	129	4.5		AFGHANISTAN-USSR BORDER REGION	111000110
94209080301	-47.278	100.224	10	5.3	5.7	SOUTHEAST INDIAN RISE	111000110
94210001745	52.398	-168.333	11	6.0	5.6	FOX ISLANDS, ALEUTIAN ISLANDS	111000110
94210075328	-16.984	167.739	14	5.7	5.8	VANUATU ISLANDS	111000110
94210220627	36.417	71.087	118	4.5		AFGHANISTAN-USSR BORDER REGION	111000110
94211103745	37.493	36.189	10	4.7		TURKEY	111000110
94211212125	40.890	142.596	57	5.1		NEAR EAST COAST OF HONSHU, JAPAN	111000100
94212051539	32.558	48.369	43	5.3	5.3	WESTERN IRAN	111000110
94214141752	52.428	158.044	145	6.0		NEAR EAST COAST OF KAMCHATKA	111000110
94215145957	21.514	93.981	34	5.7	5.1	BURMA	111000110
94216221537	-6.338	131.575	33	6.2	5.6	TANIMBAR ISLANDS REGION	111000110
94217111910	26.651	92.522	33	4.8		EASTERN INDIA	111000110
94218210214	26.991	54.363	16	5.3		SOUTHERN IRAN	111000110
94219063254	27.106	54.469	44	4.7		SOUTHERN IRAN	111000110
94220210831	24.721	95.200	122	6.0		BURMA	111000110
94222021115	26.951	54.352	44	4.8	4.4	SOUTHERN IRAN	111000110
94222145749	-58.756	-25.538	33	5.6	5.0	SOUTH SANDWICH ISLANDS REGION	111000100
94223064632	27.035	54.469	25	5.2	4.5	SOUTHERN IRAN	111000110
94223204208	-21.600	-173.768	31	5.9	5.4	TONGA ISLANDS	111000110
94224205805	37.171	69.878	33	4.2		AFGHANISTAN-USSR BORDER REGION	111000100
94226004620	44.709	150.103	17	6.0	5.9	KURIL ISLANDS REGION	111000110
94226013112	44.694	150.011	19	6.2	6.1	KURIL ISLANDS REGION	111000110
94226090652	38.794	142.075	44	5.4	5.3	NEAR EAST COAST OF HONSHU, JAPAN	111000110
94227061539	16.751	-60.739	33	5.1	5.0	LEEWARD ISLANDS	111000110
94228100932	37.842	142.462	20	5.9	5.2	OFF EAST COAST OF HONSHU, JAPAN	111000110
94229071129	36.606	71.129	145	4.4		AFGHANISTAN-USSR BORDER REGION	111000110
94230004547	-7.433	31.751	25	6.0	5.7	LAKE TANGANYIKA REGION	111000110
94230011305	35.520	-0.106	9	5.7	5.9	ALGERIA	111000110
94230044257	44.767	150.158	15	6.2	6.5	KURIL ISLANDS REGION	111000110
94230122947	39.217	72.097	33	4.1		KIRGHIZ SSR	111000100
94231100251	-26.642	-63.421	564	6.4		SANTIAGO DEL ESTERO PROV., ARG.	111000110
94231210245	17.974	96.415	12	5.6	5.6	BURMA	111000110
94232022111	44.606	149.325	23	6.0	5.2	KURIL ISLANDS	111000110

Appendix 1 (continued)

EventID	Lat	Lon	Z	Mb	Ms	Location	Key 123456789
94232043850	44.656	149.176	24	6.2	6.1	KURIL ISLANDS	111000110
94233020633	37.891	69.944	33	4.3		AFGHANISTAN-USSR BORDER REGION	011000110
94233155559	56.761	117.900	12	5.8	5.8	EAST OF LAKE BAIKAL	011000110
94234124116	70.922	-6.103	10	5.3	4.9	JAN MAYEN ISLAND REGION	011000110
94234172637	-11.509	166.452	142	6.2		SANTA CRUZ ISLANDS	011000110
94235120543	36.542	70.396	33	4.8		HINDU KUSH REGION	011000100
94235141831	40.041	78.818	33	5.0	5.0	SOUTHERN XINJIANG, CHINA	010000110
94236012826	52.302	160.336	32	5.4	4.7	OFF EAST COAST OF KAMCHATKA	010000100
94236151740	-25.076	-13.594	10	5.3	4.8	SOUTH ATLANTIC RIDGE	010000110
94237012446	42.771	145.049	72	5.4		HOKKAIDO, JAPAN REGION	010000100
94238033814	33.120	56.052	33	4.4		IRAN	010000100
94240183720	44.783	150.061	19	6.1	6.6	KURIL ISLANDS REGION	010000110
94241173620	-0.404	-19.172	10	5.5	5.3	CENTRAL MID-ATLANTIC RIDGE	010000100
94242061335	44.737	150.117	51	6.2	5.6	KURIL ISLANDS REGION	010000110
94242194246	-6.965	124.111	596	5.9		BANDA SEA	010000100
94243090725	43.719	146.013	76	6.0		KURIL ISLANDS	010000110
94244151553	40.402	-125.680	10	6.6	7.0	OFF COAST OF NORTHERN CALIFORNIA	010000110
94244161240	41.183	21.196	14	5.8		YUGOSLAVIA	010000110
94245232940	33.529	48.861	49	4.4		WESTERN IRAN	010000110
94246090253	-31.422	-111.028	7	5.8	5.4	EASTER ISLAND REGION	010000110
94246174641	-21.212	173.640	33	5.8	6.2	VANUATU ISLANDS REGION	010000110
94247022802	37.471	69.971	33	4.9		AFGHANISTAN-USSR BORDER REGION	010000110
94247071503	36.517	70.445	194	4.9		HINDU KUSH REGION	010000100
94247145034	35.941	100.080	11	5.3	4.4	QINGHAI PROVINCE, CHINA	010000110
94248052615	29.419	51.283	33	5.0		SOUTHERN IRAN	010000110
94248191317	41.905	46.231	62	4.7		EASTERN CAUCASUS	010000110
94248221347	46.782	155.226	12	5.9		KURIL ISLANDS REGION	010000110
94250135625	38.491	90.345	33	5.1	4.7	SOUTHERN XINJIANG, CHINA	010000110
94251092057	37.125	69.949	33	4.9		AFGHANISTAN-USSR BORDER REGION	010000110
94251133336	28.030	61.837	77	5.1		SOUTHERN IRAN	010000110
94252135004	36.739	70.297	33	4.8		HINDU KUSH REGION	010000100
94253045410	7.552	126.599	79	5.6		MINDANAO, PHILIPPINE ISLANDS	010000100
94254013203	19.586	99.516	33	5.1	4.6	SOUTHEAST ASIA	010000110
94255062954	-31.103	-71.706	40	5.9	5.7	NEAR COAST OF CENTRAL CHILE	010000110
94255113014	-8.910	106.476	33	5.9	5.2	SOUTH OF JAVA	010000100
94256042801	29.287	129.910	34	5.8	6.2	RYUKYU ISLANDS	010000110
94256100132	7.054	-76.678	14	5.8	5.6	NORTHERN COLOMBIA	010000110
94259062018	22.528	118.711	13	6.5	6.7	TAIWAN REGION	010000110
94260022437	37.885	41.584	9	5.1		TURKEY	010000110
94260085753	26.450	55.601	33	4.7		SOUTHERN IRAN	010000110
94261102715	38.563	71.733	33	4.6	3.9	AFGHANISTAN-USSR BORDER REGION	010000100
94262152342	42.631	43.049	33	4.4		WESTERN CAUCASUS	010000110
94263055146	32.501	48.770	33	5.0	4.4	WESTERN IRAN	010000110
94264085323	42.465	43.535	33	4.4		WESTERN CAUCASUS	010000110
94266023755	37.184	142.123	25	5.4	5.0	OFF EAST COAST OF HONSHU, JAPAN	010000100
94266075938	-3.379	148.537	33	5.7	6.0	BISMARCK SEA	010000110
94270143253	31.661	49.176	42	4.5		WESTERN IRAN	010000110
94273025616	36.412	71.067	242	4.7		AFGHANISTAN-USSR BORDER REGION	010000110
94273025716	37.551	75.025	33	5.0		TAJIK-XINJIANG BORDER REGION	010000100
94274082514	27.149	57.548	46	5.0		SOUTHERN IRAN	110001110
94274140420	13.116	50.416	10	4.9	4.4	EASTERN GULF OF ADEN	110001110
94274163520	-17.745	167.682	17	5.9	6.5	VANUATU ISLANDS	110001110
94274174637	-17.768	167.830	33	5.8	6.3	VANUATU ISLANDS	110001100
94275162016	38.554	73.888	125	4.7		TAJIK-XINJIANG BORDER REGION	100001010
94276022245	32.763	48.880	67	4.6		WESTERN IRAN	110001100
94277120940	-6.218	104.891	24	5.6	4.7	SUNDA STRAIT	100001100
94277132255	43.773	147.321	14	7.3	8.1	KURIL ISLANDS	100001100
94277152415	43.526	147.908	20	6.3		KURIL ISLANDS	101001100
94277160102	43.706	147.991	16	6.3		KURIL ISLANDS	101001100
94277191628	43.774	147.504	35	6.0	5.6	KURIL ISLANDS	101001100

Appendix 1 (continued)

EventID	Lat	Lon	Z	Mb	Ms	Location	Key 123456789
94278040047	43.398	148.078	40	5.8	5.6	KURIL ISLANDS REGION	101001110
94278203948	43.954	147.336	40	6.2	5.5	KURIL ISLANDS	101001110
94279074635	43.239	148.061	33	5.3	5.6	KURIL ISLANDS REGION	101001000
94279154214	-56.628	-141.923	10	5.8	5.2	SOUTH PACIFIC CORDILLERA	101001110
94280023609	43.614	147.289	52	6.1		KURIL ISLANDS	101001110
94280032558	41.662	88.753	0	6.0		SOUTHERN XINJIANG, CHINA	101001110
94280070052	43.117	146.866	55	5.5		KURIL ISLANDS	101001010
94280152403	42.877	146.063	24	6.0	5.2	OFF COAST OF HOKKAIDO, JAPAN	101001110
94281052826	43.319	146.676	26	5.6	5.0	KURIL ISLANDS	101001000
94281095434	43.873	148.171	9	5.9		KURIL ISLANDS REGION	101001110
94281214407	-1.258	127.980	17	6.4	6.8	HALMAHERA	101001110
94282075539	43.905	147.916	33	6.5	7.1	KURIL ISLANDS	101001110
94282122422	43.883	147.341	46	5.8	5.5	KURIL ISLANDS	101001110
94282190843	39.907	77.117	40	4.9	4.5	SOUTHERN XINJIANG, CHINA	101001010
94283210653	51.484	-173.897	33	5.6	5.2	ANDREANOF ISLANDS, ALEUTIAN IS.	101001110
94284013720	-32.100	-71.447	47	5.7	5.4	NEAR COAST OF CENTRAL CHILE	101001100
94284203117	33.558	45.678	18	4.7		IRAN-IRAQ BORDER REGION	101001110
94285060249	13.765	124.538	27	5.5	5.7	LUZON, PHILIPPINE ISLANDS	101001010
94285064339	13.773	124.529	16	5.8	6.1	LUZON, PHILIPPINE ISLANDS	101001110
94285074401	42.371	44.430	10	4.3		WESTERN CAUCASUS	101001100
94285103322	51.605	-173.770	33	5.1	4.8	ANDREANOF ISLANDS, ALEUTIAN IS.	101001000
94286050424	-1.212	127.912	11	6.1	6.3	HALMAHERA	101001110
94286231957	40.381	52.975	33	4.3		TURKMEN SSR	101001100
94286233127	45.493	21.004	10	4.7		ROMANIA	101001000
94288003925	-3.804	152.148	9	5.6	6.1	NEW IRELAND REGION	101001100
94289051000	45.749	149.167	117	6.4		KURIL ISLANDS	101001100
94289100952	38.089	56.703	33	4.5		IRAN-USSR BORDER REGION	101001100
94291171250	43.576	147.097	60	6.2		KURIL ISLANDS	101001100
94293011516	-39.187	-70.811	162	5.8		ARGENTINA	101001100
94294050621	36.391	69.708	47	5.4	5.3	HINDU KUSH REGION	101001100
94294114627	38.250	56.955	33	4.9		IRAN-USSR BORDER REGION	101001100
94297192627	43.084	147.096	57	5.7		KURIL ISLANDS	101001100
94298005434	36.359	70.957	239	5.9		HINDU KUSH REGION	101001100
94298133026	43.771	147.698	35	5.5	4.8	KURIL ISLANDS	101001100
94300131911	31.430	49.409	33	4.6		WESTERN IRAN	101001100
94300174558	43.515	-127.427	20	5.6	6.0	OFF COAST OF OREGON	101001100
94300222028	-25.778	179.339	519	5.9		SOUTH OF FIJI ISLANDS	101001100
94301091120	14.537	-103.755	33	5.2	5.5	OFF COAST OF GUERRERO, MEXICO	101001100
94303060627	-28.032	26.738	5	5.6	4.7	REPUBLIC OF SOUTH AFRICA	101000100
94303081129	-6.183	129.446	264	5.6		BANDA SEA	101000100
94304114813	3.019	96.192	29	5.7	6.2	NORTHERN SUMATERA	101000100
94304225926	9.037	-83.323	56	5.6		COSTA RICA	101000100
94305080802	-1.432	67.947	10	5.0	5.2	CARLSBERG RIDGE	101000100
94306014355	5.099	118.643	55	5.7		KALIMANTAN	101000100
94306123101	38.152	48.315	10	5.0		N.W. IRAN-USSR BORDER REGION	101000100
94307114333	28.260	52.203	33	4.9	4.4	SOUTHERN IRAN	101000100
94308011320	-9.379	-71.334	591	5.8		PERU-BRAZIL BORDER REGION	101000100
94309021603	-57.193	157.858	25	6.1	6.1	MACQUARIE ISLANDS REGION	101000100
94309120528	-9.386	-71.335	597	5.7		PERU-BRAZIL BORDER REGION	101000100
94312053122	43.271	86.960	33	5.0		NORTHERN XINJIANG, CHINA	101000100
94313182102	43.556	147.144	54	6.2	5.2	KURIL ISLANDS	101000100
94315084829	-15.626	-72.535	121	5.6		SOUTHERN PERU	101000100
94317065600	36.910	29.060	10	4.9	5.0	TURKEY	101000100
94318191530	13.525	121.067	32	6.1	7.1	MINDORO, PHILIPPINE ISLANDS	101000100
94319201811	-5.589	110.186	561	6.2		JAVA SEA	101000100
94323021801	27.818	56.887	33	4.6		SOUTHERN IRAN	101000100
94324025701	14.769	55.609	10	5.0		ARABIAN SEA	101000100
94324025715	-9.794	159.712	24	5.8	5.5	SOLOMON ISLANDS	101000100
94324143102	35.335	39.557	29	5.1	4.9	JORDAN - SYRIA REGION	101000100
94324165905	-2.001	135.932	16	5.8	6.3	WEST IRIAN REGION	101000100

Appendix 1 (continued)

EventID	Lat	Lon	Z	Mb	Ms	Location	Key 123456789
94324183434	4.330	97.591	153	5.7		NORTHERN SUMATERA	101000100
94325022130	-14.976	167.243	126	5.6		VANUATU ISLANDS	101000100
94325081634	25.540	96.657	14	5.6	5.9	BURMA	101000100
94325185516	35.902	51.884	33	4.5		IRAN	101000100
94326111157	43.961	147.293	49	5.6	5.1	KURIL ISLANDS	101000100
94328034636	37.484	72.276	33	5.2		TAJIK SSR	101000100
94330061110	-20.126	169.126	36	5.8	5.4	VANUATU ISLANDS	101000100
94330151047	71.946	-4.846	10	4.6		JAN MAYEN ISLAND REGION	101000100
94331211841	37.747	67.788	33	4.6		AFGHANISTAN-USSR BORDER REGION	101000100
94333143028	38.707	20.484	21	4.9	4.8	GREECE	101000100
94335061101	-7.639	128.173	84	5.6		BANDA SEA	101000100
94337013551	37.643	49.349	33	4.8		CASPIAN SEA	101000100
94337060251	32.624	47.307	81	4.6		IRAN-IRAQ BORDER REGION	101000100
94339162009	-8.576	159.833	49	5.8	5.1	SOLOMON ISLANDS	101000100
94340014047	40.632	27.750	10	0.0		TURKEY	101000100
94340090607	-15.316	-75.294	27	5.3	5.0	NEAR COAST OF PERU	101000100
94341033754	-23.422	-66.639	235	5.6		JUJUY PROVINCE, ARGENTINA	111000100
94341215210	30.928	51.145	28	4.9		IRAN	011000100
94342104755	36.450	70.927	200	5.1		HINDU KUSH REGION	011000100
94342125438	28.961	52.580	33	5.0		SOUTHERN IRAN	011000100
94344033931	-23.534	-70.591	37	5.8	5.6	NEAR COAST OF NORTHERN CHILE	011000100
94344121601	27.914	64.985	57	5.2		PAKISTAN	011000100
94344161738	18.136	-101.384	48	6.6	6.2	GUERRERO, MEXICO	011000100
94345022546	-5.829	104.661	51	5.7		SOUTHERN SUMATERA	011000100
94346074155	-17.477	-69.598	148	5.9		PERU-BOLIVIA BORDER REGION	010000100
94346125254	36.397	70.811	166	5.2		HINDU KUSH REGION	010000100
94346131406	42.501	43.402	33	4.4		WESTERN CAUCASUS	010000100
94346145253	-9.975	119.199	26	5.9	5.1	SUMBA ISLAND REGION	010000100
94346151203	38.175	73.021	121	5.0		TAJIK-XINJIANG BORDER REGION	010000100
94348072853	-9.519	159.411	16	5.8	5.9	SOLOMON ISLANDS	010000100
94348204353	35.104	58.633	33	5.3		IRAN	010000100
94349112022	-37.282	177.523	33	5.9	6.4	OFF E. COAST OF N. ISLAND, N.Z.	010000100
94349232448	28.956	52.641	33	4.7		SOUTHERN IRAN	010000100
94352163815	35.277	39.745	10	4.6		JORDAN - SYRIA REGION	010000100
94352203832	-17.838	-178.703	545	5.6		FIJI ISLANDS REGION	010000100
94353145958	40.934	47.816	33	4.6		EASTERN CAUCASUS	010000100
94358235147	38.588	73.897	33	5.3		TAJIK-XINJIANG BORDER REGION	010000100
94360144801	36.469	71.244	226	5.1		AFGHANISTAN-USSR BORDER REGION	010000100
94361173250	-31.965	179.860	212	6.0		KERMADEC ISLANDS REGION	010000100
94362121923	40.525	143.419	27	6.4	7.5	OFF EAST COAST OF HONSHU, JAPAN	010000100
94362205225	40.094	142.687	22	5.9	5.9	NEAR EAST COAST OF HONSHU, JAPAN	010000100
94362223746	40.375	143.636	11	5.9	6.0	OFF EAST COAST OF HONSHU, JAPAN	010000100
94363160118	35.655	80.663	33	5.5		KASHMIR-TIBET BORDER REGION	010000100
94364065616	38.179	39.670	10	4.7		TURKEY	010000100
94365025720	20.524	109.330	33	5.7	5.3	EASTERN CHINA	010000100
94365135023	40.217	142.546	43	5.7	5.6	NEAR EAST COAST OF HONSHU, JAPAN	010000100
95001065954	40.635	143.585	10	5.7	6.2	OFF EAST COAST OF HONSHU, JAPAN	010000100
95001085108	30.543	50.378	33	4.9	4.4	IRAN	010000100
95003025457	-56.211	-27.205	136	5.4		SOUTH SANDWICH ISLANDS REGION	010000110
95003161159	-57.698	-65.958	33	6.1	5.6	DRAKE PASSAGE	010000110
95003225144	34.901	23.622	33	4.8		CRETE	010000110
95004022211	27.444	56.693	33	4.6		SOUTHERN IRAN	010000110
95004085150	9.822	56.514	21	4.8		CARLSBERG RIDGE	010000110
95005124601	59.650	56.440	10	4.7		URAL MOUNTAINS REGION	010000110
95005233007	-22.036	168.838	29	5.5	5.4	NEW CALEDONIA	010000110
95006215932	9.169	126.195	61	5.7		MINDANAO, PHILIPPINE ISLANDS	010000110
95006223737	40.227	142.242	57	6.7		NEAR EAST COAST OF HONSHU, JAPAN	010000110
95007023608	40.264	142.411	48	6.2	5.6	NEAR EAST COAST OF HONSHU, JAPAN	010000110
95007203047	37.920	19.949	10	4.7	4.4	IONIAN SEA	010000110
95008092219	-8.444	-74.289	149	5.1		PERU-BRAZIL BORDER REGION	010000100

Appendix 1 (continued)

EventID	Lat	Lon	Z	Mb	Ms	Location	Key 123456789
95009180017	35.864	141.345	33	5.6	5.7	NEAR EAST COAST OF HONSHU, JAPAN	010000100
95010100951	20.040	109.153	33	5.2	5.5	EASTERN CHINA	010000100
95012102646	43.986	147.088	33	6.2	5.4	KURIL ISLANDS	010000110
95013031259	43.102	147.070	33	5.8	5.2	KURIL ISLANDS	010000100
95015024018	27.519	128.443	47	5.7	5.4	RYUKYU ISLANDS	011000000
95015235926	-5.264	152.025	66	5.7	5.9	NEW BRITAIN REGION	001000000
95016181449	51.241	179.172	33	5.5	6.0	RAT ISLANDS, ALEUTIAN ISLANDS	001000000
95016204651	34.549	135.002	16	6.4	6.8	NEAR S. COAST OF SOUTHERN HONSHU	001000000
95017165412	-20.870	-179.225	637	6.0		FIJI ISLANDS REGION	001000000
95018143858	36.608	71.233	214	4.5		AFGHANISTAN-USSR BORDER REGION	001001000
95019030023	43.326	147.010	40	5.5	5.1	KURIL ISLANDS	001001000
95019095534	-7.345	128.271	170	5.8		BANDA SEA	001001000
95019150503	5.075	-72.918	18	6.4	6.6	COLOMBIA	001001000
95020005522	-10.958	162.156	28	5.6	5.5	SOLOMON ISLANDS	001001000
95020033546	43.261	146.821	61	5.7		KURIL ISLANDS	001001000
95020154901	1.142	126.107	51	5.7	5.4	MOLUCCA PASSAGE	001001000
95021001611	47.126	152.806	33	4.9		KURIL ISLANDS	001001000
95021030231	29.040	52.073	33	4.6		SOUTHERN IRAN	001001000
95021065633	40.565	143.633	32	5.2	5.4	OFF EAST COAST OF HONSHU, JAPAN	001001000
95021073023	2.529	126.905	47	6.1	6.1	MOLUCCA PASSAGE	001001000
95021084729	43.335	146.717	63	6.5		KURIL ISLANDS	001001000
95022104127	5.126	-72.966	22	5.6	5.1	COLOMBIA	001001000
95024041426	27.640	55.652	33	4.9		SOUTHERN IRAN	001001000
95024065857	27.300	55.454	33	4.5		SOUTHERN IRAN	001001000
95024223635	-5.933	154.493	33	5.7	6.2	SOLOMON ISLANDS	001001000
95026070044	36.080	71.219	106	5.2		AFGHANISTAN-USSR BORDER REGION	001001000
95027183451	-2.332	138.883	47	5.6	5.1	WEST IRIAN	001001000
95027201653	-4.456	134.462	33	6.2	6.8	WEST IRIAN REGION	001001000
95027210753	27.954	57.012	33	4.8		SOUTHERN IRAN	001001000
95028103727	43.922	148.163	33	5.2	5.2	KURIL ISLANDS REGION	001001000
95029012011	36.978	71.552	107	5.2		AFGHANISTAN-USSR BORDER REGION	001001000
95029045337	29.234	141.202	67	5.6		SOUTH OF HONSHU, JAPAN	001001000
95030223630	36.421	71.450	54	4.6		AFGHANISTAN-USSR BORDER REGION	001001000
95032142644	-42.432	-18.449	10	5.4	5.1	SOUTH ATLANTIC RIDGE	001001000
95033123358	-1.268	127.567	33	5.5		HALMAHERA	001001000
95033125353	10.755	-42.557	10	5.6	5.4	NORTH ATLANTIC RIDGE	001001000
95033193449	39.214	67.407	33	4.6		SOUTHEASTERN UZBEK SSR	001001000
95034023134	-62.706	155.895	10	5.6	6.3	BALLENY ISLANDS REGION	001001000
95034154054	-3.416	135.538	35	5.3	4.9	WEST IRIAN REGION	001001000
95034222909	34.219	25.194	33	4.8		CRETE	001001000
95036203710	6.849	-82.675	10	5.8	5.4	SOUTH OF PANAMA	001001000
95036225110	-37.714	178.769	59	6.4		OFF E. COAST OF N. ISLAND, N.Z.	001001000
95037104357	-37.799	178.816	33	5.7	5.8	OFF E. COAST OF N. ISLAND, N.Z.	001001000
95037135135	41.124	142.188	71	5.6		HOKKAIDO, JAPAN REGION	001001000
95037211547	28.942	34.748	5	0.0		ARAB REPUBLIC OF EGYPT	001001000
95039184025	4.162	-76.644	69	6.3		COLOMBIA	001001000
95041014504	-37.968	178.472	33	5.8	6.4	OFF E. COAST OF N. ISLAND, N.Z.	001001000
95041074918	36.196	69.070	33	4.8		HINDU KUSH REGION	001001000
95041202703	-19.770	-68.544	164	5.4		CHILE-BOLIVIA BORDER REGION	001001000
95042224533	12.607	-81.603	11	5.3	5.2	CARIBBEAN SEA	001001000
95043010207	-5.796	-76.135	22	5.7	5.1	NORTHERN PERU	001001000
95044001147	-37.541	178.543	28	5.6	6.2	OFF E. COAST OF N. ISLAND, N.Z.	001001000
95044084339	-1.306	127.420	33	6.1	6.2	HALMAHERA	001001000
95044122955	-1.383	127.449	33	5.8	6.0	HALMAHERA	001001000
95044131634	40.707	22.563	10	4.8		GREECE	001001000
95044150426	-1.351	127.522	33	6.2	6.8	HALMAHERA	001001000
95045111319	37.742	42.698	10	4.8	4.2	TURKEY	001001000
95045155356	-23.290	-67.702	156	5.7		CHILE-ARGENTINA BORDER REGION	001001000
95045204741	43.991	148.098	37	5.9	5.6	KURIL ISLANDS REGION	001001000
95046130520	29.105	51.167	33	4.7		SOUTHERN IRAN	001001000

Appendix 1 (continued)

EventID	Lat	Lon	Z	Mb	Ms	Location	Key 123456789
95047145252	52.191	-30.216	10	5.1	4.8	NORTH ATLANTIC RIDGE	001001000
95048024424	27.606	92.298	35	5.2	5.1	INDIA-CHINA BORDER REGION	001001000
95049132906	46.667	145.894	355	5.6		SEA OF OKHOTSK	001001000
95050001748	5.206	126.225	104	5.9		MINDANAO, PHILIPPINE ISLANDS	001001000
95050040316	40.560	-125.527	10	6.1	6.8	OFF COAST OF NORTHERN CALIFORNIA	001001000
95050044550	43.098	146.842	33	5.8	5.8	KURIL ISLANDS	001001000
95051025912	-27.835	76.213	10	5.3	5.6	MID-INDIAN RISE	001001000
95051041224	39.255	71.054	27	5.4		TAJIK SSR	001001000
95051080733	41.225	72.498	33	5.0	4.5	KIRGHIZ SSR	001001000
95052020950	45.942	151.553	33	5.8	5.9	KURIL ISLANDS	001001000
95054050125	39.663	143.688	33	5.5	6.0	OFF EAST COAST OF HONSHU, JAPAN	001001000
95054051902	24.136	121.600	44	5.8	6.2	TAIWAN	001001000
95054210302	35.039	32.266	15	5.8	5.7	CYPRUS	001001000
95054211036	35.089	32.274	10	4.8		CYPRUS	001001000
95054214031	35.005	32.270	10	5.2		CYPRUS	001001000
95056060930	-26.670	-112.621	10	5.4	5.1	EASTER ISLAND REGION	001001000
95056094224	39.977	77.480	33	4.8		SOUTHERN XINJIANG, CHINA	001001000
95056110531	36.654	71.006	175	4.8		AFGHANISTAN-USSR BORDER REGION	001001000
95056215429	-18.235	-178.091	568	5.6		FIJI ISLANDS REGION	001001000
95057150341	1.302	97.873	33	5.0	4.7	NORTHERN SUMATERA	001001000
95059102410	38.149	73.120	88	4.2		TAJIK-XINJIANG BORDER REGION	001001000
95059211209	6.935	-81.805	21	5.2	5.5	SOUTH OF PANAMA	001001010
95062120210	-6.472	154.987	35	5.8	5.6	SOLOMON ISLANDS	001001010
95062135122	34.620	45.177	33	4.6		IRAN-IRAQ BORDER REGION	001001010
95062211237	-14.617	-175.627	22	5.6	5.7	SAMOA ISLANDS REGION	001001010
95065184342	2.662	118.218	33	5.5	5.8	CELEBES SEA	001001010
95067034559	16.555	-59.574	15	6.3	6.2	LEEWARD ISLANDS	001001010
95068183657	20.943	122.001	42	5.1	5.3	PHILIPPINE ISLANDS REGION	001001000
95069052222	46.075	143.540	350	5.4		SAKHALIN ISLAND	001001000
95070152110	44.008	148.132	33	6.0	5.7	KURIL ISLANDS	001001010
95071044045	40.187	143.489	33	5.1	5.1	OFF EAST COAST OF HONSHU, JAPAN	001001000
95071082300	17.911	73.422	33	4.7		INDIA	001001000
95071120943	-5.330	146.695	233	5.6		EAST PAPUA NEW GUINEA REGION	001001000
95072103150	-2.820	134.330	33	5.5	5.7	WEST IRIAN REGION	001001000
95073004322	6.859	-73.128	158	4.8		NORTHERN COLOMBIA	001001000
95073033233	-37.892	-73.331	33	5.2		NEAR COAST OF CENTRAL CHILE	001001000
95073102730	2.999	95.867	30	5.0	5.3	OFF W COAST OF NORTHERN SUMATERA	001001000
95073173350	54.793	-161.295	33	6.1	5.9	ALASKA PENINSULA	001001000
95075032704	30.311	67.248	25	4.8	4.2	PAKISTAN	101001010
95076021840	-13.142	166.676	33	5.7	5.2	VANUATU ISLANDS	111001010
95077180237	42.502	87.179	21	5.2		NORTHERN XINJIANG, CHINA	111000010
95078165815	36.509	70.920	201	4.7		HINDU KUSH REGION	111000010
95078174140	43.985	147.175	33	4.7	4.0	KURIL ISLANDS	111000010
95078183405	-4.270	135.061	33	5.6	6.3	WEST IRIAN REGION	111000010
95078235314	-4.148	135.087	33	6.3	7.1	WEST IRIAN REGION	111000010
95081062836	30.185	51.065	33	4.7		IRAN	111000010
95082091821	-36.263	-72.943	43	5.2	5.5	NEAR COAST OF CENTRAL CHILE	111000010
95084224428	-11.050	166.111	77	5.9		SANTA CRUZ ISLANDS	111000010
95085021616	-55.855	-28.208	77	6.1	5.9	SOUTH SANDWICH ISLANDS REGION	111000010
95089181715	34.479	24.853	10	4.9		CRETE	111000010
95090140140	38.150	135.058	365	6.0		SEA OF JAPAN	111000010
95091034933	37.924	139.177	11	5.8		HONSHU, JAPAN	111000010
95091044814	31.195	45.934	33	4.6		IRAQ	111000010
95091055020	52.279	159.133	47	5.9	5.6	OFF EAST COAST OF KAMCHATKA	111000010
95093115443	24.083	122.250	33	5.7	5.5	TAIWAN REGION	111000010
95093200815	29.638	51.052	33	4.3		SOUTHERN IRAN	111000010
95094152952	28.212	71.593	21	4.8	3.9	INDIA-PAKISTAN BORDER REG.	111000010
95097220658	-15.187	-173.594	31	6.7	8.0	TONGA ISLANDS	111000010
95098012007	-15.227	-173.521	33	5.9	6.1	TONGA ISLANDS	111000010
95098174518	21.804	142.632	319	6.3		MARIANA ISLANDS REGION	111000010

Appendix 1 (continued)

EventID	Lat	Lon	Z	Mb	Ms	Location	Key 123456789
95104003254	30.244	-103.325	5	5.7	5.6	WEST TEXAS	111000010
95106132348	-9.759	159.514	24	5.6	5.7	SOLOMON ISLANDS	111000010
95107011420	-8.585	156.613	36	5.8	6.0	SOLOMON ISLANDS	111000010
95107071435	33.778	-38.600	10	5.8	5.8	NORTH ATLANTIC RIDGE	111000010
95107232808	45.904	151.288	34	6.1	6.3	KURIL ISLANDS	111000010
95108034939	-2.088	140.449	36	5.9	5.7	NEAR N. COAST OF WEST IRIAN	111000010
95108061240	31.812	49.283	33	4.7		WESTERN IRAN	111000010
95109035005	44.027	148.204	33	5.9	5.5	KURIL ISLANDS	111000010
95110084510	6.288	126.828	85	6.2		MINDANAO, PHILIPPINE ISLANDS	111000010
95110204910	45.901	151.253	33	5.7	5.0	KURIL ISLANDS	111000010
95111000956	11.999	125.699	33	6.1	6.9	SAMAR, PHILIPPINE ISLANDS	111000010
95111003447	12.064	125.931	23	6.2	7.3	SAMAR, PHILIPPINE ISLANDS	111000010
95111051700	12.142	125.948	23	5.6	6.9	SAMAR, PHILIPPINE ISLANDS	111000010
95111080256	43.756	7.567	25	4.9		NEAR SOUTH COAST OF FRANCE	111000010
95111170317	11.997	125.877	33	5.2	5.2	SAMAR, PHILIPPINE ISLANDS	111000010
95112002149	30.912	49.843	33	5.0	4.9	WESTERN IRAN	111000000
95113025554	51.340	179.713	16	6.1	6.4	RAT ISLANDS, ALEUTIAN ISLANDS	111000000
95113050803	12.377	125.364	33	6.0	6.6	SAMAR, PHILIPPINE ISLANDS	111000000
95113235540	5.255	-72.475	33	5.3	4.7	COLOMBIA	111000000
95115061502	-5.855	147.302	33	5.6	5.7	EAST PAPUA NEW GUINEA REGION	111000010
95117124438	1.199	-84.929	10	5.3	6.0	OFF COAST OF ECUADOR	111000010
95118163000	44.058	148.055	29	6.6	6.9	KURIL ISLANDS	111000010
95118170843	44.090	148.122	33	6.2	6.2	KURIL ISLANDS	111000010
95118174413	-1.892	55.532	10	5.3		SOUTH INDIAN OCEAN	111000010
95119094400	11.766	126.044	33	5.4	6.0	PHILIPPINE ISLANDS REGION	111000010
95122060605	-3.854	-76.958	103	6.5		NORTHERN PERU	111000010
95122114811	43.824	84.607	33	5.5	5.3	NORTHERN XINJIANG, CHINA	111000010
95123024952	28.440	52.744	33	4.7		SOUTHERN IRAN	111000010
95124003412	40.673	23.466	28	5.1	5.1	GREECE	111000010
95124021851	1.857	128.488	55	6.0	6.0	HALMAHERA	111000010
95124160331	35.023	27.748	33	4.9	4.3	DODECANESE ISLANDS	111000010
95125035347	12.622	125.314	33	6.2	7.0	SAMAR, PHILIPPINE ISLANDS	111000010
95125091729	13.856	51.464	10	5.0	4.4	EASTERN GULF OF ADEN	111000010
95125130139	-10.165	118.809	33	5.7	5.4	SOUTH OF SUMBAWA ISLAND	111000010
95125224805	-18.465	168.681	123	5.8		VANUATU ISLANDS	111000010
95126015907	25.007	95.335	122	6.4		BURMA-INDIA BORDER REGION	111000010
95128174025	43.884	148.413	34	5.7	5.2	KURIL ISLANDS REGION	111000010
95129011437	40.820	20.664	10	4.8	4.2	GREECE-ALBANIA BORDER REGION	111000010
95129095420	25.260	95.136	92	5.2		BURMA-INDIA BORDER REGION	111000010
95133072041	40.750	50.635	33	4.8		CASPIAN SEA	111000010
95133084712	40.144	21.684	13	6.2	6.5	GREECE	111000010
95133105834	40.058	21.552	10	4.9		GREECE	111000010
95133114328	40.138	21.644	10	5.0		GREECE	111000010
95133210054	-5.215	108.917	554	5.7		JAVA SEA	111000010
95134024658	40.138	21.540	10	4.7		GREECE	111000010
95134044701	40.124	70.691	33	4.8	4.0	TAJIK SSR	111000010
95134113321	-8.396	125.083	33	6.1	6.9	TIMOR	111000010
95134223347	39.957	77.610	33	5.0	4.3	SOUTHERN XINJIANG, CHINA	111000010
95135001652	38.407	49.390	27	4.8		CASPIAN SEA	111000010
95135040558	41.665	88.821	0	6.1		SOUTHERN XINJIANG, CHINA	111000010
95135041355	40.047	21.619	10	5.1		GREECE	111000010
95135152654	-56.061	-27.770	100	5.4		SOUTH SANDWICH ISLANDS REGION	111000000
95135202149	13.126	49.523	10	4.9		EASTERN GULF OF ADEN	111000000
95136033503	36.485	70.896	190	5.7		HINDU KUSH REGION	111000000
95136201245	-23.014	169.893	33	6.8	7.7	LOYALTY ISLANDS REGION	111000000
95136214808	17.800	96.550	33	5.8		BURMA	111000000
95136230040	40.034	21.574	10	4.8		GREECE	111000000
95137022929	-6.290	147.398	71	5.6		EAST PAPUA NEW GUINEA REGION	111000000
95137041424	40.160	21.597	10	5.3	5.0	GREECE	111000000
95137094507	39.998	21.536	10	5.0	4.7	GREECE	111000000

Appendix 1 (continued)

EventID	Lat	Lon	Z	Mb	Ms	Location	Key 123456789
95137112351	-23.028	170.079	33	5.7	6.5	LOYALTY ISLANDS REGION	111000000
95138000626	-0.950	-21.985	10	6.2	6.1	CENTRAL MID-ATLANTIC RIDGE	111000000
95138143114	44.324	147.581	104	5.7		KURIL ISLANDS	111000000
95139064849	40.043	21.580	10	5.1	5.0	GREECE	111000000
95139214451	39.996	21.595	10	4.6		GREECE	111000000
95140134502	-56.009	-27.727	100	5.5		SOUTH SANDWICH ISLANDS REGION	111000000
95142034504	-22.771	169.931	33	5.8	6.1	LOYALTY ISLANDS REGION	111000000
95142040255	-9.683	151.475	33	5.7	6.1	DENTRECASTEAUX ISLANDS REGION	111000000
95143221011	-56.097	-3.150	10	5.3	6.6	SOUTH ATLANTIC RIDGE	111000010
95144202125	12.204	125.707	33	5.4	5.7	SAMAR, PHILIPPINE ISLANDS	111000010
95146031110	12.134	57.931	10	5.3	5.4	ARABIAN SEA	111000010
95147130355	52.563	142.814	33	6.6	7.6	SAKHALIN ISLAND	111000010
95147201529	-19.694	168.985	33	5.6	4.8	VANUATU ISLANDS	111000010
95147212128	39.041	49.056	10	4.7		CASPIAN SEA	111000010
95148195912	-29.048	-71.098	42	5.6	5.1	NEAR COAST OF CENTRAL CHILE	101000010
95149140232	32.352	141.601	33	5.1	4.6	SOUTH OF HONSHU, JAPAN	110001000
95149072946	-10.144	163.734	33	5.8	6.4	SOLOMON ISLANDS	010001000
95151135120	30.204	67.933	33	5.3	4.9	PAKISTAN	111001000
95151160840	18.949	-107.434	33	5.4	6.1	OFF COAST OF JALISCO, MEXICO	111001000
95151204411	28.194	53.264	33	5.0	4.0	SOUTHERN IRAN	111001000
95153232906	3.289	96.358	33	5.0		NORTHERN SUMATERA	111001000
95154115731	2.977	96.210	30	5.2	4.6	NORTHERN SUMATERA	111001000
95154200832	35.848	53.049	33	4.0		IRAN	111001000
95156202017	18.402	120.858	47	5.4	5.4	LUZON, PHILIPPINE ISLANDS	111001000
95157000304	26.568	67.167	33	4.6	4.2	PAKISTAN	111001000
95158005347	51.325	-179.326	30	5.2	4.7	ANDREANOF ISLANDS, ALEUTIAN IS.	111001000
95158230947	32.504	48.745	33	5.0	4.4	WESTERN IRAN	111001000
95162192050	11.711	125.867	33	5.0	5.4	SAMAR, PHILIPPINE ISLANDS	111001000
95162215549	32.556	69.618	33	5.1	5.6	PAKISTAN	111001000
95163033548	-8.308	-75.913	34	5.7	5.0	PERU	111001000
95163144759	39.169	95.365	33	5.2	4.5	GANSU PROVINCE, CHINA	111001000
95165054233	36.286	58.515	33	4.4	4.1	IRAN	111001000
95165111149	12.204	-88.349	39	5.6	6.0	OFF COAST OF CENTRAL AMERICA	111001000
95165121159	42.388	21.421	10	5.1		YUGOSLAVIA	111001000
95166001548	38.401	22.269	14	6.0	6.5	GREECE	111001000
95166003100	38.395	22.430	10	5.3	6.0	GREECE	111001000
95166183729	38.668	69.964	33	4.6		TAJIK SSR	111001001
95168013711	-8.255	123.020	38	5.2	5.4	FLORES ISLAND REGION	111001001
95170005744	44.031	150.473	33	5.3	4.8	KURIL ISLANDS REGION	111001001
95172152851	-61.621	154.714	10	5.6	6.7	BALLENY ISLANDS REGION	111001001
95172163305	-11.546	-77.564	70	5.5		NEAR COAST OF PERU	111001001
95173010121	50.325	89.915	33	5.5	5.3	USSR-MONGOLIA BORDER REGION	111001001
95175065806	-3.979	153.945	386	6.2		NEW IRELAND REGION	011001001
95176021041	-3.281	150.365	45	5.5	6.3	NEW IRELAND REGION	011001001
95176065905	24.599	121.713	47	5.8	5.7	TAIWAN	011001001
95177034142	-55.361	-27.843	33	5.4	5.1	SOUTH SANDWICH ISLANDS REGION	111001001
95177211255	36.327	51.060	33	4.1		IRAN	111001001
95177212649	7.106	-34.331	10	4.9	5.3	CENTRAL MID-ATLANTIC RIDGE	111001001
95177232735	39.852	48.310	33	4.4		N.W. IRAN-USSR BORDER REGION	111001001
95178004642	39.837	48.324	33	4.5		N.W. IRAN-USSR BORDER REGION	111001001
95178040929	-55.365	-27.980	33	5.3	5.2	SOUTH SANDWICH ISLANDS REGION	111001001
95178100958	18.847	-81.730	10	5.7	5.6	CARIBBEAN SEA	111001001
95178211256	-17.228	66.829	10	5.0	6.3	MASCARENE ISLANDS REGION	111001001
95179211449	-1.617	127.365	33	5.6	5.4	HALMAHERA	111001001
95180074509	48.784	154.459	62	5.9		KURIL ISLANDS	111001001
95180122403	-19.464	169.241	144	6.2		VANUATU ISLANDS	111001001
95180230231	51.923	103.075	33	5.6	5.5	LAKE BAIKAL REGION	111001001
95181115856	24.621	-110.264	10	5.8	6.3	BAJA CALIFORNIA	111001001
95182041055	12.942	57.468	10	5.2		ARABIAN SEA	111001001
95182235744	-55.516	-27.819	33	5.2	5.2	SOUTH SANDWICH ISLANDS REGION	111001001

Appendix 1 (continued)

EventID	Lat	Lon	Z	Mb	Ms	Location	Key 123456789
95184195050	-29.198	-177.612	33	6.5	7.2	KERMADEC ISLANDS	111001001
95184215651	-29.052	-177.676	55	6.0		KERMADEC ISLANDS	111001001
95188104004	-53.561	9.186	10	5.4	5.2	SOUTHWEST OF AFRICA	111001001
95188211518	33.947	137.122	324	5.8		NEAR S. COAST OF HONSHU, JAPAN	111001001
95189054256	39.640	143.353	40	5.7	5.5	OFF EAST COAST OF HONSHU, JAPAN	111001001
95189113905	4.329	62.417	10	5.5	5.1	CARLSBERG RIDGE	111001001
95189171528	53.646	-163.546	33	5.8	5.7	UNIMAK ISLAND REGION	111001001
95189234947	-24.153	-176.478	51	5.7		SOUTH OF FIJI ISLANDS	111001001
95190022945	37.330	71.823	121	5.0		AFGHANISTAN-USSR BORDER REGION	111001001
95190203131	22.003	99.196	12	5.7	5.9	BURMA-CHINA BORDER REGION	111001001
95191024232	12.399	141.651	55	5.2	4.9	SOUTH OF MARIANA ISLANDS	111001001
95192214639	21.933	99.162	13	6.1	7.2	BURMA-CHINA BORDER REGION	111001001
95193154659	-23.237	170.824	33	5.9	6.4	LOYALTY ISLANDS REGION	111001001
95193183849	12.316	125.037	33	5.8	5.6	SAMAR, PHILIPPINE ISLANDS	111001001
95194000023	-23.308	170.636	33	5.6	5.7	LOYALTY ISLANDS REGION	111001001
95195140307	42.818	48.825	33	4.2		CASPIAN SEA	111001001
95198231815	40.265	21.404	10	5.3	4.8	GREECE	111001001
95199143545	-3.855	135.293	33	5.4	5.7	WEST IRIAN REGION	111001001
95200002417	-22.685	169.736	32	5.8	5.6	LOYALTY ISLANDS REGION	111001001
95202224407	36.443	103.105	33	5.7	5.4	GANSU PROVINCE, CHINA	111001001
95205191321	55.597	-35.059	10	5.4	5.2	NORTH ATLANTIC OCEAN	111000001
95206151326	10.694	-41.211	10	5.4	5.5	NORTH ATLANTIC RIDGE	111000001
95206223923	44.120	148.446	33	5.5	4.7	KURIL ISLANDS	111000001
95207234202	2.562	127.692	66	5.9		MOLUCCA PASSAGE	111000001
95208055117	-12.578	79.237	10	6.2	5.9	SOUTH INDIAN OCEAN	111000001
95209142912	-21.097	-175.485	102	6.1		TONGA ISLANDS	111000001
95210080125	4.210	126.698	51	5.5	5.3	TALAUD ISLANDS	111000001
95211051123	-23.364	-70.312	47	6.6	7.3	NEAR COAST OF NORTHERN CHILE	111000001
95211210550	-23.317	-70.590	33	5.6	5.6	NEAR COAST OF NORTHERN CHILE	111000001
95213021039	46.342	153.903	33	5.6	4.7	KURIL ISLANDS	111000001
95214001409	-23.152	-70.578	33	5.4	5.5	NEAR COAST OF NORTHERN CHILE	111000001
95214110539	-23.100	-70.405	33	5.2	5.1	NEAR COAST OF NORTHERN CHILE	111000001
95215015721	-23.132	-70.602	33	5.4	5.9	NEAR COAST OF NORTHERN CHILE	111000001
95215081853	-28.346	-69.198	104	5.9		CHILE-ARGENTINA BORDER REGION	111000001
95219194424	4.081	143.680	10	5.5	5.7	CAROLINE ISLANDS REGION	111000001
95220003524	11.780	125.791	33	5.3	5.0	SAMAR, PHILIPPINE ISLANDS	111000001
95226043717	-4.827	151.507	126	6.3	6.3	NEW BRITAIN REGION	111000001
95228102726	-5.809	154.212	16	6.4	7.8	SOLOMON ISLANDS	111000001
95228162426	-5.418	153.765	21	5.6	6.8	NEW IRELAND REGION	111000001
95228231028	-5.782	154.256	74	6.1	7.2	SOLOMON ISLANDS	111000001
95229005957	41.587	88.782	0	6.0		SOUTHERN XINJIANG, CHINA	111000001
95229100127	-5.176	153.404	33	5.5	6.4	NEW IRELAND REGION	111000001
95229231419	36.465	71.156	239	5.4		AFGHANISTAN-USSR BORDER REGION	111000001
95230021626	-55.898	-28.901	36	5.6	5.8	SOUTH SANDWICH ISLANDS REGION	111000001
95231214332	5.096	-75.690	125	6.1		COLOMBIA	001000001

Prof. Thomas Ahrens
Seismological Lab, 252-21
Division of Geological & Planetary Sciences
California Institute of Technology
Pasadena, CA 91125

Prof. Keiiti Aki
Center for Earth Sciences
University of Southern California
University Park
Los Angeles, CA 90089-0741

Prof. Shelton Alexander
Geosciences Department
403 Deike Building
The Pennsylvania State University
University Park, PA 16802

Prof. Charles B. Archambeau
University of Colorado
JSPC
Campus Box 583
Boulder, CO 80309

Dr. Thomas C. Bache, Jr.
Science Applications Int'l Corp.
10260 Campus Point Drive
San Diego, CA 92121 (2 copies)

Prof. Muawia Barazangi
Cornell University
Institute for the Study of the Continent
3126 SNEE Hall
Ithaca, NY 14853

Dr. Jeff Barker
Department of Geological Sciences
State University of New York
at Binghamton
Vestal, NY 13901

Dr. Douglas R. Baumgardt
ENSCO, Inc
5400 Port Royal Road
Springfield, VA 22151-2388

Dr. Susan Beck
Department of Geosciences
Building #77
University of Arizona
Tuscon, AZ 85721

Dr. T.J. Bennett
S-CUBED
A Division of Maxwell Laboratories
11800 Sunrise Valley Drive, Suite 1212
Reston, VA 22091

Dr. Robert Blandford
AFTAC/TT, Center for Seismic Studies
1300 North 17th Street
Suite 1450
Arlington, VA 22209-2308

Dr. Stephen Bratt
ARPA/NMRO
3701 North Fairfax Drive
Arlington, VA 22203-1714

Dale Breding
U.S. Department of Energy
Recipient, IS-20, GA-033
Office of Arms Control
Washington, DC 20585

Dr. Lawrence Burdick
C/O Barbara Wold
Dept of Biology
CA Inst. of Technology
Pasadena, CA 91125

Dr. Robert Burridge
Schlumberger-Doll Research Center
Old Quarry Road
Ridgefield, CT 06877

Dr. Jerry Carter
Center for Seismic Studies
1300 North 17th Street
Suite 1450
Arlington, VA 22209-2308

Dr. Martin Chapman
Department of Geological Sciences
Virginia Polytechnical Institute
21044 Derring Hall
Blacksburg, VA 24061

Mr Robert Cockerham
Arms Control & Disarmament Agency
320 21st Street North West
Room 5741
Washington, DC 20451,

Prof. Vernon F. Cormier
Department of Geology & Geophysics
U-45, Room 207
University of Connecticut
Storrs, CT 06268

Prof. Steven Day
Department of Geological Sciences
San Diego State University
San Diego, CA 92182

Dr. Zoltan Der
ENSCO, Inc.
5400 Port Royal Road
Springfield, VA 22151-2388

Dr. Stanley K. Dickinson
AFOSR/NM
110 Duncan Avenue
Suite B115
Bolling AFB, DC 20332-6448

Prof. Adam Dziewonski
Hoffman Laboratory, Harvard University
Dept. of Earth Atmos. & Planetary Sciences
20 Oxford Street
Cambridge, MA 02138

Prof. John Ebel
Department of Geology & Geophysics
Boston College
Chestnut Hill, MA 02167

Dr. Petr Firbas
Institute of Physics of the Earth
Masaryk University Brno
Jecna 29a
612 46 Brno, Czech Republic

Dr. Mark D. Fisk
Mission Research Corporation
735 State Street
P.O. Drawer 719
Santa Barbara, CA 93102

Prof. Donald Forsyth
Department of Geological Sciences
Brown University
Providence, RI 02912

Dr. Cliff Frolich
Institute of Geophysics
8701 North Mopac
Austin, TX 78759

Dr. Holly Given
IGPP, A-025
Scripps Institute of Oceanography
University of California, San Diego
La Jolla, CA 92093

Dr. Jeffrey W. Given
SAIC
10260 Campus Point Drive
San Diego, CA 92121

Dr. Indra N. Gupta
Multimax, Inc.
1441 McCormick Drive
Landover, MD 20785

Dan N. Hagedon
Pacific Northwest Laboratories
Battelle Boulevard
Richland, WA 99352

Dr. James Hannon
Lawrence Livermore National Laboratory
P.O. Box 808, L-205
Livermore, CA 94550

Prof. Danny Harvey
University of Colorado, JSPC
Campus Box 583
Boulder, CO 80309

Prof. Donald V. Helmberger
Division of Geological & Planetary Sciences
California Institute of Technology
Pasadena, CA 91125

Prof. Eugene Herrin
Geophysical Laboratory
Southern Methodist University
Dallas, TX 75275

Prof. Robert B. Herrmann
Department of Earth & Atmospheric Sciences
St. Louis University
St. Louis, MO 63156

Prof. Lane R. Johnson
Seismographic Station
University of California
Berkeley, CA 94720

Prof. Thomas H. Jordan
Department of Earth, Atmospheric &
Planetary Sciences
Massachusetts Institute of Technology
Cambridge, MA 02139

Prof. Alan Kafka
Department of Geology & Geophysics
Boston College
Chestnut Hill, MA 02167

U.S. Dept of Energy
Max Koontz, NN-20, GA-033
Office of Research and Develop.
1000 Independence Avenue
Washington, DC 20585

Dr. Richard LaCoss
MIT Lincoln Laboratory, M-200B
P.O. Box 73
Lexington, MA 02173-0073

Dr. Fred K. Lamb
University of Illinois at Urbana-Champaign
Department of Physics
1110 West Green Street
Urbana, IL 61801

Prof. Charles A. Langston
Geosciences Department
403 Deike Building
The Pennsylvania State University
University Park, PA 16802

Jim Lawson, Chief Geophysicist
Oklahoma Geological Survey
Oklahoma Geophysical Observatory
P.O. Box 8
Leonard, OK 74043-0008

Prof. Thorne Lay
Institute of Tectonics
Earth Science Board
University of California, Santa Cruz
Santa Cruz, CA 95064

Dr. William Leith
U.S. Geological Survey
Mail Stop 928
Reston, VA 22092

Mr. James F. Lewkowicz
Phillips Laboratory/GPE
29 Randolph Road
Hanscom AFB, MA 01731-3010(2 copies)

Prof. L. Timothy Long
School of Geophysical Sciences
Georgia Institute of Technology
Atlanta, GA 30332

Dr. Randolph Martin, III
New England Research, Inc.
76 Olcott Drive
White River Junction, VT 05001

Dr. Robert Masse
Denver Federal Building
Box 25046, Mail Stop 967
Denver, CO 80225

Dr. Gary McCartor
Department of Physics
Southern Methodist University
Dallas, TX 75275

Prof. Thomas V. McEvilly
Seismographic Station
University of California
Berkeley, CA 94720

Dr. Art McGarr
U.S. Geological Survey
Mail Stop 977
U.S. Geological Survey
Menlo Park, CA 94025

Dr. Keith L. McLaughlin
S-CUBED
A Division of Maxwell Laboratory
P.O. Box 1620
La Jolla, CA 92038-1620

Stephen Miller & Dr. Alexander Florence
SRI International
333 Ravenswood Avenue
Box AF 116
Menlo Park, CA 94025-3493

Prof. Bernard Minster
IGPP, A-025
Scripps Institute of Oceanography
University of California, San Diego
La Jolla, CA 92093

Prof. Brian J. Mitchell
Department of Earth & Atmospheric Sciences
St. Louis University
St. Louis, MO 63156

Mr. Richard J. Morrow
USACDA/IVI
320 21st St. N.W.
Washington , DC 20451

Mr. Jack Murphy
S-CUBED
A Division of Maxwell Laboratory
11800 Sunrise Valley Drive, Suite 1212
Reston, VA 22091 (2 Copies)

Dr. Keith K. Nakanishi
Lawrence Livermore National Laboratory
L-025
P.O. Box 808
Livermore, CA 94550

Prof. John A. Orcutt
IGPP, A-025
Scripps Institute of Oceanography
University of California, San Diego
La Jolla, CA 92093

Prof. Jeffrey Park
Kline Geology Laboratory
P.O. Box 6666
New Haven, CT 06511-8130

Dr. Howard Patton
Lawrence Livermore National Laboratory
L-025
P.O. Box 808
Livermore, CA 94550

Dr. Frank Pilotte
HQ AFTAC/TT
1030 South Highway A1A
Patrick AFB, FL 32925-3002

Dr. Jay J. Pulli
Radix Systems, Inc.
6 Taft Court
Rockville, MD 20850

Dr. Robert Reinke
ATTN: FCTVTD
Field Command
Defense Nuclear Agency
Kirtland AFB, NM 87115

Prof. Paul G. Richards
Lamont-Doherty Earth Observatory
of Columbia University
Palisades, NY 10964

Mr. Wilmer Rivers
Teledyne Geotech
1300 17th St N #1450
Arlington, VA 22209-3803

Dr. Alan S. Ryall, Jr.
Lawrence Livermore National Laboratory
P.O. Box 808, L-205
Livermore, CA 94550

Dr.Chandan K. Saikia
Woodward Clyde- Consultants
566 El Dorado Street
Pasadena, CA 91101

Dr. Richard Sailor
TASC, Inc.
55 Walkers Brook Drive
Reading, MA 01867

Prof. Charles G. Sammis
Center for Earth Sciences
University of Southern California
University Park
Los Angeles, CA 90089-0741

Prof. Christopher H. Scholz
Lamont-Doherty Earth Observatory
of Columbia University
Palisades, NY 10964

Dr. Susan Schwartz
Institute of Tectonics
1156 High Street
Santa Cruz, CA 95064

Mr. Dogan Seber
Cornell University
Inst. for the Study of the Continent
3130 SNEE Hall
Ithaca, NY 14853-1504

Secretary of the Air Force
(SAFRD)
Washington, DC 20330

Office of the Secretary of Defense
DDR&E
Washington, DC 20330

Thomas J. Sereno, Jr.
Science Application Int'l Corp.
10260 Campus Point Drive
San Diego, CA 92121

Dr. Michael Shore
Defense Nuclear Agency/SPSS
6801 Telegraph Road
Alexandria, VA 22310

Dr. Robert Shumway
University of California Davis
Division of Statistics
Davis, CA 95616

Dr. Matthew Sibol
Virginia Tech
Seismological Observatory
4044 Derring Hall
Blacksburg, VA 24061-0420

Prof. David G. Simpson
IRIS, Inc.
1616 North Fort Myer Drive
Suite 1050
Arlington, VA 22209

Donald L. Springer
Lawrence Livermore National Laboratory
L-025
P.O. Box 808
Livermore, CA 94550

Dr. Jeffrey Stevens
S-CUBED
A Division of Maxwell Laboratory
P.O. Box 1620
La Jolla, CA 92038-1620

Prof. Brian Stump
Los Alamos National Laboratory
EES-3
Mail Stop C-335
Los Alamos, NM 87545

Prof. Jeremiah Sullivan
University of Illinois at Urbana-Champaign
Department of Physics
1110 West Green Street
Urbana, IL 61801

Prof. L. Sykes
Lamont-Doherty Earth Observatory
of Columbia University
Palisades, NY 10964

Dr. Steven R. Taylor
Los Alamos National Laboratory
P.O. Box 1663
Mail Stop C335
Los Alamos, NM 87545

Prof. Tuncay Taymaz
Istanbul Technical University
Dept. of Geophysical Engineering
Mining Faculty
Maslak-80626, Istanbul Turkey

Prof. Clifford Thurber
University of Wisconsin-Madison
Department of Geology & Geophysics
1215 West Dayton Street
Madison, WS 53706

Prof. M. Nafi Toksoz
Earth Resources Lab
Massachusetts Institute of Technology
42 Carleton Street
Cambridge, MA 02142

Dr. Larry Turnbull
CIA-OSWR/NED
Washington, DC 20505

Dr. Gregory van der Vink
IRIS, Inc.
1616 North Fort Myer Drive
Suite 1050
Arlington, VA 22209

Dr. Karl Veith
EG&G
2341 Jefferson Davis Highway
Suite 801
Arlington, VA 22202-3809

Prof. Terry C. Wallace
Department of Geosciences
Building #77
University of Arizona
Tuscon, AZ 85721

Dr. Thomas Weaver
Los Alamos National Laboratory
P.O. Box 1663
Mail Stop C335
Los Alamos, NM 87545

Dr. William Wortman
Mission Research Corporation
8560 Cinderbed Road
Suite 700
Newington, VA 22122

Prof. Francis T. Wu
Department of Geological Sciences
State University of New York
at Binghamton
Vestal, NY 13901

Prof Ru-Shan Wu
University of California, Santa Cruz
Earth Sciences Department
Santa Cruz, CA 95064

ARPA, OASB/Library
3701 North Fairfax Drive
Arlington, VA 22203-1714

HQ DNA
ATTN: Technical Library
Washington, DC 20305

TACTEC
Battelle Memorial Institute
505 King Avenue
Columbus, OH 43201 (Final Report)

Phillips Laboratory
ATTN: XPG
29 Randolph Road
Hanscom AFB, MA 01731-3010

Phillips Laboratory
ATTN: GPE
29 Randolph Road
Hanscom AFB, MA 01731-3010

Phillips Laboratory
ATTN: TSML
5 Wright Street
Hanscom AFB, MA 01731-3004

Phillips Laboratory
ATTN: PL/SUL
3550 Aberdeen Ave SE
Kirtland, NM 87117-5776 (2 copies)

Dr. Michel Bouchon
I.R.I.G.M.-B.P. 68
38402 St. Martin D'Heres
Cedex, FRANCE

Dr. Michel Campillo
Observatoire de Grenoble
I.R.I.G.M.-B.P. 53
38041 Grenoble, FRANCE

Prof. Hans-Peter Harjes
Institute for Geophysic
Ruhr University/Bochum
P.O. Box 102148
4630 Bochum 1, GERMANY

Prof. Eystein Husebye
IFJF
Jordskjelvstasjonen
Allegaten, 5007 BERGEN NORWAY

David Jepsen
Acting Head, Nuclear Monitoring Section
Bureau of Mineral Resources
Geology and Geophysics
G.P.O. Box 378, Canberra, AUSTRALIA

Ms. Eva Johannisson
Senior Research Officer
FOA
S-172 90 Sundbyberg, SWEDEN

Dr. Peter Marshall
Procurement Executive
Ministry of Defense
Blacknest, Brimpton
Reading FG7-FRS, UNITED KINGDOM

Dr. Bernard Massinon, Dr. Pierre Mechler
Societe Radiomana
27 rue Claude Bernard
75005 Paris, FRANCE (2 Copies)

Dr. Svein Mykkeltveit
NTNT/NORSAR
P.O. Box 51
N-2007 Kjeller, NORWAY (3 Copies)

Prof. Keith Priestley
University of Cambridge
Bullard Labs, Dept. of Earth Sciences
Madingley Rise, Madingley Road
Cambridge CB3 OEZ, ENGLAND

Dr. Jorg Schlittenhardt
Federal Institute for Geosciences & Nat'l Res.
Postfach 510153
D-30631 Hannover , GERMANY

Dr. Johannes Schweitzer
Institute of Geophysics
Ruhr University/Bochum
P.O. Box 1102148
4360 Bochum 1, GERMANY

Trust & Verify
VERTIC
Carrara House
20 Embankment Place
London WC2N 6NN, ENGLAND

Prof. Dr. M. Namik YALCIN
Dept. of Earth Sciences
P.O. Box 21,
41470
GEBZE-KOCAELI, TURKEY

Defense Technical Information Center
8725 John J. Kingman Road
Ft. Belvoir, VA 22060-6218 (2 copies)